

## Effect of steady shear deformation on electrically conductive PP/PS/MWCNT composites

Daria Strugova, Éric David and Nicole R. Demarquette \*

Mechanical Engineering Department, École de Technologie Supérieure, Montréal, Québec H3C 1K3, Canada;

\* Correspondence: [NicoleR.Demarquette@etsmtl.ca](mailto:NicoleR.Demarquette@etsmtl.ca)

### Abstract

Conductive polymeric materials are commonly obtained adding conductive nanoparticles to blends of immiscible polymers that form a co-continuous morphology. However, during processing, morphology changes affecting materials properties. This study investigates the impact of steady shear deformation on the morphological and electrical properties of a model system consisting of polypropylene/polystyrene/multiwall carbon nanotubes (PP/PS/MWCNT). The findings reveal that the deformation results in coarsening of the blend morphology and disruption of the electrical network, increasing both the rheological and electrical percolation threshold concentrations. The evolution of both electrical and morphological properties depends on MWCNT concentration, strain amplitude, and shear rate. MWCNT concentration, below a certain level, leads to a disruption in electrical conductivity at high shear rates. However, if the MWCNT concentration is above 1 wt.%, the balance between filler network breakup and nanoparticle diffusion is maintained, resulting in stable electrical conductivity and morphology.

### I. INTRODUCTION

Blending two polymers, along with a nanoparticles' filler, can be an effective way to enhance the properties of thermoplastic nanocomposites, as it provides a tool to engineer the distribution of the nanoparticles within the matrix. For example, adding electrically conductive nanofillers to blends with a co-continuous morphology can lower the electrical percolation threshold (PT), which is the fillers' concentration at which the material conducts electricity. Indeed, if two immiscible polymers with appropriate rheological properties are mixed in the right proportions, a blend forming a co-continuous morphology is obtained [1, 2]. If conductive particles are added to the blend, in such a way that they end up locating in one of the blend components or at the interface between the two polymers, the percolation threshold decreases drastically. This phenomenon known as double percolation [3-23], was observed in several studies using various carbonaceous nanofillers, such as carbon black (CB) [14-24], carbon nanotubes (CNT) [4, 6, 8, 25-33], or graphene [10, 12, 13, 34-40].

The potential for low percolation threshold, predicted by the double percolation theory, can be hampered by changes to the co-continuous morphology during both processing and post-processing stages. In particular, the characteristic domain size can coarsen resulting in a decrease of electrical conductivity [12, 14, 41-44]. Overall, achieving good electrical properties in composites with a double percolation structure requires careful control of processing and post-processing parameters to mitigate the negative effects of morphology changes on the conductive



filler network. Optimizing post-treatment temperature and duration can positively alter the electrical conductivity of the composite and decrease the percolation threshold concentration [13, 45]. In practice, however, it can be challenging to control all relevant parameters. Therefore, further research is needed to fully understand the effects of processing and post-processing on the electrical properties, in order to develop effective strategies to control the morphology and achieve optimal electrical conductivity.

Several strategies have been proposed in the literature to mitigate the negative effects of morphology changes on the electrical properties of composites with double percolation structures, including increasing filler content [13, 44], using different fillers, or applying thermal treatments [13, 44, 46, 47]. The success of these strategies, however, is influenced by various factors, such as the type or geometry of the employed filler [13, 38, 45, 46], as well as the post-processing temperature and duration. For example, in a study involving a polylactic acid/polystyrene (PLA/PS) co-continuous blend, filled with thermally reduced graphene oxide (r-GO), after 30 min of annealing at 180 °C the characteristic domain size increased significantly for composites containing 0-0.28 vol.% r-GO (it increased, for example, from ~2.5 μm to ~23 μm for composite with r-GO concentration of 0.028 vol.%), but remained unchanged for composites containing 0.56-1.12 vol.% r-GO [13]. In our previous work [45], we demonstrated that the characteristic domain size was slightly reduced after 30 min of annealing at 200 °C for a polypropylene/polystyrene (PP/PS) blend filled with different concentrations of MWCNT presenting a co-continuous morphology [45]. This reduction in domain size was attributed to a refinement of the co-continuous morphology. This refinement led to an increase in the specific interfacial area between the two polymers, which is inversely proportional to the domain size. Our previous work has demonstrated progress in this field by introducing a tool/technique that correlates morphology and electrical properties in filled polymer composites with a co-continuous morphology [45]. Further investigation of the evolution of double percolation-type morphologies, however, is necessary to develop effective strategies for optimizing the electrical properties of such composites.

To investigate the evolution of properties during, as well as, after applying deformation, a series of steps must be taken. A test design consisting of three steps should be carried out. The first step is to use small amplitude oscillatory shear (SAOS) tests within the linear viscoelastic region, which are commonly employed to characterize the morphology of polymer blends by fitting the data to appropriate constitutive equations [22, 26, 48-52]. The second step is to apply a non-linear deformation. The third step is to use another SAOS to assess the evolution of the blend's morphology as a result of the applied deformations.

This strategy has been widely used to study the evolution of dispersed droplet shape morphology [53-59], using the well-known Palierne's model and its derivatives [48, 49]. This approach can be used to investigate the evolution of a double-percolation morphology. The rheological behavior of the filled blend-based composite with a co-continuous morphology is subjected to SAOS and fitted to a modified Yu et al. (YZZ) model (1):

$$G'_{blend}(\omega) = G'_{components}(\omega) + G'_{interface}(\omega) + G'_0 \quad (1)$$

The contribution of components, denoted by  $G'_{components}(\omega)$ , can be calculated using equation (4) presented in reference [60], which takes into account the storage moduli of each polymer in the polymer blend, as well as geometrical parameters of a simplified co-continuous morphology. The contribution of the interface, denoted by  $G'_{interface}(\omega)$  can be calculated using equation (15) presented in reference [61]. The calculation of  $G'_{interface}(\omega)$  takes into account both the geometrical parameters of the co-continuous morphology and the physical properties of the components in the polymer blend, such as the viscosity of each polymer and the interfacial tension between them. Finally, an adjustable constant, denoted by  $G'_0$  is included to account the rigidity of the filler network, as described in references [45, 62]. It should be noted that Equation (1) refers to different mechanical models that are purely empirical. More details can be found in Yu et al. and Strugova et al. [45, 61].

As mentioned above, the evolution of the blend morphology that is subjected to a deformation flow depends on the kinematics and kinetics of the undergone deformation. In the case of dispersed droplet morphology, the magnitude of the shear rate will either result in a droplet break-up or droplet coalescence [57-59, 63, 64]. The shear rate value which determines the transition from coalescence to break-up can be calculated using the well-known Grace diagram [65] (presented in Figure S1 of the Supplementary material). This diagram provides the critical capillary number  $Ca = \frac{F_{viscous}}{F_{interfacial}} = \frac{\eta_m \dot{\gamma} R_v}{\alpha}$  as a function of the viscosity ratio,  $p = \frac{\eta_d}{\eta_m}$ , for rotational shear. Here  $\eta_m$  is the viscosity of the matrix,  $\eta_d$  is the viscosity of the dispersed phase,  $\dot{\gamma}$  is the shear rate,  $R_v$  is the volume average radius of the drops, and  $\alpha$  is the interfacial tension [66]. The capillary number is a function of shear rate, therefore, the transition, for a certain viscosity ratio can be predicted by the shear rate value or the capillary number. The value of the transition, from coalescence to breakup, capillary number, was measured by Grace [65], by gradually increasing the strain rate up to breakup. Tucker et al. [67] suggested an empirical fit to Grace's data shown in Figure S1, according to Equation (2):

$$\text{Log}(Ca_c) = -0.506 - 0.0995 \log(p) + 0.124(\log(p))^2 - \frac{0.115}{\log(p) - \log(4.08)}, \quad (2)$$

While this theory was developed for a dispersed droplet type morphology it can be used to, approximately, determine the critical transition shear rate, from coalescence to breakup.

In the present work, PP/PS/MWCNT composites manifesting double percolation, with MWCNT concentrations equal to or above the PT, were subjected to different sequences of SAOS-steady shear-SAOS tests. The values of steady shear rate to which the blends were subjected during deformation were chosen to promote coalescence and break-up in order to induce two types of morphology evolution. The evolution of morphology of the blend during deformation was evaluated using the modified YZZ model [45]. The electrical properties of the materials were monitored during the deformation step and were attributed to the morphology evolution. The

possibility of recovering the morphological and electrical properties after applied deformation was also investigated.

## II. MATERIALS AND METHODS

### A. Materials

The study employed PP (PP4712E1 grade) from ExxonMobil and PS (MC3650 grade) from PolyOne. Their respective characteristics are detailed in Table 1. Additionally, MWCNT (NC7000™ grade) with an average diameter of 9.5 nm and length of 1.5  $\mu\text{m}$ , and a nominal electrical conductivity of  $10^6 \text{ Sm}^{-1}$ , were obtained from Nanocyl.

Table 1. Properties of the polymers.

Polymers	$M_w$ (g/mol)	$M_w/M_n$	Density ( $\text{g}\cdot\text{cm}^{-3}$ )	$\eta_0$ (Pa·s) at 200 °C
PP	317 420	6.65	0.9	7 800
PS	105 000	2.37	1.04	4 080

\*  $\eta_0$  – zero-shear viscosity. Zero shear viscosity of neat PP and PS was found by fitting the experimental data to the Carreau model [68, 69].

### B. Composites preparation

In this study, PP/PS/MWCNT composites with 50/50/x wt.% (where x is the weight concentration of MWCNT ranging from 0 to 5 wt.%) were prepared using a melt-mixing process with a Haake Rheomix OS PTW16 twin-screw extruder. The compositions were prepared by initially producing a masterbatch of PP containing 10 wt.% MWCNT, which was then diluted with PP and PS to achieve the desired MWCNT concentrations in PP/PS/MWCNT composites. During extrusion, a temperature of 220 °C was maintained in all zones, and the screw speed was fixed at 100 rpm for all compositions.

To promote MWCNT migration to the interface, the MWCNT was added to the PP phase, as it exhibited better affinity towards PS. Young's equation was utilized to predict the preferred location of MWCNT in the PP/PS blend, by estimating the wetting coefficient [6, 9, 70].

Further details regarding the selection of PP and PS weight fractions in order to obtain a co-continuous morphology can be found in our previous works [3, 45].

## C. Characterization

### *Rheological analysis*

The rheological properties of the composites were evaluated using a controlled-stress MCR 501 rotational rheometer from Anton Paar (Graz, Austria), in a dry nitrogen atmosphere. The experiments were conducted using a parallel-plates geometry with a 1 mm gap and 25 mm diameter plates, with all tests performed at a temperature of 200 °C. To determine the linear viscoelastic (LVE) region of the composites, dynamic strain sweep tests (DSST) were conducted. Following the DSST, a strain of 0.3% was selected for all subsequent tests, as it corresponds to the LVE region of the composite. The thermal stability of polymers was tested using time sweep tests on pure PP and PS. The employed polymers were found to be thermally stable for 6 hours. SAOS tests were carried out to investigate the morphology evolution. The parameters for all the above-mentioned tests can be found in Table S1 of the Supplementary material.

Rheological properties' evolution can be investigated by using sequences of SAOS, followed by a steady shear (simulating the processing route), followed by another SAOS, as shown in Figure 1(a) [58, 59, 71]. Parameters for the steady shear steps were chosen in order to perform/mimic coalescence and break-up phenomena of a dispersed droplet morphology type blend, composed of the same polymers (see Table 2, below). To assess any possible relaxation of the morphology after steady shear a stress relaxation step consisting of 30 min of rotation at 0.05 rad/s was added to the sequence (depicted in Figure 1(a)). The parameters of the stress relaxation step are similar to the parameters of annealing, explained in our previous work [45].

It is important to note that the parallel-plates geometry is not ideal for performing deformation tests to assess the morphology of polymer blends because the shear rate across the sample is not uniform. However, when measuring electrical properties at the same time as rheological properties under applied deformation, the parallel-plates geometry is the most suitable option as it allows for simpler extraction of electrical properties. Furthermore, in the case of cone-plate geometry, where the deformation is uniform across the diameter of the samples when steady shear tests are performed, the order of magnitude of the size of the dispersed phase is comparable to the gap between the tip of the cone and the upper plate. This is the reason why many studies carried out with polymer blends are carried out using parallel-plates geometries [57-59, 72-80]. Although the parallel-plates geometry may not be ideal for characterizing the morphology, we assumed that we could study the evolution of morphology using this geometry since we are measuring bulk properties rather than point-specific properties. To obtain a more comprehensive understanding of the co-continuous morphology, the samples for scanning electron microscopy were broken across the diameter and observations were done at a fixed position from the center of the samples. To determine the presence of a slip effect, the viscosity of the composites (pure blend and filled with 0.5 wt.% of MWCNT) was measured at a constant shear rate of 0.05 s<sup>-1</sup> for 2000s (100% of shear strain) for two plate-plate gaps: 1 mm and 2 mm. It was found that no significant change in viscosity was observed. The data for this experiment is presented in Figures S2(a) and S2(b) of the Supplementary material.

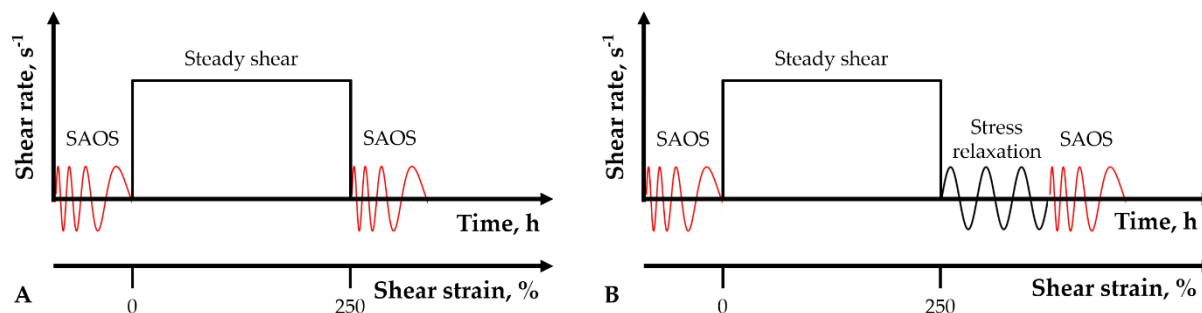


Figure 1. Experimental protocols.

Equation (2) was used to determine the critical shear rate ( $\dot{\gamma}_c$ ), above and below which break-up or coalescence occurs. Although this theory was originally developed for dispersed droplets morphology, calculating the critical shear rates for a co-continuous morphology can be done by estimating of the critical shear rates for different ratios of the dispersion. This would yield a curve of the of shear rate versus dispersion approaching a plateau. The plateau value of the shear rate is considered to be the critical shear rate for the co-continuous morphology. For this purpose, PP/PS blends with PS disperse phase ranging from 0 to 30 wt.% were prepared. 30wt.% of PS was deemed adequate since the co-continuous range was approached. The droplets volume average radius ( $R_v$ ) for each blend was measured by scanning electron microscopy (SEM). The interfacial tension value was taken from the literature [81]. Table 2 summarizes the experimental data required for the proposed experimental protocol.

Table 2. Experimental data for PP/PS blend with different weight concentration of components.

PP/PS wt.%	$Ca_c$	$\alpha$ , mNm	$R_v$ , $\mu\text{m}$	$\dot{\gamma}_c$ , $\text{s}^{-1}$
90/10			0.76	0.5
80/20	0.46	6	3.2	0.1
70/30			4.9	0.07
50/50			-	-

Values of steady shear rate for the experimental protocol presented in Figure 1(a) and Figure 1(b) are reported in Table 3. These values were chosen based on the experimental data presented in Table 2.

This is the author's peer reviewed, accepted manuscript. However, the online version of record will be different from this version once it has been copyedited and typeset.  
PLEASE CITE THIS ARTICLE AS DOI: 10.1122/1.8.0000647

Table 3. Parameters of the experimental protocol presented in Figure 1.

Coalescence		Break-up	
Shear strain, %	$\dot{\gamma}$ , s <sup>-1</sup>	Shear strain, %	$\dot{\gamma}$ , s <sup>-1</sup>
0		0	
10		10	
25	0.05	25	1
100		100	
250		250	

*Electrical conductivity analysis*

Electrical characterization, in conjunction with a rheological one, was carried out, using the MCR501 rheometer equipped with a dielectro-rheological device (DRD with ST2826/A high-frequency LCR meter). The plates of the parallel-plates geometry are made of stainless steel. In the employed arrangement two ceramic insulating discs about 5mm in height are added to both shafts holding the plates to provide electrical insulation as shown in Figure 2. Electrical (electronic) conductivity was measured during the steady shear and stress relaxation steps, see Figure 1(a) and Figure 1(b). More technical details for electrical conductivity measurements can be found in our previous work [45].

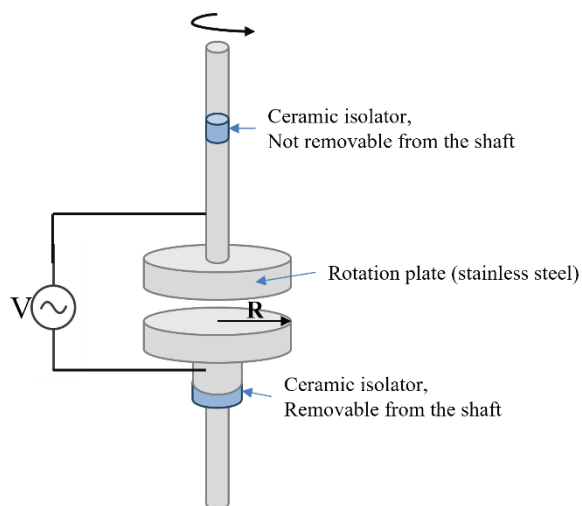


Figure 2. The illustration of the dielectro-rheological-device (DRD) setup.

In the parallel-plates geometry of a rotational rheometer, the shear rate is not constant as a function of the plate radius as can be seen in Equation (3):

$$\dot{\gamma} = \frac{\Omega R}{h}, \quad (3)$$

where  $h$  is the gap between the plates (mm),  $\Omega$  is the angular frequency (rad/s), and  $R$  is the distance from the center (mm). A full derivation of the equation can be found elsewhere [82].

In the present paper the shear rate at the rim ( $R=12.5$  mm) is either  $0.05\text{ s}^{-1}$  or  $1\text{ s}^{-1}$ . The rate decreases until it become  $0\text{ s}^{-1}$  at the center of the plate ( $R=0$  mm), where no deformation takes place. As a result, all the applied  $\dot{\gamma}$  values are average.

### *Microscopy analysis*

The morphology of PP/PS/MWCNT 50/50/x wt.% composites, before and after 250% of applied shear strain at two steady shear rates, one corresponding to coalescence,  $0.05\text{ s}^{-1}$ , and other to breakup,  $1\text{ s}^{-1}$ , was observed by scanning electron microscopy (SEM) using a S3600 Hitachi microscope (Hitachi, Ltd., Tokyo, Japan), operated at 5 kV in the secondary electrons mode. The samples, deformed in the rheometer, were quenched by opening the rheometer oven and cooling them, by convection, with compressed air. The cooling time was around 30 s which was not enough for the sample to undergo a change of morphology. More details for sample preparation can be found in Strugova et al. [3, 45].

Using the parallel-plates geometry, the samples were sheared at rates of  $0.05\text{ s}^{-1}$ , and  $1\text{ s}^{-1}$ . It is then true that the largest effect of shear was experienced by the sample at a distance of 12.5 mm from the center of the plate and was absent at the center of the sample (see Equation (3) and Figure S3 of the Supplementary material). In order to show morphology evolution after shearing, the micrographs of the samples' morphology were taken at a fixed position of 12.5 mm from the center. Those micrographs were added to the manuscript to support the model predictions but were not used in the calculations.

The state of dispersion and localization of MWCNT in PP/PS/MWCNT composites were evaluated by transmission electron microscopy (TEM). The investigated samples were embedded in an epoxy resin in order to obtain 50–100 nm ultrathin sections. The sectioning was performed using a Leica Microsystems UC7/FC7 cryo-ultramicrotome operated at  $-160\text{ }^{\circ}\text{C}$ . Imaging was carried out with a Thermo Scientific Talos F200X G2 S/TEM at an accelerating voltage of 200 kV.

### **III. RESULTS**

Figures 3(a) and 3(b) depict the co-continuous morphology of PP/PS 50/50 wt.% and PP/PS/MWCNT 50/50/0.5 wt.%. Figures 3(c) and 3(d) illustrate the localization of MWCNT in PP/PS/MWCNT 50/50/0.5 wt.% composite. It was observed that the addition of MWCNT refined the co-continuous morphology of the 50/50 wt.% PP/PS matrix, as previously observed in our earlier works [3, 45]. Moreover, due to MWCNT' thermodynamic affinity to PS, it tends to move towards that more favorable phase.



This is the author's peer reviewed, accepted manuscript. However, the online version of record will be different from this version once it has been copyedited and typeset.  
PLEASE CITE THIS ARTICLE AS DOI: 10.1122/1.50000647

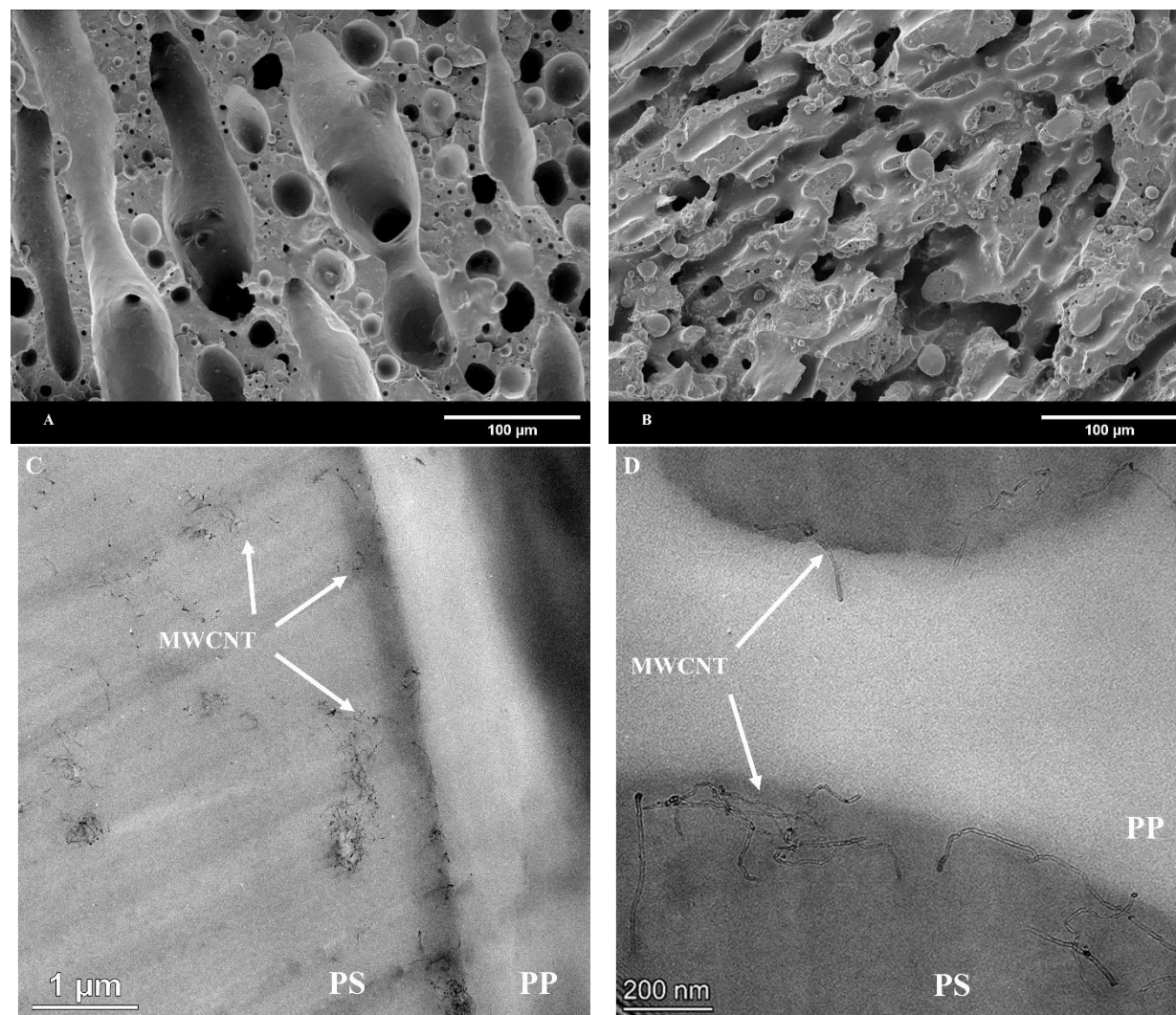


Figure 3. SEM observations for (a) PP/PS 50/50 wt.% and (b) PP/PS/MWCNT 50/50/0.5 wt.%. TEM of PP/PS/MWCNT 50/50/0.5 wt.%. composite with different magnification.

Figures 4(a) and 4(b) show electrical conductivity versus shear strain at steady shear rates of  $0.05 \text{ s}^{-1}$  and  $1 \text{ s}^{-1}$ , respectively. The results demonstrate a significant impact of the MWCNT concentration on the electrical conductivity of composites during the steady shear step. For the composite containing 0.3 wt.% MWCNT, the electrical conductivity decreased noticeably in the early stages of deformation for both studied steady shear rates. It eventually levelled off at a value close to the one for pure PP/PS matrix, exhibiting a dielectric behavior. However, for a steady shear rate of  $0.05 \text{ s}^{-1}$ , corresponding to coalescence, the electrical conductivity gradually decreased at a much lower pace, while for a steady shear rate of  $1 \text{ s}^{-1}$ , corresponding to break-up, the conductivity decreased very sharply to within 75% of its value. The electrical conductivity of composites with 0.5 wt.% and 1 wt.% of MWCNT decreased by two orders of magnitude (or four orders of magnitude for the composite containing 0.5 wt.% of MWCNT sheared at a shear rate of  $1 \text{ s}^{-1}$ ), while composites containing 2 wt.% and 5 wt.% of MWCNT showed either no change or

an increase in electrical conductivity during steady shear. Figure 13 (presented later in the paper) provides a clear illustration of the effect of morphology coarsening during applied deformation on the distribution of the filler within the matrix, and the resulting impact on electrical conductivity of the composites. Similar behavior of electrical conductivity for polycarbonate/MWCNT composites containing 0.75, 1, and 1.5 wt.% of MWCNT was observed by Skipa et al. [78]. For these concentrations of MWCNT, electrical conductivity decreased with increasing deformation time, within the first 300 s, and within the following 300 s, it stabilized and approached a plateau [78].

Transient shear viscosity behavior versus shear strain is presented in Figures 4(c) and 4(d) for composites deformed at a steady shear rate of  $0.05 \text{ s}^{-1}$  and  $1 \text{ s}^{-1}$ , respectively. To aid visualization, the results are presented for the first 50% of applied deformation only. This is because, beyond this point, the transient viscosity reaches a plateau for both steady shear rates. Figures S4(a) and S4(b) in the Supplementary material illustrate this trend. The results show that the composites subjected to a deformation rate of  $1 \text{ s}^{-1}$  exhibit a stress overshoot, whereas the ones subjected to a deformation rate of  $0.05 \text{ s}^{-1}$  do not. This stress overshoot corresponds not only to the reaction of PP and PS phases to the deformation applied but also to the reorientation of the MWCNT network [62]. Its magnitude is larger for the larger compositions of MWCNT as the network is expected to be more robust.

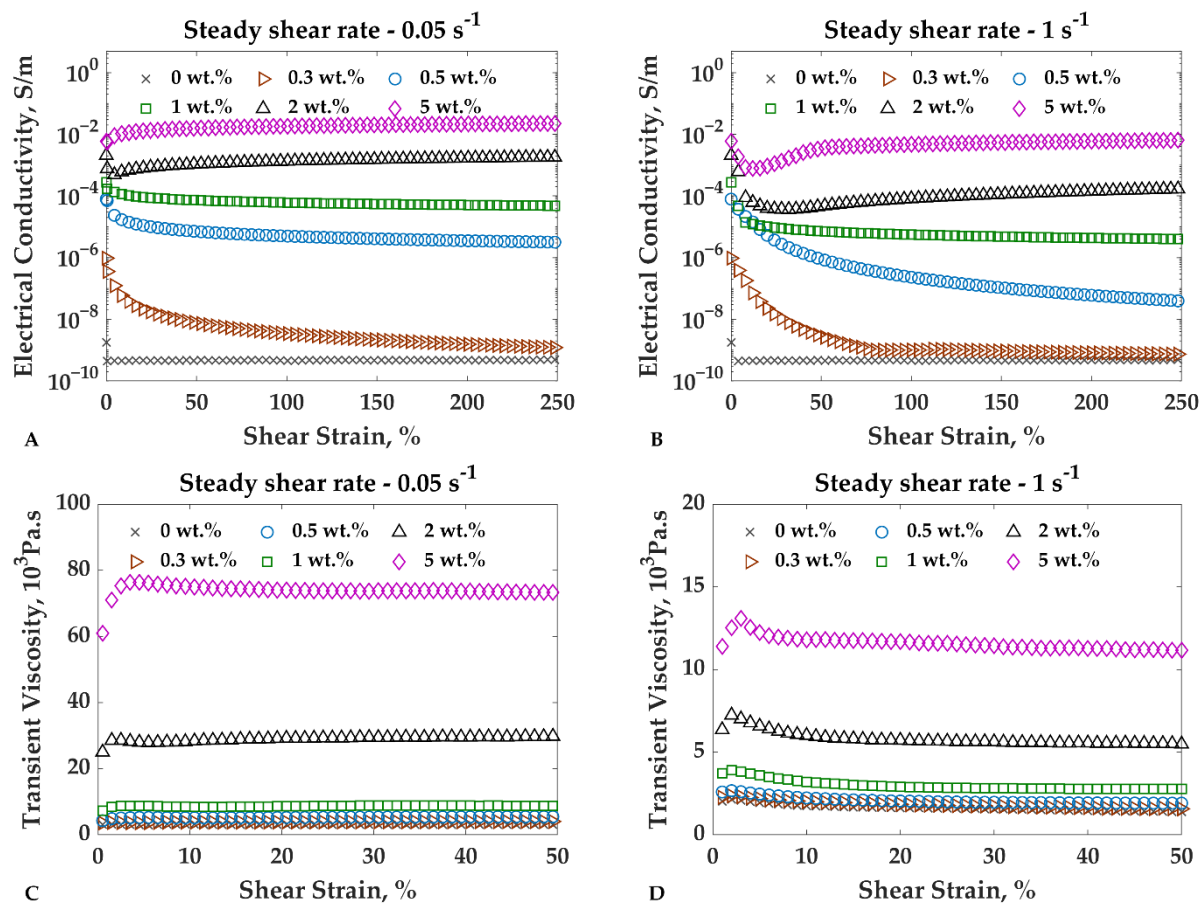


Figure 4. Electrical conductivity and transient shear viscosity vs. applied shear strain for PP/PS/MWCNTs 50/50/x wt.% composites at 200 °C at: a and c) steady shear rate of 0.05 s<sup>-1</sup>; b and d) steady shear rate of 1 s<sup>-1</sup>.

The DC electrical conductivity of PP/PS/MWCNT composites before and after applying 250% of shear strain at steady shear rates of 0.05 s<sup>-1</sup> and 1 s<sup>-1</sup> is presented in Figure 5. In comparison to the undeformed composites, the results indicate that the behavior of the electrical conductivity of deformed composites can be categorized into three distinct groups based on MWCNT concentration. Composites with 0.3 wt.% MWCNT and below experienced a significant decrease in electrical conductivity, exhibiting dielectric behavior. For composites containing 0.5-1 wt.% MWCNT, the electrical conductivity decreased by one order of magnitude when subjected to steady shear at a shear rate of 0.05 s<sup>-1</sup>, and by 2-3 orders of magnitude at a shear rate of 1 s<sup>-1</sup>, compared to composites before any deformation. Finally, composites containing 2 wt.% and 5 wt.% of MWCNT either demonstrated no change or exhibited an increase in electrical conductivity after 250% of applied deformation at both shear rates. The observed results suggest that the effect of shear strain on the electrical conductivity of PP/PS/MWCNT composites is highly dependent on the MWCNT concentration. Additionally, the applied shear rate also plays a crucial role in determining the behavior of electrical conductivity. The decrease in electrical conductivity for composites with lower MWCNT wt.% can be attributed to the reduction in MWCNT network connectivity caused by the deformation. However, for composites with higher MWCNT wt.%, the increase in electrical conductivity can be attributed to the alignment and re-orientation of the MWCNT network, resulting in enhanced connectivity.

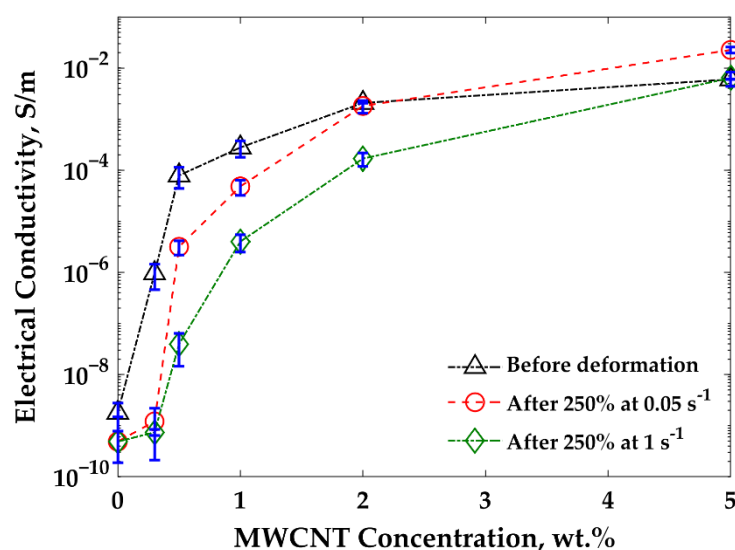


Figure 5. Electrical conductivity vs. MWCNT wt.% for composites before and after 250% of applied shear strain at different steady shear rates.

The percolation threshold concentrations for PP/PS/MWCNT (50/50/x wt.%) composites, subjected to 250% of applied deformation at both  $0.05 \text{ s}^{-1}$  and  $1 \text{ s}^{-1}$  shear rates, were evaluated using Equation (3) and the data presented in Figure 5.

$$\sigma = k \cdot (p - p_c)^t, \text{ with } p > p_c, \quad (3)$$

where  $\sigma$  is the electrical conductivity of PP/PS/MWCNT 50/50/x wt.% composite,  $p$  is the mass fraction of MWCNT,  $p_c$  is the percolation threshold concentration,  $t$  is a fitted exponent that depends, only, on the dimensionality of the system, and  $k$  is a scaling factor. The fitting parameters are presented in Table 4 and in Figure S5 of the Supplementary material.

Table 4.  $p_c$  and fitted coefficients for PP/PS/MWCNT composites before and after 250% of shear strain applied at different steady shear rates.

Parameters	Before deformation	After 250% of shear strain	
		at a steady shear rate of:	
		$0.05 \text{ s}^{-1}$	$1 \text{ s}^{-1}$
$p_c$ , wt.%	0.29	0.43	0.75
$k$ , S/m	$7 \times 10^{-4}$	$6 \times 10^{-4}$	$1 \times 10^{-4}$
$t$	1.4	2.2	2.6
$R^2$	0.99	0.96	0.99

As presented in Figure 5 and Table 4, an increase in the percolation threshold concentration was observed after the application of 250% shear strain at both shear rates. The concentration increased to 0.43 wt.% and 0.75 wt.% compared to 0.29 wt.% MWCNT for composites subjected to 250% applied strain at shear rates of  $0.05 \text{ s}^{-1}$  and  $1 \text{ s}^{-1}$ , respectively. Nevertheless, the filler network was not completely destroyed for highly filled composites containing more than 1 wt.% MWCNT, even in composites subjected to a shear rate of  $1 \text{ s}^{-1}$ , as the electrical conductivity of these composites exhibited minimal reduction. In the following section, the changes in electrical properties are elucidated in terms of the morphological evolution, as assessed by rheological measurements.

Figure 6 shows a typical example of the frequency-dependent evolution of the storage modulus ( $G'(\omega)$ ) after subjecting the composites to a certain shear strain at steady shear rates of  $0.05 \text{ s}^{-1}$  (Figures 6(a) and 6(c)), and  $1 \text{ s}^{-1}$  (Figures 6(b) and 6(d)). The  $G'(\omega)$  behavior for PP/PS/MWCNT 50/50/0.5 wt.% and 50/50/2 wt.% composites is shown in this case, although similar behavior was observed for the other samples, as presented in Figure S6 of the Supplementary material. Example of the frequency-dependent evolution of the loss modulus ( $G''(\omega)$ ) after subjecting

This is the author's peer reviewed, accepted manuscript. However, the online version of record will be different from this version once it has been copyedited and typeset.  
PLEASE CITE THIS ARTICLE AS DOI: 10.1122/1.50000647

PP/PS/MWCNT composites with 0.5 wt.% and 2 wt.% of MWCNT to a certain shear strain at a steady shear rate of  $1 \text{ s}^{-1}$  are reported in Figure S7(a-b) of the Supplementary material.

Notably, a nonterminal behavior characterized by the presence of a plateau of  $G'(\omega)$  is observed at low frequencies, indicating the presence of a rigid nanoparticle network [10, 26, 27], independently of the shear conditions to which the samples were exposed. However, the magnitude of this plateau modulus decreases with increasing shear strain indicating that the strength of the MWCNT network decreases, although it was not fully destroyed during the applied deformation. Similar results were observed for all composites with MWCNT concentration above 0.5 wt.% (see Figure S6 of the Supplementary material), except for the composites containing 2 wt.% and 5wt.% of MWCNT, subjected to steady shear at a shear rate of  $0.05 \text{ s}^{-1}$ , for which plateau values of  $G'(\omega)$  remains nearly unchanged or even increased as a function of applied shear strain.

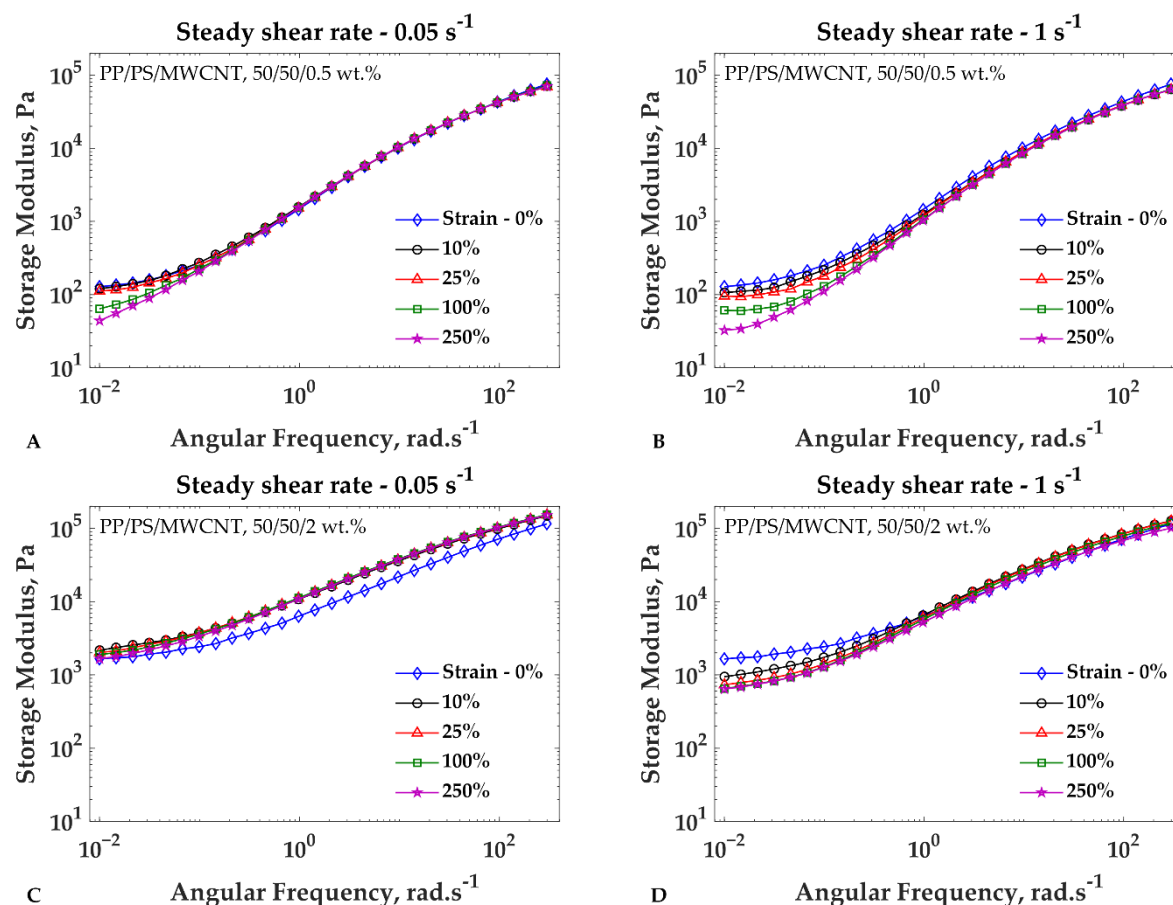


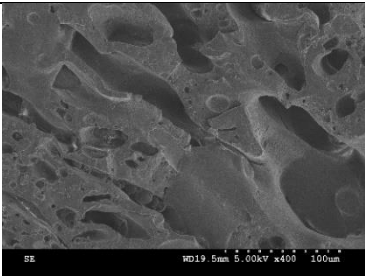
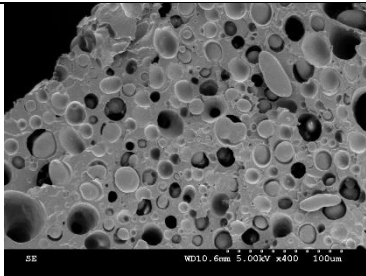
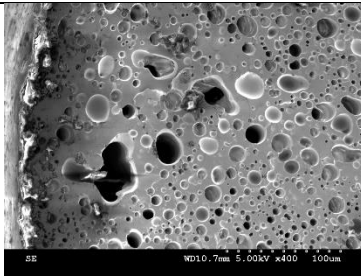
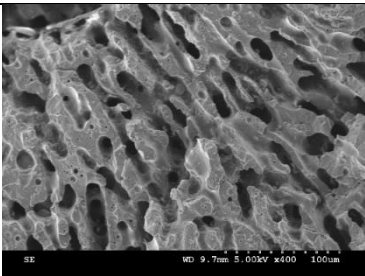
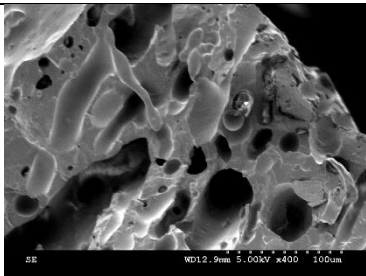
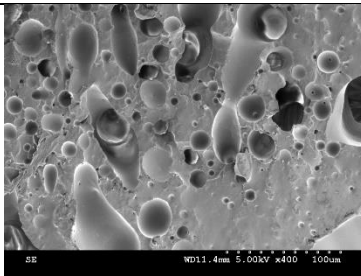
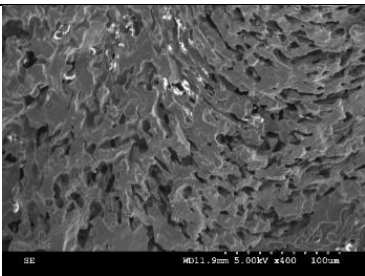
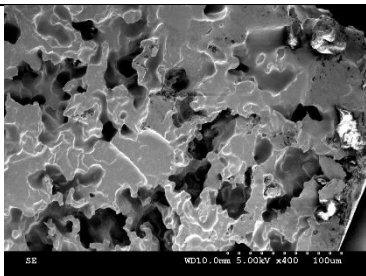
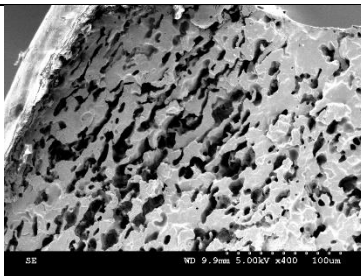
Figure 6.  $G'$  versus frequency for PP/PS/MWCNT composites with 0.5 and 2 wt.% of MWCNT after shear strain applied at a steady shear rate of: (a) and (c)  $0.05 \text{ s}^{-1}$ , and (b) and (d)  $1 \text{ s}^{-1}$ .

Table 5 presents SEM observations of co-continuous morphology evolution in neat PP/PS (50/50 wt.%) blend, as well as PP/PS/MWCNT composites with 0.5 wt.% and 2 wt.% of MWCNT, before

This is the author's peer reviewed, accepted manuscript. However, the online version of record will be different from this version once it has been copyedited and typeset.  
PLEASE CITE THIS ARTICLE AS DOI: 10.1122/1.50000647

and after 250% of applied shear strain, at steady shear rates of  $0.05 \text{ s}^{-1}$  and  $1 \text{ s}^{-1}$ . The results indicate that the co-continuous morphology of the 50/50 wt.% PP/PS blend transforms into a droplet-type morphology following 250% of applied shear strain at both shear rates. However, when MWCNT are added into the blend, this transformation does not occur. Instead, the co-continuous morphology undergoes coarsening following the applied shear strain but does not lose its continuity.

Table 5. Morphology of neat PP/PS, 50/50 wt.% blend and PP/PS/MWCNT composites, containing 0.5 wt.% and 2 wt.% of MWCNT wt.% before any deformation and after 250% of shear strain at different steady shear rates.

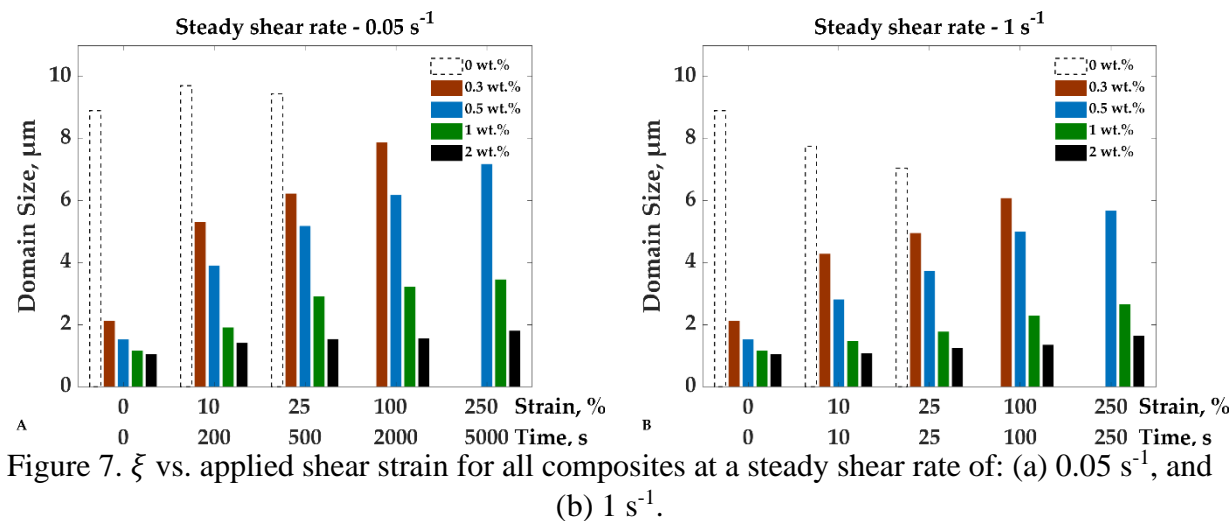
	Before any deformation	After 250% at $0.05 \text{ s}^{-1}$	After 250% at $1 \text{ s}^{-1}$
PP/PS, 50/50 wt. %			
	a	b	c
50/50/0.5 wt. %			
	d	e	f
50/50/2 wt. %			
	g	h	i

To study the rate of morphology coarsening following deformation at different shear rates, the characteristic domain size was determined by fitting the storage moduli data to Equation (1) for all the sheared composites, except for composites containing 5 wt.% of MWCNT. This is because the presence of a high amount of MWCNT (i.e., more than 2 wt.%) stabilizes the morphology and rheological properties. As a result, no significant changes in  $G'$  (as can be seen in Figure S6 of the Supplementary material) or in morphology were observed. Furthermore, in such composites, the behavior of  $G'(\omega)$  at low frequencies was largely dominated by the MWCNT network, making the modelling method less sensitive to the assessment of the morphology. As a result, the characteristic domain sizes could not be extracted for PP/PS/MWCNT composites containing more than 2 wt.% of MWCNT. Additionally, for the neat blend without MWCNT and the blend containing 0.3 wt.% MWCNT, the characteristic domain size could not be calculated for shear strains equal to or greater than 100% and 250%, respectively. This was because the morphology of these blends transformed from a co-continuous structure to a dispersed droplet type one, which made the calculation of the characteristic domain size impossible.

Figures 7(a) and 7(b) show the characteristic domain size ( $\xi$ ) as a function of shear strain applied at steady shear rates of  $0.05 \text{ s}^{-1}$  (Figure 7(a)), and  $1 \text{ s}^{-1}$  (Figure 7(b)), for composites with different MWCNT concentrations. The neat blend showed no change in morphology when sheared at a shear rate of  $0.05 \text{ s}^{-1}$ , but refinement was observed when sheared at a shear rate of  $1 \text{ s}^{-1}$ . In contrast, all composites containing MWCNT exhibited an increase in the characteristic domain sizes, indicating morphology coarsening. However, the degree of coarsening was less pronounced for composites with higher MWCNT concentrations, and almost absent at a concentration of 2 wt.%, indicating that 2 wt.% MWCNT stabilizes the morphology.

Table 5 shows variations in morphologies for composites containing 2 wt.% MWCNT following 250% of shear strain at different shear rates, although the values of the characteristic domain size for these composites are close. The variations in morphology were primarily due to slight orientation along the direction of shear at the higher rate of  $1/\text{s}$ , which was observed for composites with high MWCNT loadings (1-2 wt.%). As a result, co-continuous domains of the composites appear to be slightly elongated, but the specific surface area values remain relatively constant, as well as the characteristic domain size, which is inversely proportional to it.

The results also indicate that all filled composites exhibit a greater increment in the characteristic domain when sheared at a steady shear rate of  $0.05 \text{ s}^{-1}$  compared to  $1 \text{ s}^{-1}$ . This can be attributed to the longer time required to achieve a strain of 250% at a lower shear rate, allowing more time for morphology evolution/coarsening. Moreover, the increase in characteristic domain size is dependent on the MWCNT concentration, with a greater increase observed for lower concentrations. Interestingly, the coarsening observed at different shear rates can lead to either an increase or decrease in electrical conductivity. The results reveal that when the deformation is applied at a shear rate of  $0.05 \text{ s}^{-1}$ , the electrical conductivity of the composites increases, whereas it decreases when the deformation is applied at a shear rate of  $1 \text{ s}^{-1}$ . These results indicate that the evolution of electrical conductivity depends on a delicate balance between changes in blend morphology, leading to the destruction of the conductive network, and the diffusion of MWCNT particles toward the interface.



The stability of the filler network of the PP/PS/MWCNT composites can be investigated by fitting the values of  $G'_0$ , the frequency-independent elastic modulus, obtained by fitting the SAOS data to Equation (1), to the following equation (values predicted by the modified YZZ [45]) [83]:

$$G'_0 = k \cdot (\gamma - \gamma_c)^{-\nu} \quad (4)$$

where  $\gamma$  is the applied shear strain,  $\gamma_c$  is the critical shear strain at which MWCNT rheological network is destroyed,  $\nu$  is a fitted exponent that depends, only, on the dimensionality of the system, and  $k$  is a scaling factor responsible for strength of the filler network.

The  $G'_0$  data for PP/PS/MWCNT composites with different MWCNT concentrations, subjected to deformation at  $0.05 \text{ s}^{-1}$  and  $1 \text{ s}^{-1}$  are presented in Table S2 and Table S3 of the Supplementary material, respectively. Linear regression analysis was used to obtain critical shear strains, represented by the equation,  $\log(G'_0) = \log(\gamma - \gamma_c)$ . The results of these regressions, for PP/PS/MWCNT composites with varying concentrations of 0.5 wt.%, 1 wt.%, and 2 wt.% MWCNT, deformed at  $0.05 \text{ s}^{-1}$  and  $1 \text{ s}^{-1}$ , are illustrated in Figures S8(a-c) of the Supplementary material. The critical shear strain values for composites sheared at steady shear rates of  $0.05 \text{ s}^{-1}$  and  $1 \text{ s}^{-1}$  are reported in Table 6.

It can be seen that the critical strain at which the rheological network is destroyed increases with increasing MWCNT concentration and decreases with increasing shear rate. However, it should be noted that the critical strain values obtained indicate that the rheological network is destroyed at lower strains compared to the electrical network.

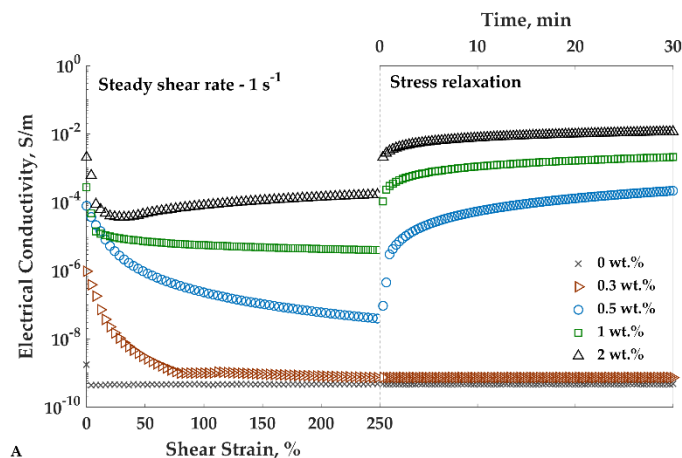


Table 6. Critical shear strain for composites sheared at  $0.05 \text{ s}^{-1}$  and  $1 \text{ s}^{-1}$  of steady shear rates.

MWCNT, wt.%	$\gamma_c$ , %	
	$0.05 \text{ s}^{-1}$	$1 \text{ s}^{-1}$
0.5	9	5
1	18	10
2	53	25

Figure 8(a) presents the electrical conductivity as a function of shear strain of PP/PS/MWCNT 50/50/x wt.% composites sheared at  $1 \text{ s}^{-1}$ , as well as a function of time during the stress relaxation step (see to Figure 1(b) for the deformation history). It can be seen that for composites with MWCNT concentrations above 0.5 wt.%, the electrical conductivity increases during stress relaxation, reaching values even greater than those prior to shearing as shown in Figure 9.

Figure 8(b) shows the shear stress growth function during steady shear at  $1 \text{ s}^{-1}$  and stress relaxation for the first 10 minutes. The experimental values of stress during stress relaxation step (Figure 8(b-right)) were oscillating during the early stage of a stress relaxation step. These oscillations were attributed to measurement artifacts and in order to mitigate their effects the experimental data was smoothed. The results indicate that there is a significant relaxation step following the steady shear step that occurs within the first few seconds. Furthermore, the relaxation takes longer in the PP/PS/MWCNT composites filled with MWCNT compared to the neat PP/PS blend. This behavior of stress is likely due to the presence of a rigid filler network, which is building-up during the stress relaxation step and this process incorporates long time relaxation mechanisms into the system as well as leads to stabilization of the co-continuous morphology [45] and to a decrease in a stress. This happened because nothing prevents filler diffusion towards the more favorable PS phase, where at a high enough concentration of MWCNT, significant number of nanoparticles are trapped at the interface rebuilding of filler network.



This is the author's peer reviewed, accepted manuscript. However, the online version of record will be different from this version once it has been copyedited and typeset.  
PLEASE CITE THIS ARTICLE AS DOI: 10.1122/1.50000647

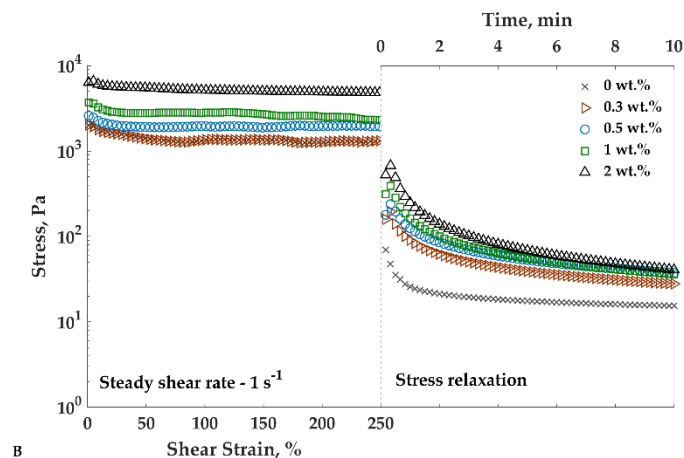


Figure 8. (a) Electrical conductivity vs. shear strain at a steady shear step and as a function of time at a stress relaxation step for all composites; (b) Stress vs. shear strain and time for all composites.

Figure 9 presents the DC electrical conductivity as a function of MWCNT wt.% before any deformation, after 250% shear strain applied at steady shear rate of  $1 \text{ s}^{-1}$ , and after 250% shear strain applied at steady shear rate of  $1 \text{ s}^{-1}$  plus 30 min of stress relaxation step at an angular frequency of  $0.05 \text{ rad/s}$ . As previously mentioned, the electrical conductivity values for composites containing 0.5 wt.% or more MWCNT after deformation and stress relaxation are even greater than those prior to deformation. For PP/PS/MWCNT composite containing 2 wt.% of MWCNT, the electrical conductivity after 250 % of applied shear strain plus 30 min of stress relaxation at  $0.05 \text{ rad/s}$  is  $0.015 \text{ S/m}$ , compared to  $0.002 \text{ S/m}$  and  $0.00017 \text{ S/m}$  prior to deformation and just after 250 % of applied strain at  $1 \text{ s}^{-1}$ , respectively. This indicates that the filler network rebuilds and strengthens itself although it was partially destroyed during the deformation steps [77, 78, 84]. Moreover, the co-continuous morphology of the composite undergoes further refinement after the stress relaxation step, resulting in improved connections of the filler particles trapped at the interphase (the illustration of the effect of morphology coarsening during applied deformation and morphology refinement after the stress relaxation step can be seen in Figure 13).

Similar results on the electrical conductivity behavior were obtained by other researchers who worked with a single polymer containing MWCNT. In particular, in a study conducted by Alig et al., using polycarbonate (PC)/MWCNT composites, the electrical conductivity after steady shear decreased from  $4 \times 10^{-5} \text{ S/m}$  to  $3 \times 10^{-8} \text{ S/m}$  but recovered to a value of  $2 \times 10^{-2} \text{ S/m}$  [77]. Similarly, in another investigation of the PC/MWCNT composites containing 0.75 to 1.5 wt.% MWCNT, Skipa et al. observed a decrease in electrical conductivity with increasing deformation time at an angular frequency of  $0.02 \text{ rad/s}$  for 600s. However, the electrical conductivity bounced back to its initial value after 600 s of stress relaxation step, which was equivalent to the deformation time [78].

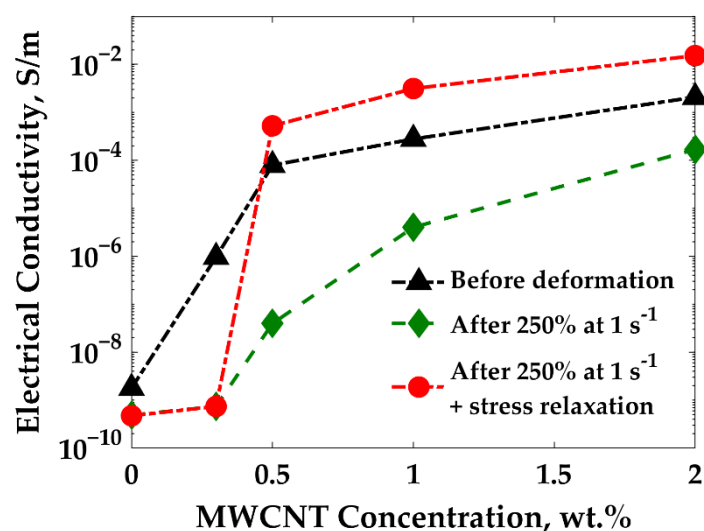


Figure 9. Electrical conductivity vs. MWCNT wt.% for composites before, after 250% of applied shear strain at 1 s<sup>-1</sup>, and after 250% of applied shear strain at 1 s<sup>-1</sup> plus 30 min of stress relaxation at 0.05 rad/s.

Figure 10 shows a comparison of characteristic domain sizes for PP/PS/MWNT composite containing 0.5 wt.% MWCNT before deformation, after deformation following the protocol of Figure 1(a), and after deformation along with 30 minutes of stress relaxation, see Figure 1(b). Figure 11 shows the morphology of the composites at the same conditions. Such analysis was performed to visualize the evolution of the morphology and electrical conductivity of the blends containing 0.5 wt.% MWCNT, as both parameters showed the most significant changes after steady shear (see Figure 7) and stress relaxation (see Figure 8(a)). The results indicate that the stress relaxation step led to a recovery of the co-continuous morphology. Specifically, the characteristic domain size decreased from 5.7  $\mu\text{m}$  to 3  $\mu\text{m}$  after the stress relaxation step was applied. However, it did not reach the initial value of 1.5  $\mu\text{m}$  observed in the composites before deformation. Notably, as shown in Figure 11(b) and Figure 11(c), shearing transformed the morphology from co-continuous to dispersed droplet shape type (Figure 11(b)). However, after recovery, it reverted to its co-continuous state (Figure 11(c)).

This is the author's peer reviewed, accepted manuscript. However, the online version of record will be different from this version once it has been copyedited and typeset.  
PLEASE CITE THIS ARTICLE AS DOI: 10.1122/1.50000647

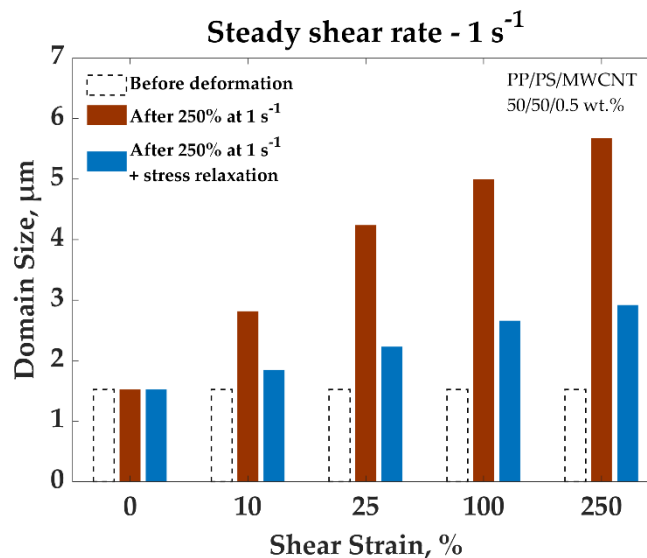


Figure 10. Evolution of characteristic domain size for PP/PS/MWCNT 50/50/0.5 wt.% composite before any deformation, after shear strain applied at a steady shear rate of 1 s<sup>-1</sup>, and after shear strain applied at a steady shear rate of 1 s<sup>-1</sup> plus stress relaxation step of 10 min.

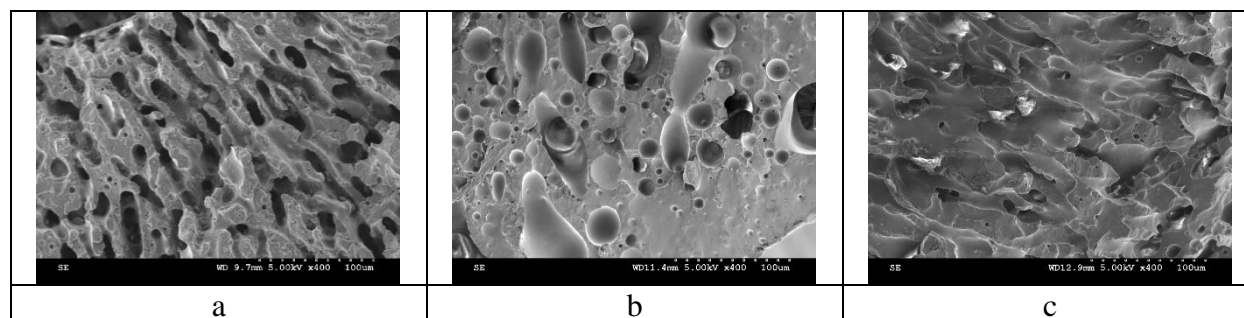


Figure 11. Morphology of PP/PS/MWCNT 50/50/0.5 wt.% composite: (a) before any deformation, (b) after 250% of shear strain at a shear rate of 1 s<sup>-1</sup>, and (c) after 250% of shear strain at a shear rate of 1 s<sup>-1</sup> + 30 min of stress relaxation step.

#### IV. DISCUSSION

The experimental results found in this work indicate that the evolution of the electrical conductivity of the composites, when subjected to steady shear, depends on the carbon nanotubes concentration, as well as, the rate (steady shear rate), and amplitude (strain) of deformation. In turn, those three variables will affect 1) the blend morphology, 2) the coverage of interface by conductive nanoparticles, 3) the diffusion of conductive nanoparticles towards the interface. Indeed, the evolution of electrical conductivity during deformation and/or stress relaxation depends on both the evolution of morphology of the blend and location of the filler [3, 10-13, 45].

The maximum interface coverage ( $\Sigma$ ), assuming that all MWCNT are at the PP/PS interface can be found as:

$$\Sigma = \frac{A_{MWCNT}}{S_V} * wt. \%PS * 100\% \quad (5)$$

where  $A_{MWCNT}$  is the total area of a triangular array which is created by MWCNT as shown in Figure 12,  $S_V$  is the specific interphase area per weight fraction of PS.

In order to determine the maximum area covered by the MWCNT within the composite we assumed that the carbon nanotubes formed a triangular array as illustrated in Figure 12. The total surface area of the array, denoted as  $A_{MWCNT}$ , was calculated by multiplying the area of a single triangular unit by the total number of triangular units in the array, taking into account the surface fraction of the network. By knowing the concentration of the nanotubes in the composites, as well as their length and density, it was possible to determine the number of nanotubes within a composite. This allowed us to calculate the area occupied by the nanotubes when arranged in the triangular array configuration as shown in Figure 12.

Table 7 presents the MWCNT weight concentrations,  $S_V$ ,  $A_{MWCNT}$ , and  $\Sigma$ .

Table 7. Maximum surface coverage of PP/PS/MWCNT 50/50/x wt.% composite interface by MWCNT mesh.

MWCNT, wt.%	$S_V, m^2/g,$ for pure PP/PS	$A_{MWCNT}, m^2$	$\Sigma, \%$
0.1		509	23
0.3		1528	68
0.5	112364	2547	113
1		5093	227
2		10187	453

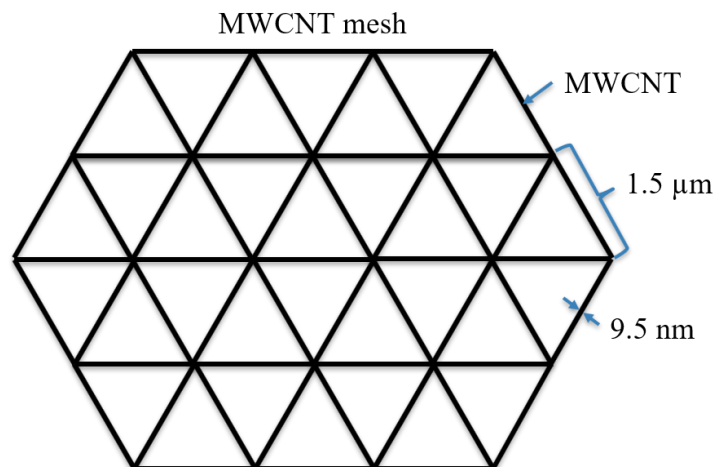


Figure 12. Schematic of a triangular array of MWCNT.

The results presented in Table 7 suggest that a complete surface coverage can be reached with as little as 0.5 wt.% of MWCNT and that a surface coverage of 68% is sufficient to reach the percolation threshold concentration of 0.3 wt.% for these composites. However, it is important to note that our assumption of complete coverage by MWCNT at the interface is not a common occurrence, as it is often difficult to achieve. Nonetheless, we do believe that a complete surface coverage can be achieved with a less dense MWCNT array, as the creation of a conductive pathway through the sample volume does not necessarily require interconnections in the array once the pathway has been established.

Figure 13 provides a summary of the results obtained in this work. It presents a sketch of the co-continuous morphology and of the conductive filler network evolutions for composites containing three MWCNT concentrations (0, 0.5 and 2 wt.%) before and after undergoing 250% deformation (strain) under steady shear rates of  $0.05 \text{ s}^{-1}$  and  $1 \text{ s}^{-1}$ , as well as after a stress relaxation step following the strain. The corresponding electrical conductivity values are also reported. The chosen concentrations correspond to a blend without addition of MWCNT, a blend with complete coverage of the PP/PS interface by MWCNT (0.5 wt.%), as was calculated using Equation (5), and a blend with high MWCNT concentration (2 wt.%) in order to illustrate the effects of deformation and MWCNT concentration on morphology coarsening and electrical conductivity changes. Note that MWCNT were always present in the PP phase.

The results showed that when no MWCNT were added to the blend, the co-continuous morphology transformed into a droplet type morphology after undergoing 250% strain at both steady shear rates ( $0.05 \text{ s}^{-1}$  and  $1 \text{ s}^{-1}$ ), as shown in Table 5. When 0.5 wt.% of MWCNT were added to the blend, the morphology coarsened, and the distance between MWCNT at the PP/PS interface increased, resulting in a decrease in electrical conductivity. However, during stress relaxation, the remaining MWCNT in PP were able to migrate to the interface, leading to a recovery of the electrical conductivity to its pre-deformation values. While the morphology was able to recover, it did not return to its initial state. When 2 wt.% MWCNT were added to the blend, the morphology was

This is the author's peer reviewed, accepted manuscript. However, the online version of record will be different from this version once it has been copyedited and typeset.  
 PLEASE CITE THIS ARTICLE AS DOI: 10.1122/1.50000647

stabilized by the presence of MWCNT. However, when a high shear rate ( $1 \text{ s}^{-1}$ ) was applied in order to deform the blend, the electrical conductivity decreased slightly, most likely due to a disruption of the electrical network. Nonetheless, during stress relaxation, the MWCNTs were once again able to migrate to the interface and contribute to an increase in electrical conductivity, as a large amount of MWCNTs remained at the interphase at all times, preventing any morphology coarsening.

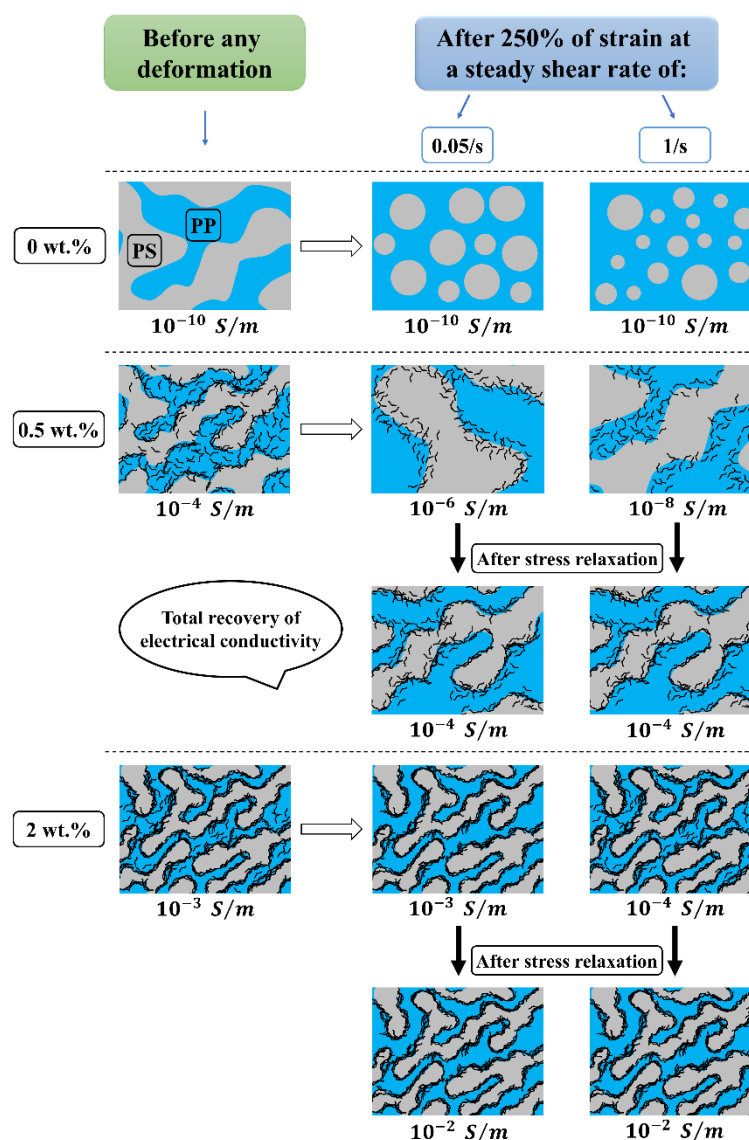


Figure 13. Schematic summary of the results.

The results of this study are general and can be applied to a broad range of blend systems based on thermoplastic polymers that exhibit a co-continuous morphology, provided that the viscosity ratio between the components does not exceed 3. This is due to the fact that a higher viscosity ratio

would hinder the droplets break-up and coalescence, and it will not be possible to mimic droplets break-up and coalescence in order to perform steady shear deformation tests which are critical for predicting morphological and electrical properties evolutions.

Moreover, the results of this study can be extended to any commonly added conductive filler.

It should be emphasized that these findings have significant industrial implications, as they offer a reliable and cost-effective way to predict and optimize the electrical conductivity of polymer composites during processing. This can be particularly relevant for the development of advanced materials for a broad range of applications, such as electromagnetic shielding, energy storage and conversion, and sensing technologies.

## V. CONCLUSION

Blends consisting of two immiscible polymers and presenting a co-continuous morphology have been widely used to obtain electrically conductive polymeric materials. The morphology of such blends is characterized by a double percolation of the polymer and filler phases, which significantly reduces the concentration of electrically conductive fillers required to attain conductivity, known as the percolation threshold. However, the morphology of multiphase materials is prone to evolution during processing involving various flows at different magnitudes and speeds. These changes in morphology can lead to a negative impact on materials properties and need to be understood and ultimately controlled. In this study, the effect of steady shear deformation on the morphological and electrical properties of a model system, polypropylene/polystyrene/multiwall carbon nanotubes (PP/PS/MWCNT), which presents a double percolation morphology, was investigated.

The results obtained in this work showed that deformation results in evolutions of blend morphology (coarsening) and electrical network, leading to an increase in both the rheological and electrical percolation thresholds. These evolutions depend on three key factors: MWCNT concentration, strain, and shear rate applied on the composites. High shear rates can have a disruptive effect on composites with low MWCNT concentration, causing coarsening of the blend morphology and a drastic reduction in electrical conductivity. Once the MWCNT concentration reaches a certain critical level, where the surface coverage is high enough, the co-continuous morphology and electrical network are stabilized. However, even if the morphology coarsens and the electrical network is disrupted, resulting in a decrease in electrical conductivity, it is possible to restore both the morphology and electrical conductivity through a stress relaxation if the MWCNT concentration is large enough. This can be achieved by promoting the diffusion of nanoparticles towards the PP/PS interface by applying thermal treatments. Nonetheless, when the MWCNT concentration is very low, it becomes impossible to recover from the disruptive effects of applied strain and shear rate. The changes in electrical conductivity and co-continuous morphology are governed by the balance between the breakup of the filler network and nanoparticles diffusion.



## SUPPLEMENTARY MATERIAL

See supplementary material for the additional information of experimental data: Grace diagram. Tables with tests parameters. Viscosity of composites measured at different plate-plate gaps. Transient shear viscosity for all composite as a function of applied shear strain. Electrical conductivity versus reduced filler content. Storage modulus as a function of frequency for all composites. Network elasticity as a function of reduced shear strain.

## ACKNOWLEDGMENTS

Financial support from the Natural Sciences and Engineering Research Council of Canada (NSERC), PRIMA and École de technologie supérieure (ÉTS) are gratefully acknowledged. The help of Mazen Samara in reviewing the English in this paper is highly appreciated.

## REFERENCES

1. Miles, I.S. and A. Zurek, *Preparation, structure, and properties of two-phase co-continuous polymer blends*. Polymer Engineering & Science, 1988. **28**(12): p. 796-805.
2. Jordhamo, G., J. Manson, and L. Sperling, *Phase continuity and inversion in polymer blends and simultaneous interpenetrating networks*. Polymer Engineering & Science, 1986. **26**(8): p. 517-524.
3. Strugova, D., et al., *Ultra-Low Percolation Threshold Induced by Thermal Treatments in Co-Continuous Blend-Based PP/PS/MWCNTs Nanocomposites*. Nanomaterials, 2021. **11**(6): p. 1620.
4. Yang, Y., et al., *Achieving improved electromagnetic interference shielding performance and balanced mechanical properties in polyketone nanocomposites via a composite MWCNTs carrier*. Composites Part A: Applied Science and Manufacturing, 2020. **136**: p. 105967.
5. Shi, Y., et al., *Simultaneously improved electromagnetic interference shielding and flame retarding properties of poly (butylene succinate)/thermoplastic polyurethane blends by constructing segregated flame retardants and multi-walled carbon nanotubes double network*. Composites Part A: Applied Science and Manufacturing, 2020. **137**: p. 106037.
6. Otero-Navas, I., M. Arjmand, and U. Sundararaj, *Carbon nanotube induced double percolation in polymer blends: Morphology, rheology and broadband dielectric properties*. Polymer, 2017. **114**: p. 122-134.
7. Zhang, H., et al., *Thermal annealing induced enhancement of electrical properties of a co-continuous polymer blend filled with carbon nanotubes*. Composites Science and Technology, 2018. **167**: p. 522-528.
8. Chen, J., et al., *Design of superior conductive polymer composite with precisely controlling carbon nanotubes at the interface of a co-continuous polymer blend via a balance of  $\pi$ - $\pi$  interactions and dipole-dipole interactions*. Carbon, 2017. **114**: p. 441-448.
9. Hwang, T.Y., Y. Yoo, and J.W. Lee, *Electrical conductivity, phase behavior, and rheology of polypropylene/polystyrene blends with multi-walled carbon nanotube*. Rheologica acta, 2012. **51**(7): p. 623-636.
10. Helal, E., et al., *Correlation between morphology, rheological behavior, and electrical behavior of conductive cocontinuous LLDPE/EVA blends containing commercial graphene nanoplatelets*. Journal of Rheology, 2019. **63**(6): p. 961-976.

This is the author's peer reviewed, accepted manuscript. However, the online version of record will be different from this version once it has been copyedited and typeset.  
PLEASE CITE THIS ARTICLE AS DOI: 10.1122/1.5000647

11. Kurusu, R.S., et al., *The role of selectively located commercial graphene nanoplatelets in the electrical properties, morphology, and stability of EVA/LLDPE blends*. Macromolecular Materials and Engineering, 2018. **303**(9): p. 1800187.
12. Bai, L., et al., *Kinetic control of graphene localization in co-continuous polymer blends via melt compounding*. Langmuir, 2018. **34**(3): p. 1073-1083.
13. Bai, L., et al., *Localizing graphene at the interface of cocontinuous polymer blends: Morphology, rheology, and conductivity of cocontinuous conductive polymer composites*. Journal of Rheology, 2017. **61**(4): p. 575-587.
14. Luo, Y., et al., *Preparation of conductive polylactic acid/high density polyethylene/carbon black composites with low percolation threshold by locating the carbon black at the Interface of co-continuous blends*. Journal of Applied Polymer Science, 2021. **138**(17): p. 50291.
15. Sun, X.-R., et al., *Effect of phase coarsening under melt annealing on the electrical performance of polymer composites with a double percolation structure*. Physical Chemistry Chemical Physics, 2018. **20**(1): p. 137-147.
16. Zhang, Q., et al., *Comparison between the efficiencies of two conductive networks formed in carbon black-filled ternary polymer blends by different hierarchical structures*. Polymer Testing, 2017. **63**: p. 141-149.
17. Qi, X., et al., *Enhanced shape memory property of polylactide/thermoplastic poly (ether) urethane composites via carbon black self-networking induced co-continuous structure*. Composites Science and Technology, 2017. **139**: p. 8-16.
18. Chen, J., et al., *Balance the electrical properties and mechanical properties of carbon black filled immiscible polymer blends with a double percolation structure*. Composites Science and Technology, 2017. **140**: p. 99-105.
19. Soares, B.G., et al., *Effect of double percolation on the electrical properties and electromagnetic interference shielding effectiveness of carbon-black-loaded polystyrene/ethylene vinyl acetate copolymer blends*. Journal of Applied Polymer Science, 2016. **133**(7).
20. Pan, Y., et al., *Enhancing the electrical conductivity of carbon black-filled immiscible polymer blends by tuning the morphology*. European Polymer Journal, 2016. **78**: p. 106-115.
21. Gong, T., et al., *Low percolation threshold and balanced electrical and mechanical performances in polypropylene/carbon black composites with a continuous segregated structure*. Composites Part B: Engineering, 2016. **99**: p. 348-357.
22. Scherzer, S.L., et al., *Phase structure, rheology and electrical conductivity of co-continuous polystyrene/polymethylmethacrylate blends filled with carbon black*. Composites Science and Technology, 2015. **119**: p. 138-147.
23. Gao, C., et al., *High-performance conductive materials based on the selective location of carbon black in poly (ether ether ketone)/polyimide matrix*. Composites Part B: Engineering, 2015. **79**: p. 124-131.
24. Calberg, C., et al., *Electrical and dielectric properties of carbon black filled co-continuous two-phase polymer blends*. Journal of Physics D: Applied Physics, 1999. **32**(13): p. 1517.
25. Bizhani, H., et al., *Double percolated MWCNTs loaded PC/SAN nanocomposites as an absorbing electromagnetic shield*. European Polymer Journal, 2018. **100**: p. 209-218.
26. Bose, S., et al., *Electrical, rheological and morphological studies in co-continuous blends of polyamide 6 and acrylonitrile-butadiene-styrene with multiwall carbon nanotubes prepared by melt blending*. Composites Science and Technology, 2009. **69**(3-4): p. 365-372.
27. Chen, J., et al., *A promising strategy for efficient electromagnetic interference shielding by designing a porous double-percolated structure in MWCNT/polymer-based composites*. Composites Part A: Applied Science and Manufacturing, 2020. **138**: p. 106059.

This is the author's peer reviewed, accepted manuscript. However, the online version of record will be different from this version once it has been copyedited and typeset.  
PLEASE CITE THIS ARTICLE AS DOI: 10.1122/1.5111111

28. Ellingford, C., et al., *Electrical dual-percolation in MWCNTs/SBS/PVDF based thermoplastic elastomer (TPE) composites and the effect of mechanical stretching*. European Polymer Journal, 2019. **112**: p. 504-514.
29. Liu, T., et al., *Facile preparation of rapidly electro-active shape memory thermoplastic polyurethane/polylactide blends via phase morphology control and incorporation of conductive fillers*. Polymer, 2017. **114**: p. 28-35.
30. Roman, C., et al., *On the phase affinity of multi-walled carbon nanotubes in PMMA: LDPE immiscible polymer blends*. Polymer, 2017. **118**: p. 1-11.
31. Soares, B.G., et al., *Conducting melt blending of polystyrene and EVA copolymer with carbon nanotube assisted by phosphonium-based ionic liquid*. Journal of Applied Polymer Science, 2018. **135**(24): p. 45564.
32. Soares, B.G., et al., *The effect of the noncovalent functionalization of CNT by ionic liquid on electrical conductivity and electromagnetic interference shielding effectiveness of semi-biodegradable polypropylene/poly (lactic acid) composites*. Polymer Composites, 2020. **41**(1): p. 82-93.
33. Soares da Silva, J.P., et al., *Double Percolation of Melt-Mixed PS/PBAT Blends Loaded With Carbon Nanotube: Effect of Molding Temperature and the Non-covalent Functionalization of the Filler by Ionic Liquid*. Frontiers in Materials, 2019. **6**: p. 191.
34. Lan, Y., et al., *Electrically conductive thermoplastic polyurethane/polypropylene nanocomposites with selectively distributed graphene*. Polymer, 2016. **97**: p. 11-19.
35. Mao, C., Y. Zhu, and W. Jiang, *Design of electrical conductive composites: tuning the morphology to improve the electrical properties of graphene filled immiscible polymer blends*. ACS applied materials & interfaces, 2012. **4**(10): p. 5281-5286.
36. Rafeie, O., et al., *Conductive poly (vinylidene fluoride)/polyethylene/graphene blend-nanocomposites: Relationship between rheology, morphology, and electrical conductivity*. Journal of Applied Polymer Science, 2018. **135**(23): p. 46333.
37. Lin, Y., et al., *A highly stretchable and sensitive strain sensor based on graphene-elastomer composites with a novel double-interconnected network*. Journal of Materials Chemistry C, 2016. **4**(26): p. 6345-6352.
38. Mun, S.C., et al., *Strategies for interfacial localization of graphene/polyethylene-based cocontinuous blends for electrical percolation*. AIChE Journal, 2019. **65**(6): p. e16579.
39. Sadeghi, A., R. Moeini, and J.K. Yeganeh, *Highly conductive PP/PET polymer blends with high electromagnetic interference shielding performances in the presence of thermally reduced graphene nanosheets prepared through melt compounding*. Polymer Composites, 2019. **40**(S2): p. E1461-E1469.
40. Shen, Y., et al., *Selective localization of reduced graphene oxides at the interface of PLA/EVA blend and its resultant electrical resistivity*. Polymer Composites, 2017. **38**(9): p. 1982-1991.
41. Fenouillot, F., P. Cassagnau, and J.-C. Majesté, *Uneven distribution of nanoparticles in immiscible fluids: Morphology development in polymer blends*. Polymer, 2009. **50**(6): p. 1333-1350.
42. Gödel, A., et al., *The kinetics of CNT transfer between immiscible blend phases during melt mixing*. Polymer, 2012. **53**(2): p. 411-421.
43. Huang, J., et al., *Control of carbon nanotubes at the interface of a co-continuous immiscible polymer blend to fabricate conductive composites with ultralow percolation thresholds*. Carbon, 2014. **73**: p. 267-274.
44. Trifkovic, M., et al., *Stabilization of PE/PEO cocontinuous blends by interfacial nanoclays*. Macromolecules, 2015. **48**(13): p. 4631-4644.
45. Strugova, D., É. David, and N.R. Demarquette, *Linear viscoelasticity of PP/PS/MWCNT composites with co-continuous morphology*. Journal of Rheology, 2022. **66**(4): p. 671-681.

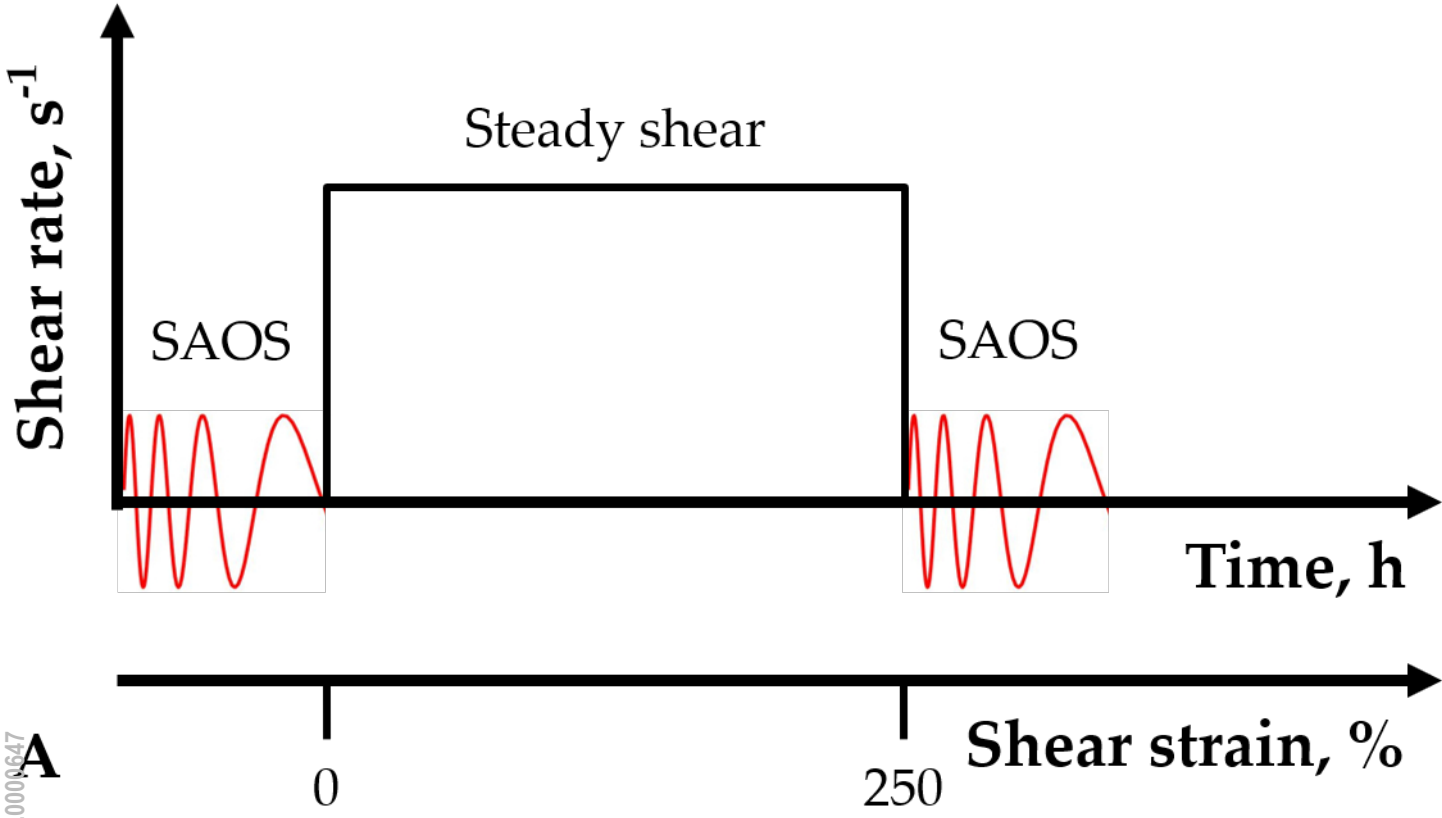
This is the author's peer reviewed, accepted manuscript. However, the online version of record will be different from this version once it has been copyedited and typeset.  
PLEASE CITE THIS ARTICLE AS DOI: 10.1122/1.50000647

46. Helal, E., et al., *Interfacial molecular dynamics of styrenic block copolymer-based nanocomposites with controlled spatial distribution*. Polymer, 2017. **113**: p. 9-26.
47. Liu, X.-Q., et al., *Suppressing phase retraction and coalescence of co-continuous polymer blends: effect of nanoparticles and particle network*. RSC Advances, 2014. **4**(90): p. 49429-49441.
48. Palierne, J., *Linear rheology of viscoelastic emulsions with interfacial tension*. Rheologica acta, 1990. **29**(3): p. 204-214.
49. Gramespacher, H. and J. Meissner, *Interfacial tension between polymer melts measured by shear oscillations of their blends*. Journal of Rheology, 1992. **36**(6): p. 1127-1141.
50. Bousmina, M., *Effect of interfacial tension on linear viscoelastic behavior of immiscible polymer blends*. Rheologica acta, 1999. **38**(3): p. 251-254.
51. Souza, A.M.C.d., P.S. Calvao, and N.R. Demarquette, *Linear viscoelastic behavior of compatibilized PMMA/PP blends*. Journal of applied polymer science, 2013. **129**(3): p. 1280-1289.
52. Omonov, T., et al., *Phase continuity detection and phase inversion phenomena in immiscible polypropylene/polystyrene blends with different viscosity ratios*. Polymer, 2007. **48**(20): p. 5917-5927.
53. Vandebril, S., J. Vermant, and P. Moldenaers, *Efficiently suppressing coalescence in polymer blends using nanoparticles: role of interfacial rheology*. Soft Matter, 2010. **6**(14): p. 3353-3362.
54. Thareja, P., K. Moritz, and S.S. Velankar, *Interfacially active particles in droplet/matrix blends of model immiscible homopolymers: Particles can increase or decrease drop size*. Rheologica acta, 2010. **49**(3): p. 285-298.
55. Thareja, P. and S. Velankar, *Rheology of immiscible blends with particle-induced drop clusters*. Rheologica acta, 2008. **47**(2): p. 189-200.
56. Vermant, J., et al., *Coalescence suppression in model immiscible polymer blends by nano-sized colloidal particles*. Rheologica acta, 2004. **43**(5): p. 529-538.
57. Bose, S., et al., *Phase separation as a tool to control dispersion of multiwall carbon nanotubes in polymeric blends*. ACS applied materials & interfaces, 2010. **2**(3): p. 800-807.
58. Genoyer, J., N.R. Demarquette, and J. Soulestin, *Effect of clay particles size and location on coalescence in PMMA/PS blends*. Journal of Rheology, 2019. **63**(6): p. 883-893.
59. Genoyer, J., J. Soulestin, and N.R. Demarquette, *Influence of the molar masses on compatibilization mechanism induced by two block copolymers in PMMA/PS blends*. Journal of Rheology, 2018. **62**(3): p. 681-693.
60. Veenstra, H., et al., *On the mechanical properties of co-continuous polymer blends: experimental and modelling*. Polymer, 2000. **41**(5): p. 1817-1826.
61. Yu, W., W. Zhou, and C. Zhou, *Linear viscoelasticity of polymer blends with co-continuous morphology*. Polymer, 2010. **51**(9): p. 2091-2098.
62. Kou, Y., et al., *Robust networks of interfacial localized graphene in cocontinuous polymer blends*. Journal of Rheology, 2021. **65**(6): p. 1139-1153.
63. Moghimi, E., F. Goharpey, and R. Foudazi, *Role of droplet bridging on the stability of particle-containing immiscible polymer blends*. Rheologica Acta, 2014. **53**(2): p. 165-180.
64. Zou, Z.-M., Z.-Y. Sun, and L.-J. An, *Effect of fumed silica nanoparticles on the morphology and rheology of immiscible polymer blends*. Rheologica Acta, 2014. **53**(1): p. 43-53.
65. Grace, H.P., *Dispersion phenomena in high viscosity immiscible fluid systems and application of static mixers as dispersion devices in such systems*. Chemical Engineering Communications, 1982. **14**(3-6): p. 225-277.
66. Taylor, G.I., *The viscosity of a fluid containing small drops of another fluid*. Proceedings of the Royal Society of London. Series A, Containing Papers of a Mathematical and Physical Character, 1932. **138**(834): p. 41-48.

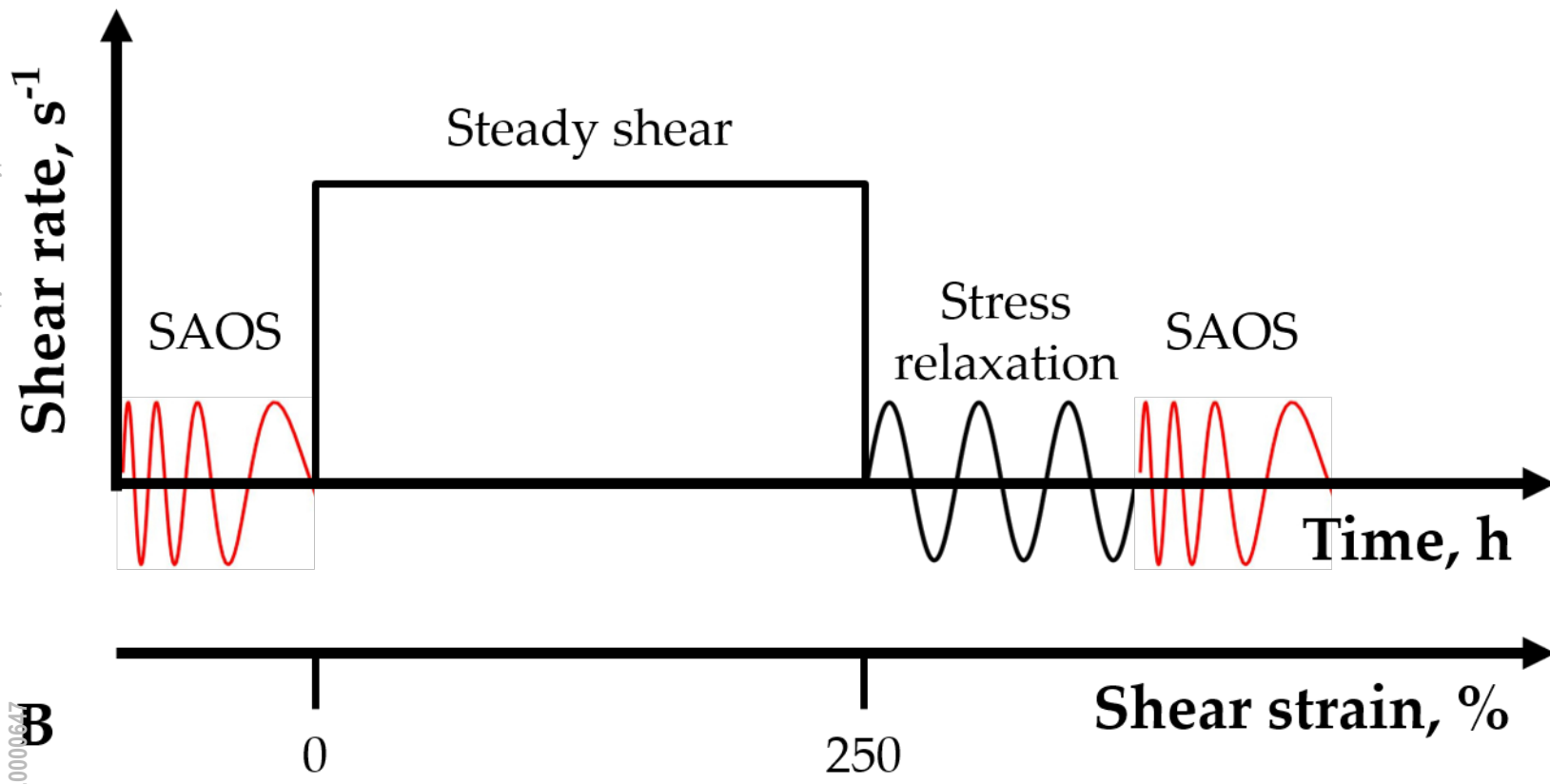
This is the author's peer reviewed, accepted manuscript. However, the online version of record will be different from this version once it has been copyedited and typeset.  
PLEASE CITE THIS ARTICLE AS DOI: 10.1122/1.511111

67. Tucker III, C.L. and P. Moldenaers, *Microstructural evolution in polymer blends*. Annual Review of Fluid Mechanics, 2002. **34**: p. 177.
68. Bird, R.B., R.C. Armstrong, and O. Hassager, *Dynamics of polymeric liquids. Vol. 1: Fluid mechanics*. 1987.
69. Carreau, P.J., D.C. De Kee, and R.P. Chhabra, *Rheology of polymeric systems: principles and applications*. 2021: Carl Hanser Verlag GmbH Co KG.
70. Chen, J., et al., *Combined effect of compatibilizer and carbon nanotubes on the morphology and electrical conductivity of PP/PS blend*. Polymers for advanced technologies, 2014. **25**(6): p. 624-630.
71. Vinckier, I., et al., *Droplet size evolution during coalescence in semiconcentrated model blends*. AIChE journal, 1998. **44**(4): p. 951-958.
72. Nofar, M., et al., *Interfacial and rheological properties of PLA/PBAT and PLA/PBSA blends and their morphological stability under shear flow*. Journal of Rheology, 2015. **59**(2): p. 317-333.
73. Nofar, M., et al., *Coalescence in PLA-PBAT blends under shear flow: Effects of blend preparation and PLA molecular weight*. Journal of Rheology, 2016. **60**(4): p. 637-648.
74. Zhu, X., et al., *Selective distribution of nanoparticles in immiscible blends: Effects on the morphology evolution and rheology in quiescent annealing, shear and extensional flow*. Journal of Rheology, 2020. **64**(6): p. 1357-1371.
75. Jordan, A.M., et al., *Rheology of polymer multilayers: Slip in shear, hardening in extension*. Journal of Rheology, 2019. **63**(5): p. 751-761.
76. Bharati, A., et al., *Tuning the phase separated morphology and resulting electrical conductivity of carbon nanotube filled PαMSAN/PMMA blends by compatibilization with a random or block copolymer*. Polymer, 2017. **108**: p. 483-492.
77. Alig, I., et al., *Destruction and formation of a carbon nanotube network in polymer melts: Rheology and conductivity spectroscopy*. Polymer, 2008. **49**(16): p. 3524-3532.
78. Skipa, T., et al., *Influence of shear deformation on carbon nanotube networks in polycarbonate melts: Interplay between build-up and destruction of agglomerates*. Polymer, 2010. **51**(1): p. 201-210.
79. Pan, Y., et al., *Conductivity and phase morphology of carbon black-filled immiscible polymer blends under creep: An experimental and theoretical study*. Physical Chemistry Chemical Physics, 2016. **18**(47): p. 32125-32131.
80. Salehiyan, R., et al., *Shear-induced carbon nanotube migration and morphological development in polylactide/poly (vinylidene fluoride) blend nanocomposites and their impact on dielectric constants and rheological properties*. The Journal of Physical Chemistry C, 2020. **124**(17): p. 9536-9547.
81. Macaubas, P. and N. Demarquette, *Morphologies and interfacial tensions of immiscible polypropylene/polystyrene blends modified with triblock copolymers*. Polymer, 2001. **42**(6): p. 2543-2554.
82. Macosko, C., *Rheology principles, measurements, and applications*, VCH Publ. Inc, New York, 1994.
83. Filippone, G. and M. Salzano de Luna, *A unifying approach for the linear viscoelasticity of polymer nanocomposites*. Macromolecules, 2012. **45**(21): p. 8853-8860.
84. Alig, I., et al., *Establishment, morphology and properties of carbon nanotube networks in polymer melts*. Polymer, 2012. **53**(1): p. 4-28.

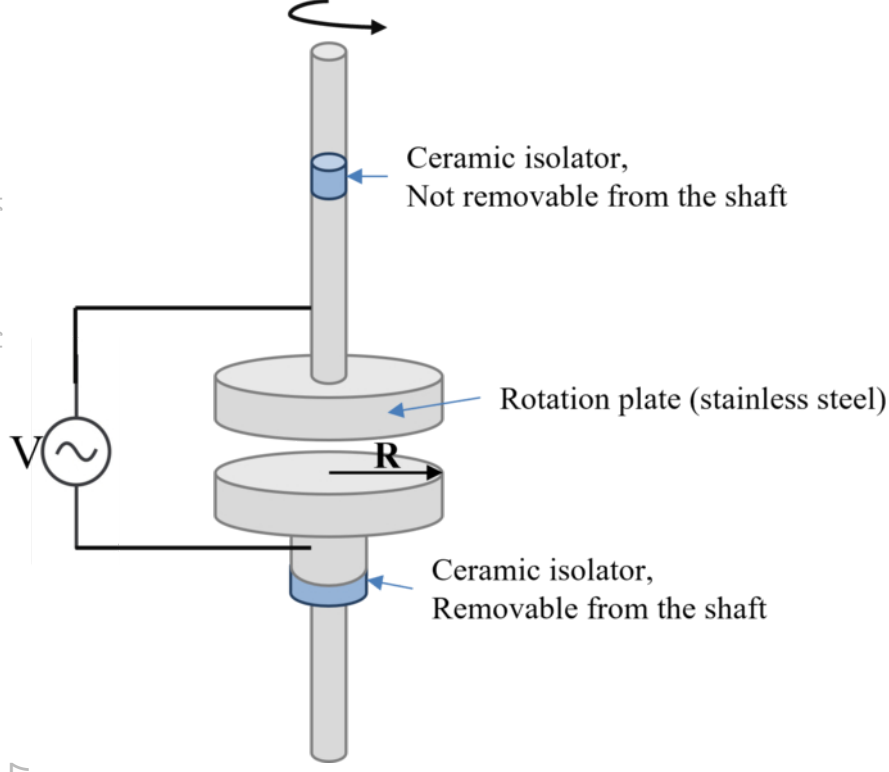
This is the author's peer reviewed, accepted manuscript. However, the online version of record will be different from this version once it has been copyedited and typeset.  
PLEASE CITE THIS ARTICLE AS DOI: 10.1122/1.50000647



This is the author's peer reviewed, accepted manuscript. However, the online version of record will be different from this version once it has been copyedited and typeset.  
PLEASE CITE THIS ARTICLE AS DOI: 10.1122/1.5000064

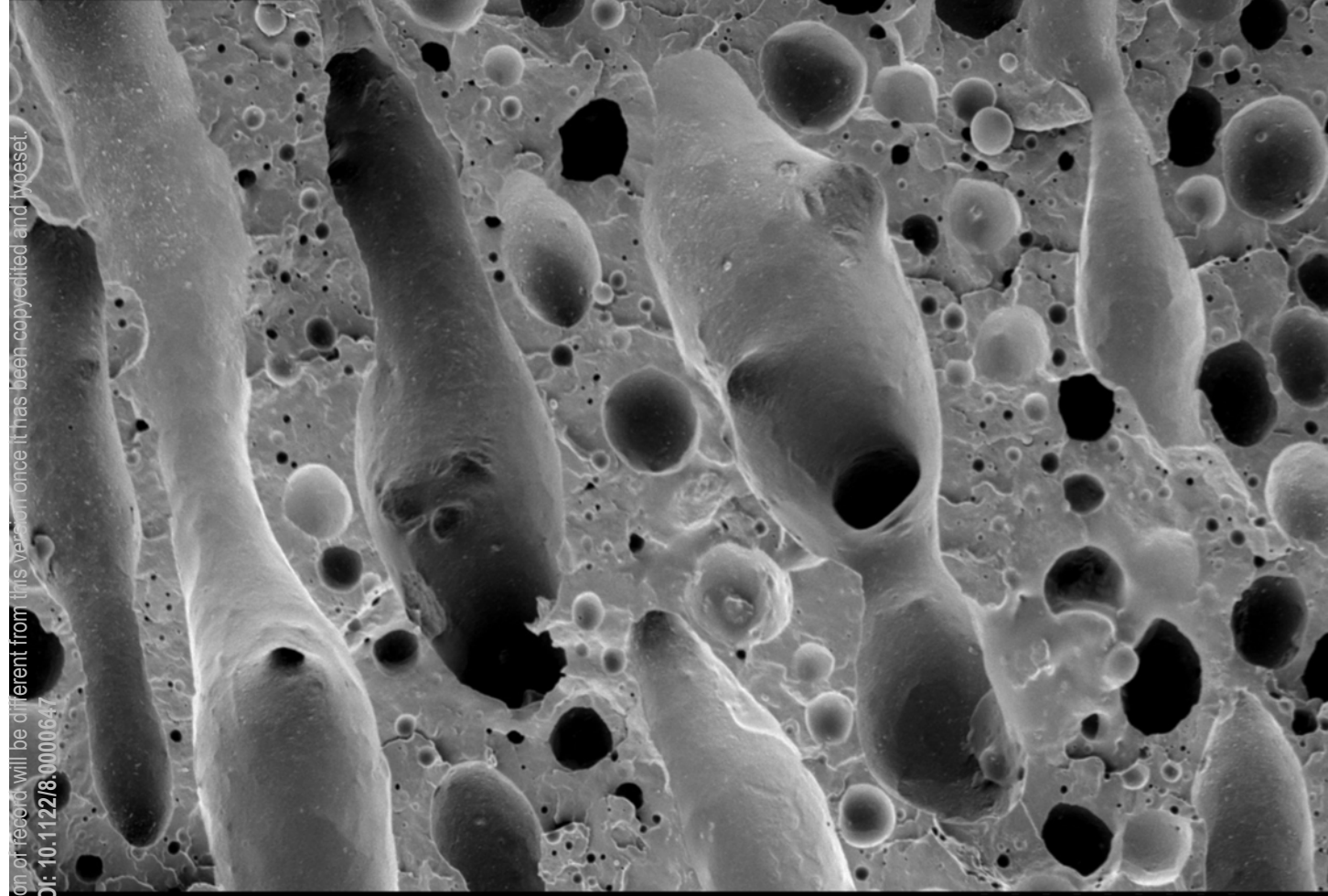


This is the author's peer reviewed, accepted manuscript. However, the online version of record will be different from this version once it has been copyedited and typeset.  
PLEASE CITE THIS ARTICLE AS DOI: 10.1122/8.0000647





This is the author's peer reviewed, accepted manuscript. However, the online version of record will be different from this version once it has been copyedited and typeset.  
PLEASE CITE THIS ARTICLE AS DOI: 10.1122/1.50000647

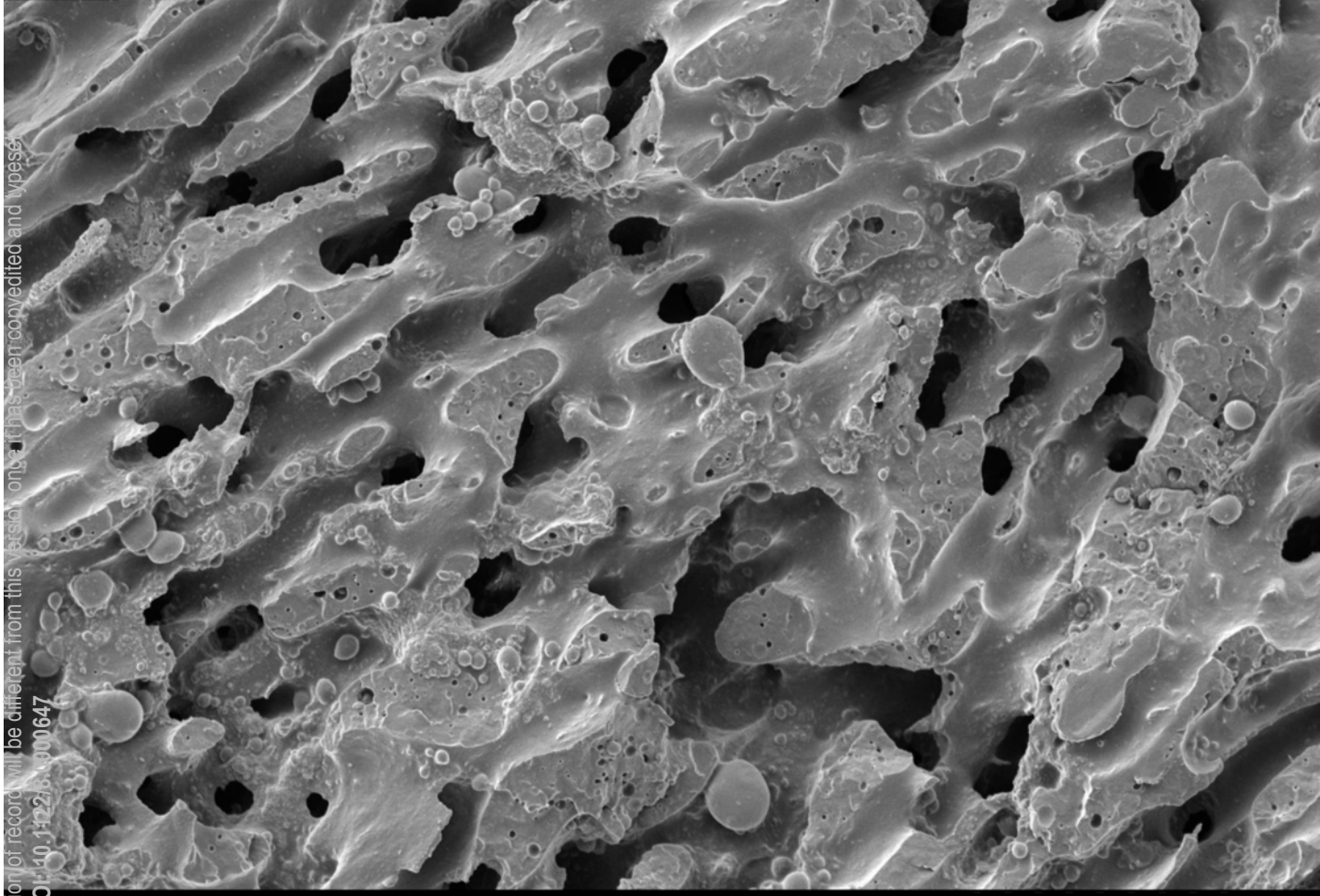


A

100  $\mu\text{m}$

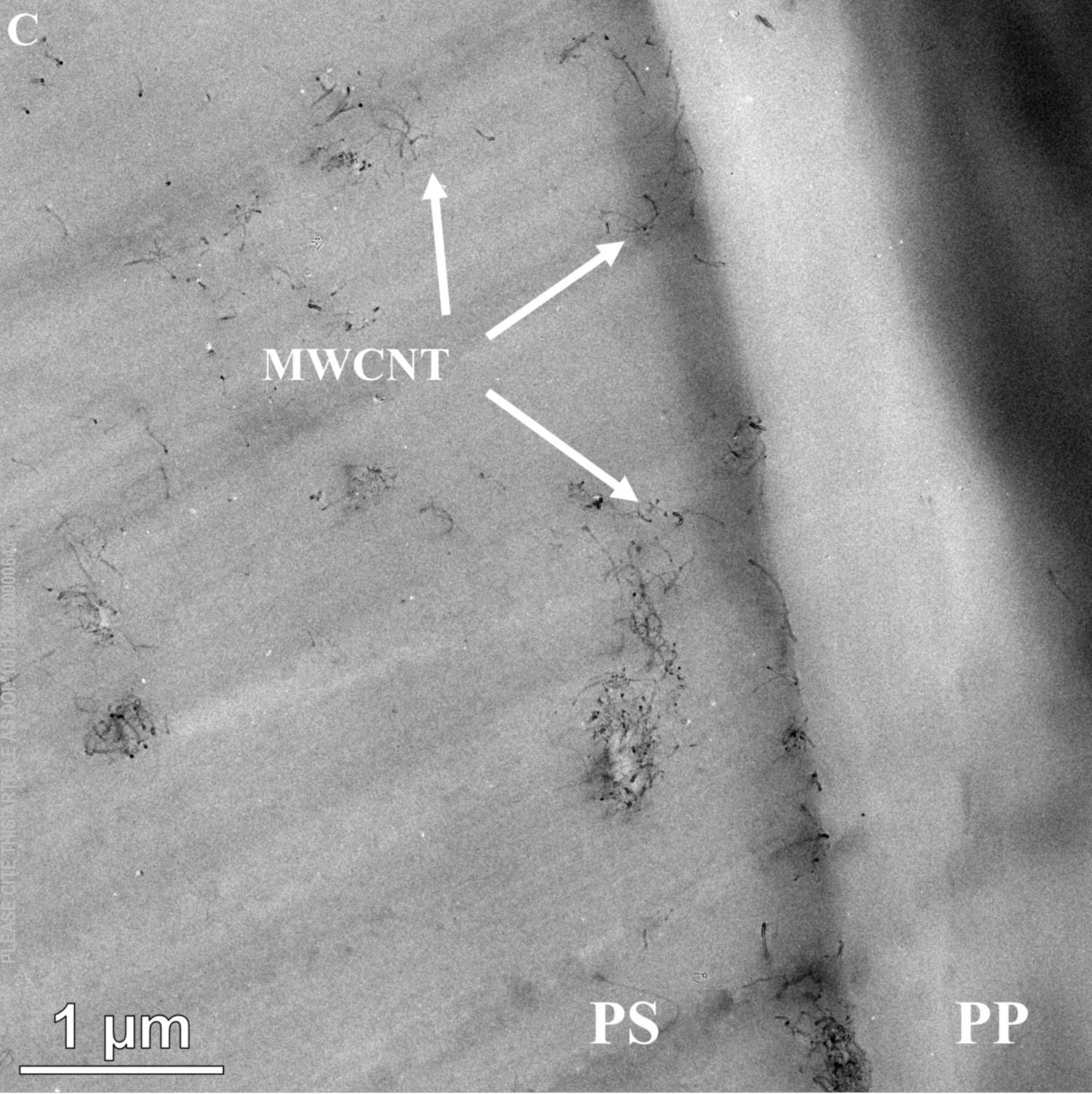
This is the author's peer reviewed, accepted manuscript. However, the online version of record will be different from this version once it has been copyedited and typeset.  
PLEASE CITE THIS ARTICLE AS DOI:10.1122/j.1400-0479.2016.000647

**B**

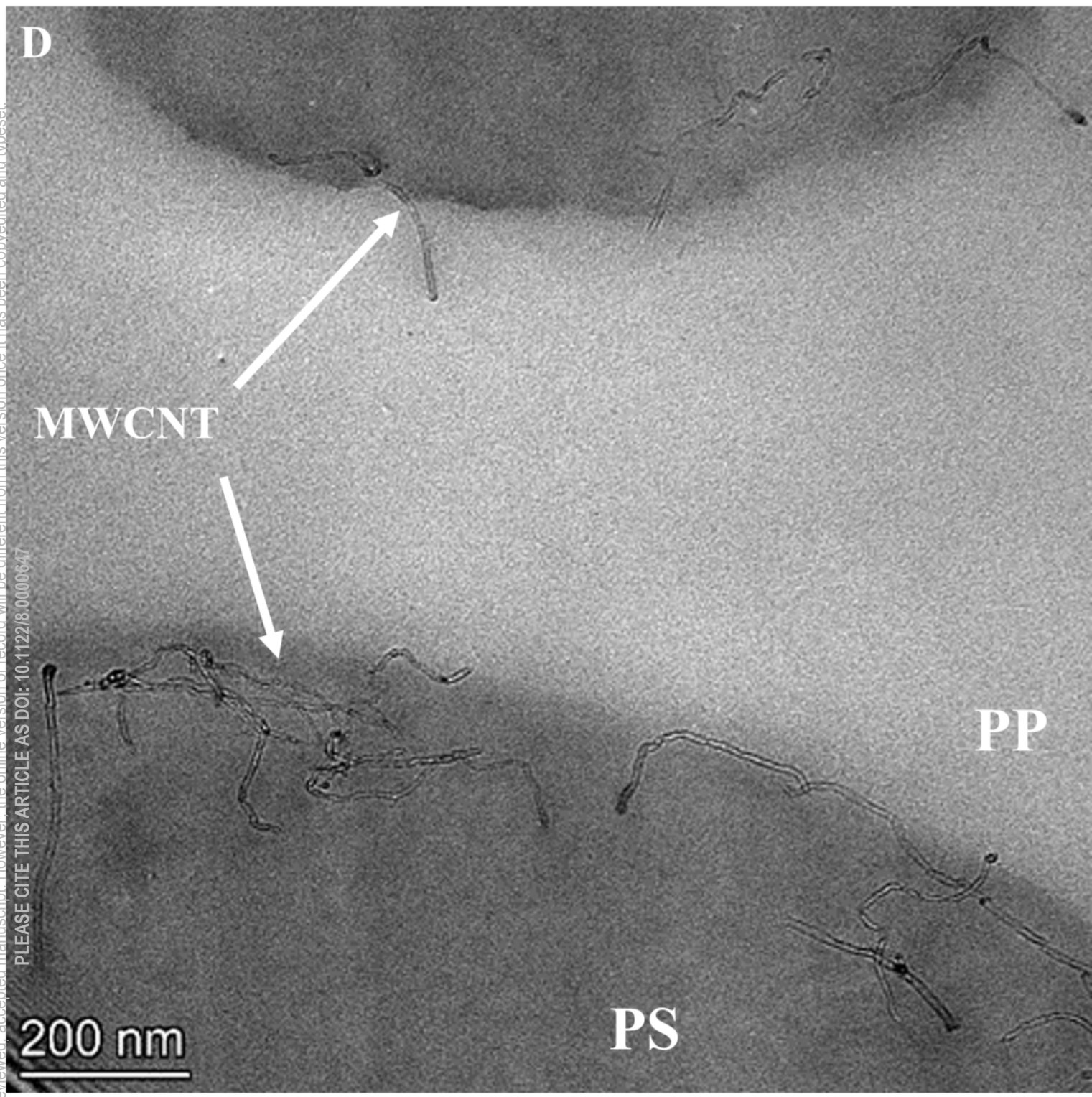


100  $\mu\text{m}$

This is the author's peer reviewed, accepted manuscript. However, the online version of record will be different from this version once it has been copyedited and typeset.  
PLEASE CITE THIS ARTICLE AS DOI: 10.1122/1.5000064

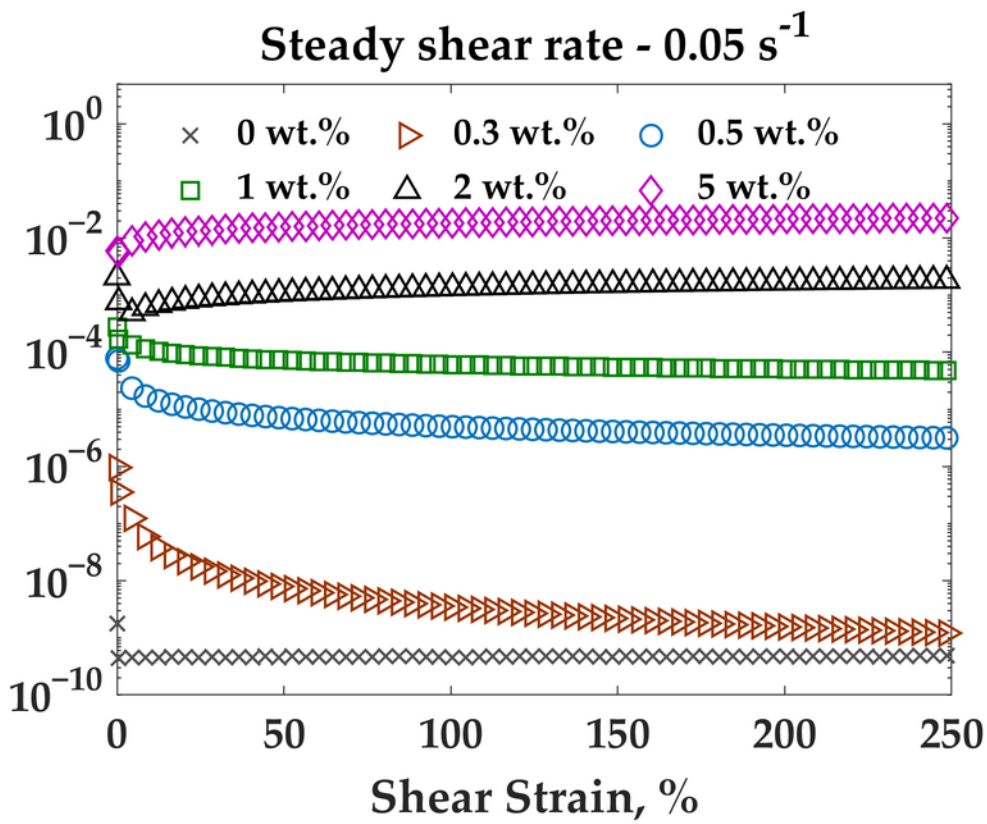


This is the author's peer reviewed, accepted manuscript. However, the online version of record will be different from this version once it has been copyedited and typeset.  
PLEASE CITE THIS ARTICLE AS DOI: 10.1122/8.00000647



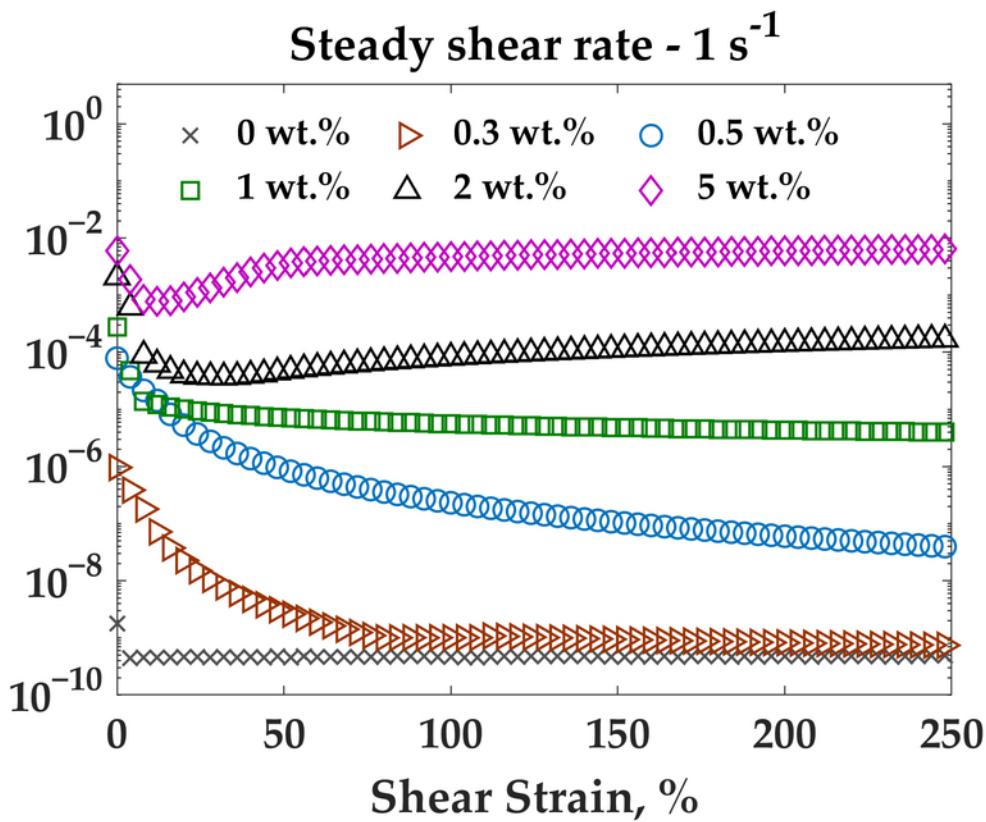
This is the author's peer reviewed, accepted manuscript. However, the online version of record will be different from this version once it has been copyedited and typeset.  
PLEASE CITE THIS ARTICLE AS DOI: 10.1122/1.506647

Electrical Conductivity, S/m



This is the author's peer reviewed, accepted manuscript. However, the online version of record will be different from this version once it has been copyedited and typeset.  
 PLEASE CITE THIS ARTICLE AS DOI: 10.1122/1.5006647

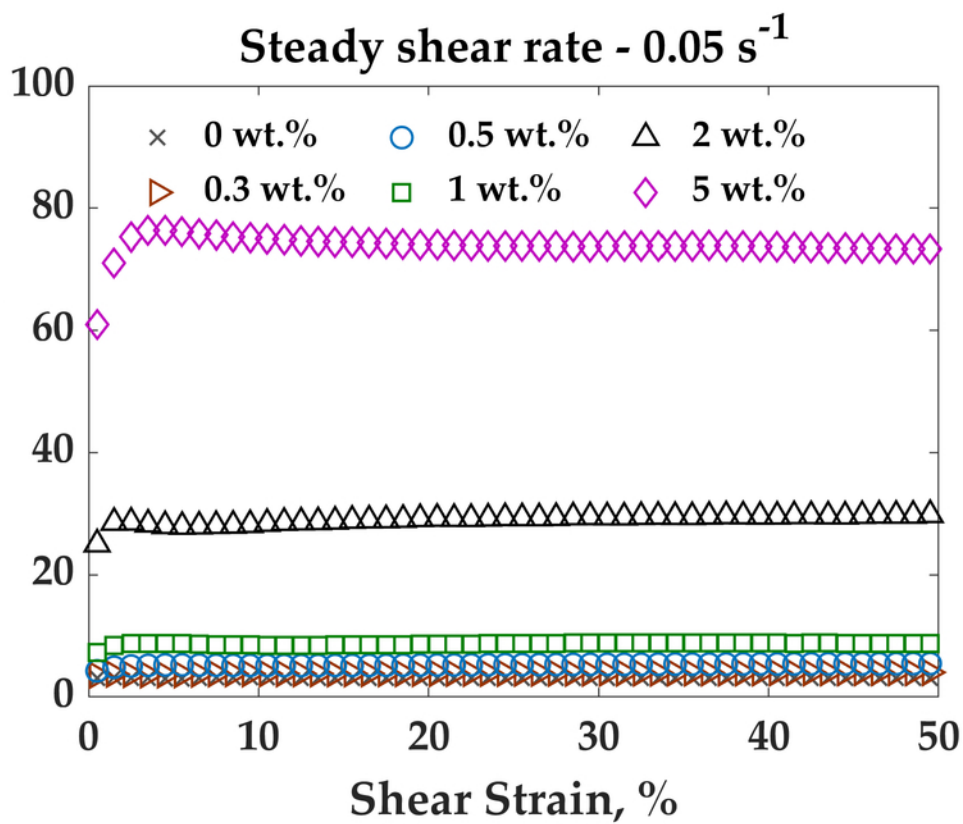
Electrical Conductivity, S/m



This is the author's peer reviewed, accepted manuscript. However, the online version of record will be different from this version once it has been copyedited and typeset.

PLEASE CITE THIS ARTICLE AS DOI: 10.1122/8.00000647

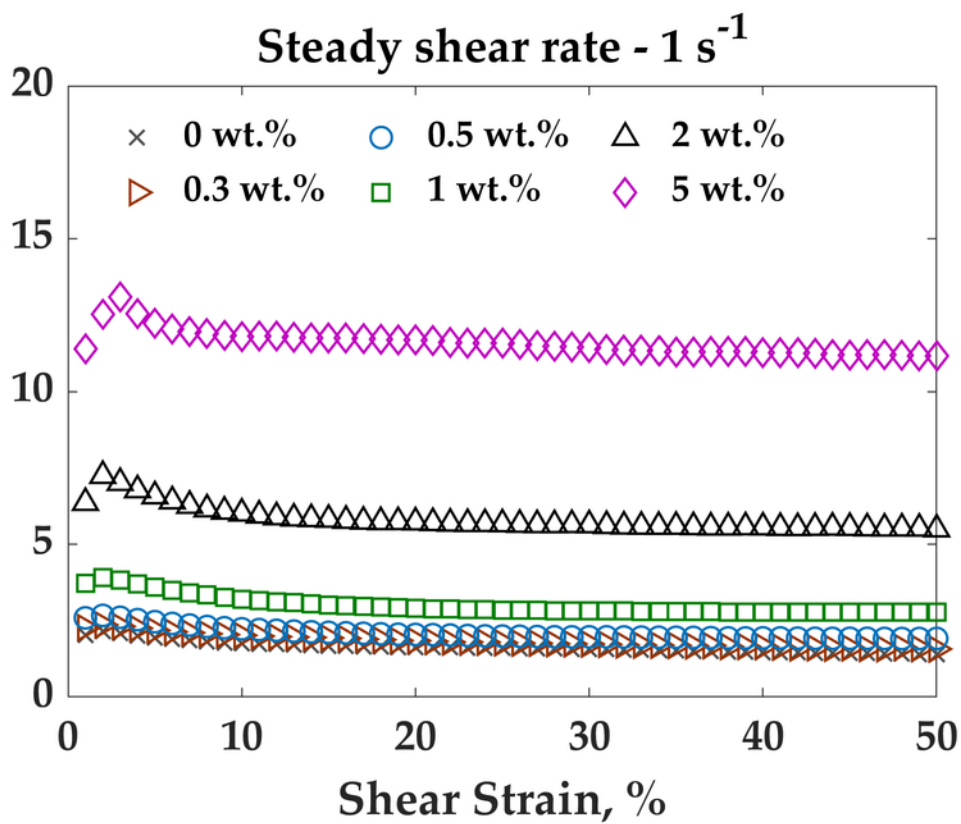
Transient Viscosity,  $10^3$  Pa.s



This is the author's peer reviewed, accepted manuscript. However, the online version of record will be different from this version once it has been copyedited and typeset.

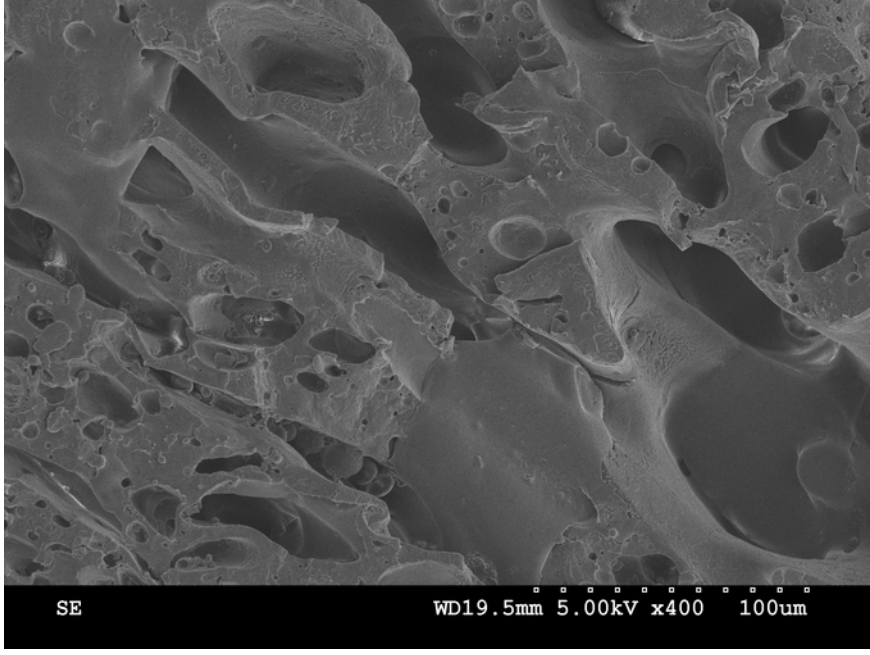
PLEASE CITE THIS ARTICLE AS DOI: 10.1122/8.00000000000000000000000000000000

Transient Viscosity,  $10^3$  Pa.s

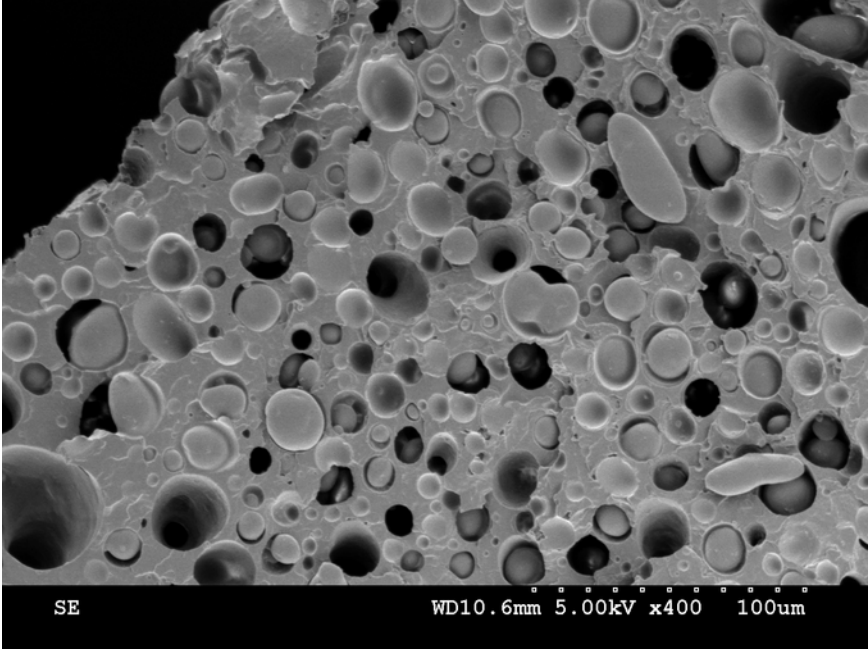




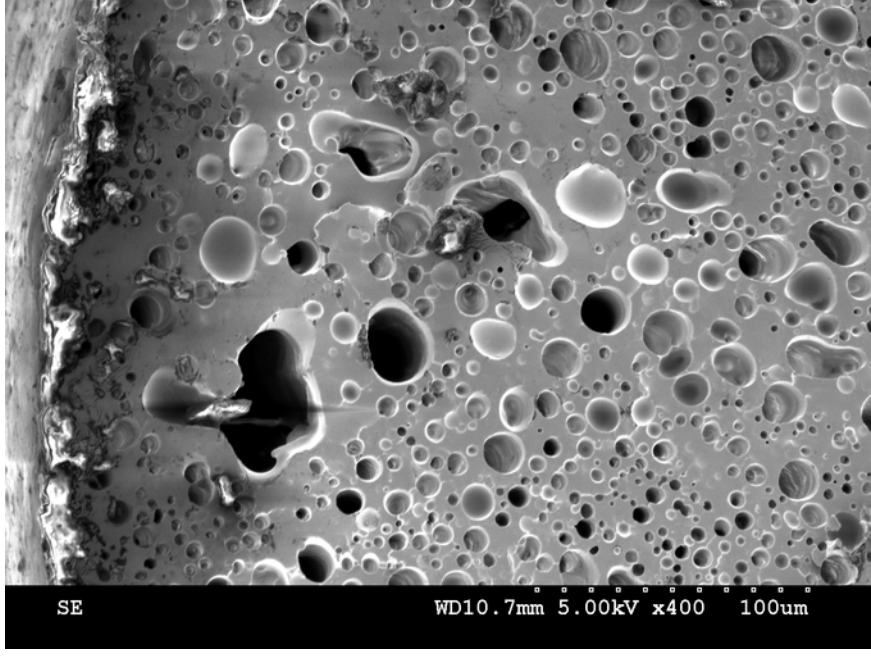
This is the author's peer reviewed, accepted manuscript. However, the online version of record will be different from this version once it has been copyedited and typeset.  
PLEASE CITE THIS ARTICLE AS DOI: 10.1122/8.0000647



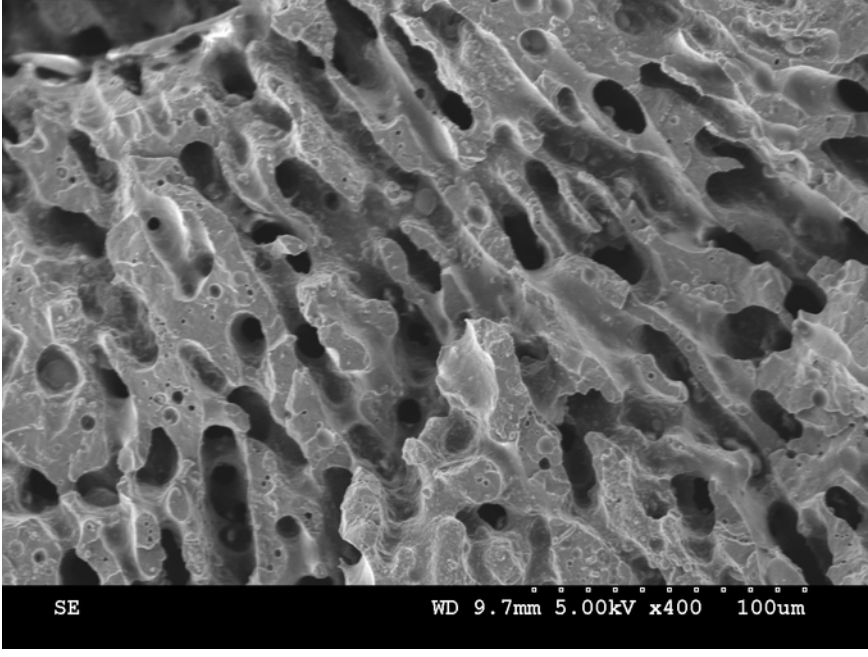
This is the author's peer reviewed, accepted manuscript. However, the online version of record will be different from this version once it has been copyedited and typeset.  
PLEASE CITE THIS ARTICLE AS DOI: 10.1122/8.0000647



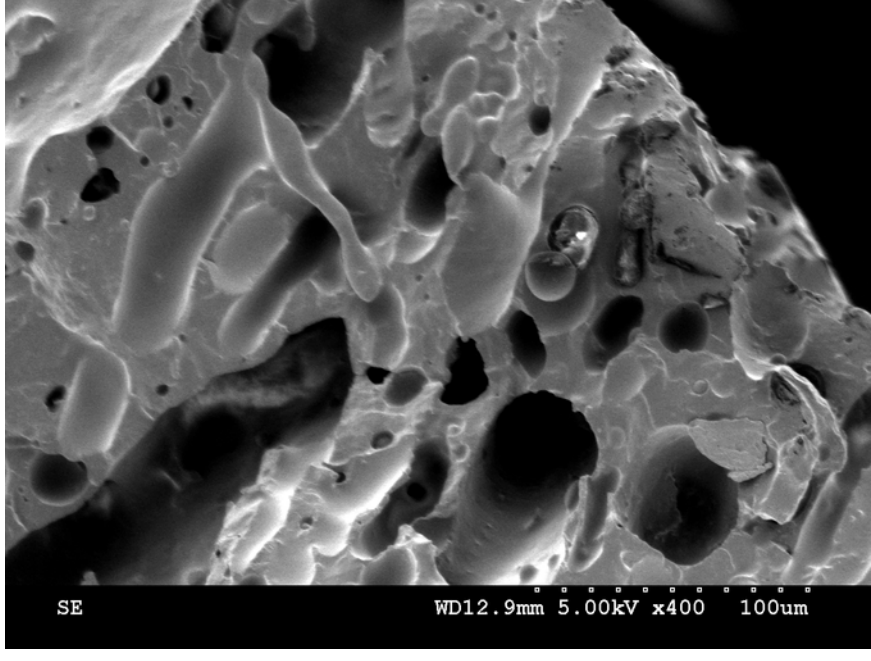
This is the author's peer reviewed, accepted manuscript. However, the online version of record will be different from this version once it has been copyedited and typeset.  
PLEASE CITE THIS ARTICLE AS DOI: 10.1122/8.0000647



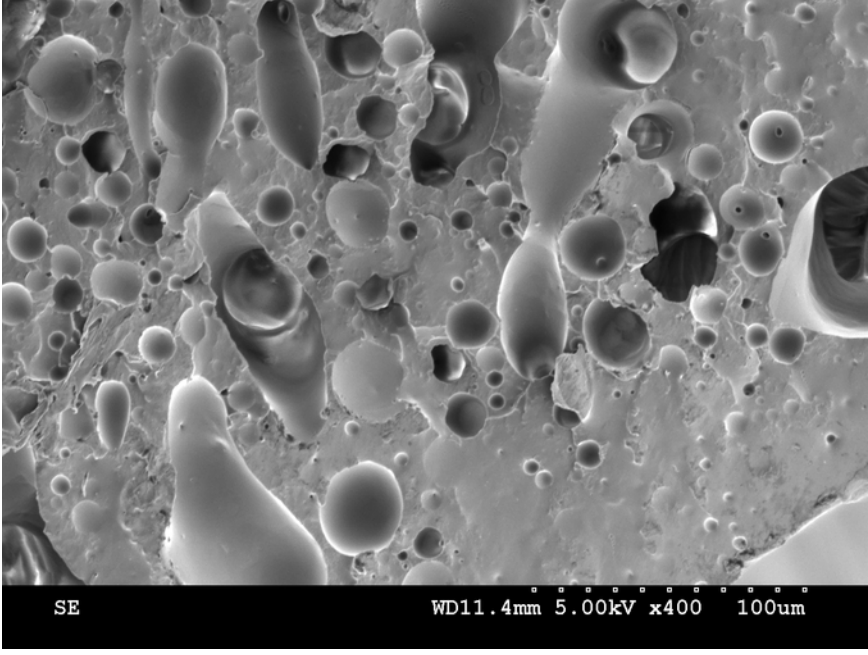
This is the author's peer reviewed, accepted manuscript. However, the online version of record will be different from this version once it has been copyedited and typeset.  
PLEASE CITE THIS ARTICLE AS DOI: 10.1122/8.0000647



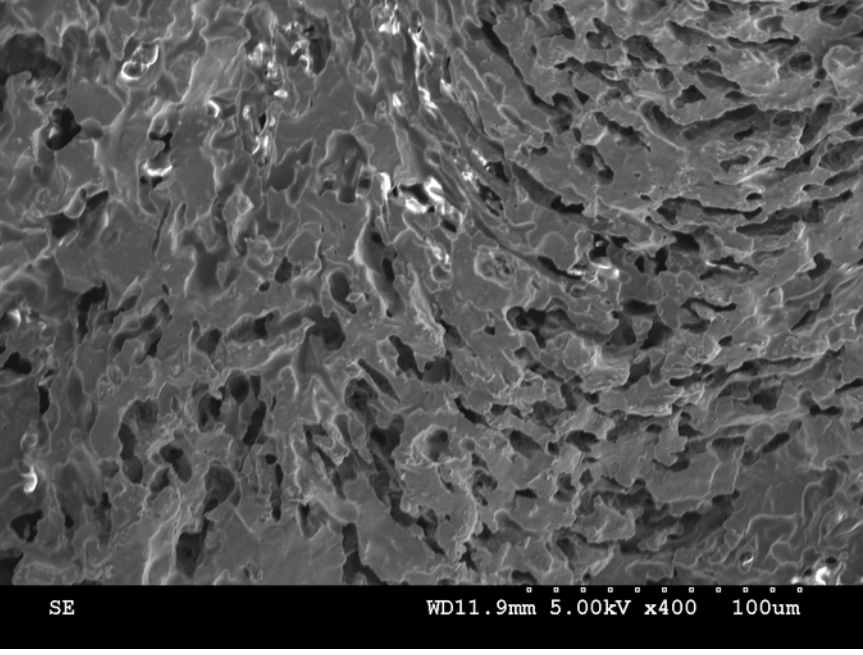
This is the author's peer reviewed, accepted manuscript. However, the online version of record will be different from this version once it has been copyedited and typeset.  
PLEASE CITE THIS ARTICLE AS DOI: 10.1122/8.0000647



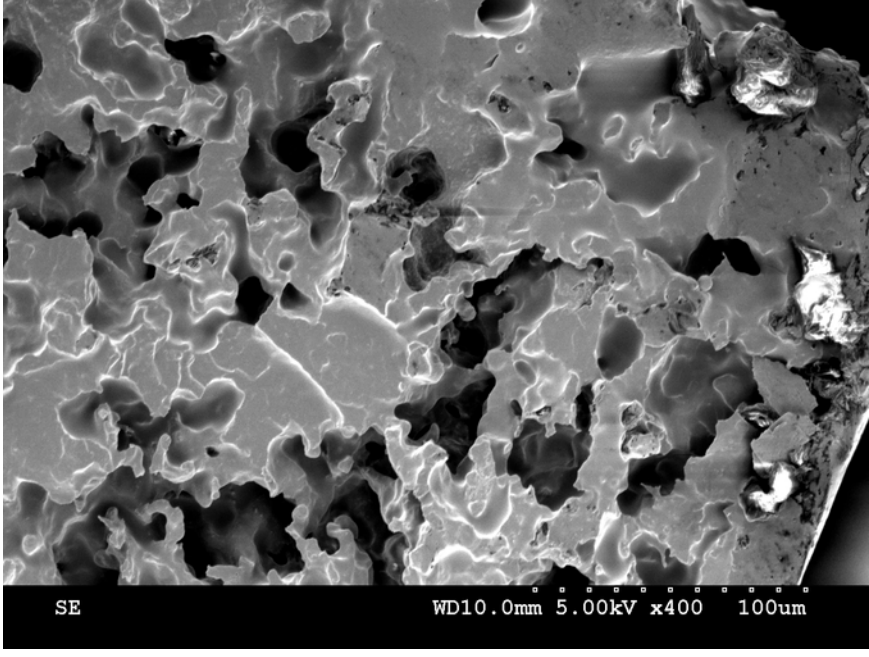
This is the author's peer reviewed, accepted manuscript. However, the online version of record will be different from this version once it has been copyedited and typeset.  
PLEASE CITE THIS ARTICLE AS DOI: 10.1122/8.0000647



This is the author's peer reviewed, accepted manuscript. However, the online version of record will be different from this version once it has been copyedited and typeset.  
PLEASE CITE THIS ARTICLE AS DOI: 10.1122/8.0000647

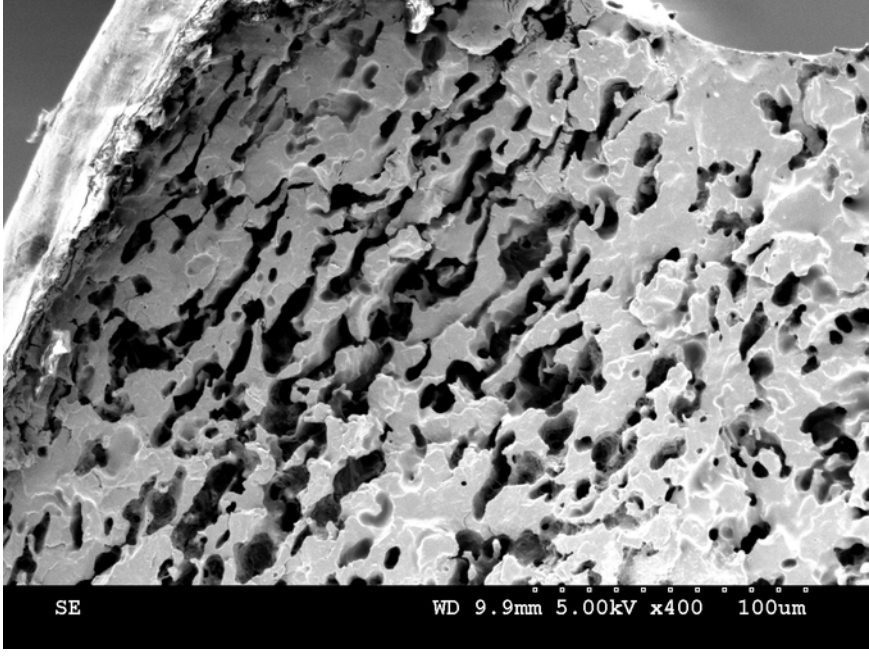


This is the author's peer reviewed, accepted manuscript. However, the online version of record will be different from this version once it has been copyedited and typeset.  
PLEASE CITE THIS ARTICLE AS DOI: 10.1122/8.0000647



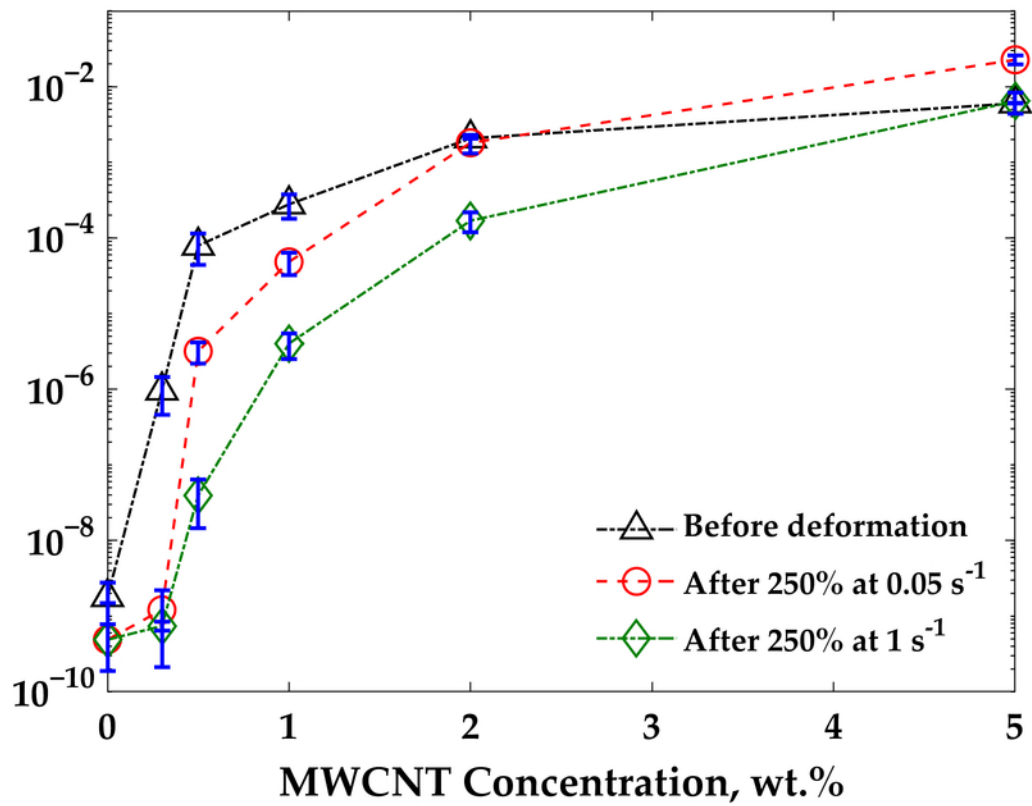


This is the author's peer reviewed, accepted manuscript. However, the online version of record will be different from this version once it has been copyedited and typeset.  
PLEASE CITE THIS ARTICLE AS DOI: 10.1122/8.0000647



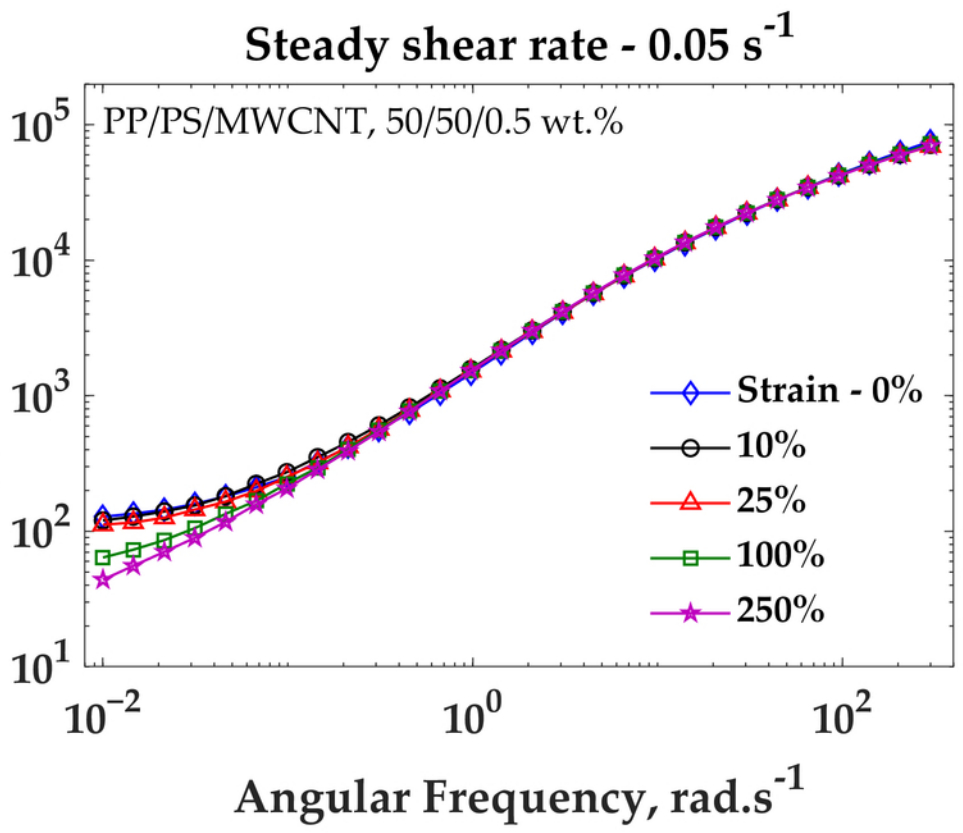
This is the author's peer reviewed, accepted manuscript. However, the online version of record will be different from this version once it has been copyedited and typeset.  
PLEASE CITE THIS ARTICLE AS DOI: 10.1122/8.0000647

Electrical Conductivity, S/m



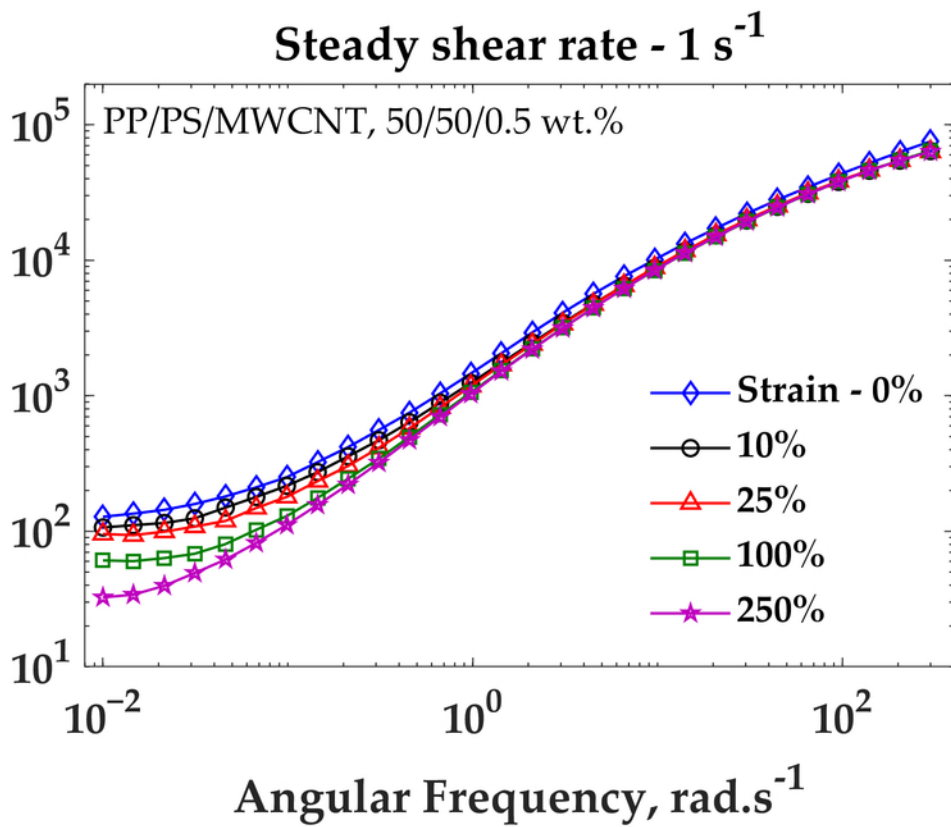
This is the author's peer reviewed, accepted manuscript. However, the online version of record will be different from this version once it has been copyedited and typeset.  
 PLEASE CITE THIS ARTICLE AS DOI: 10.1122/1.5116647

Storage Modulus, Pa



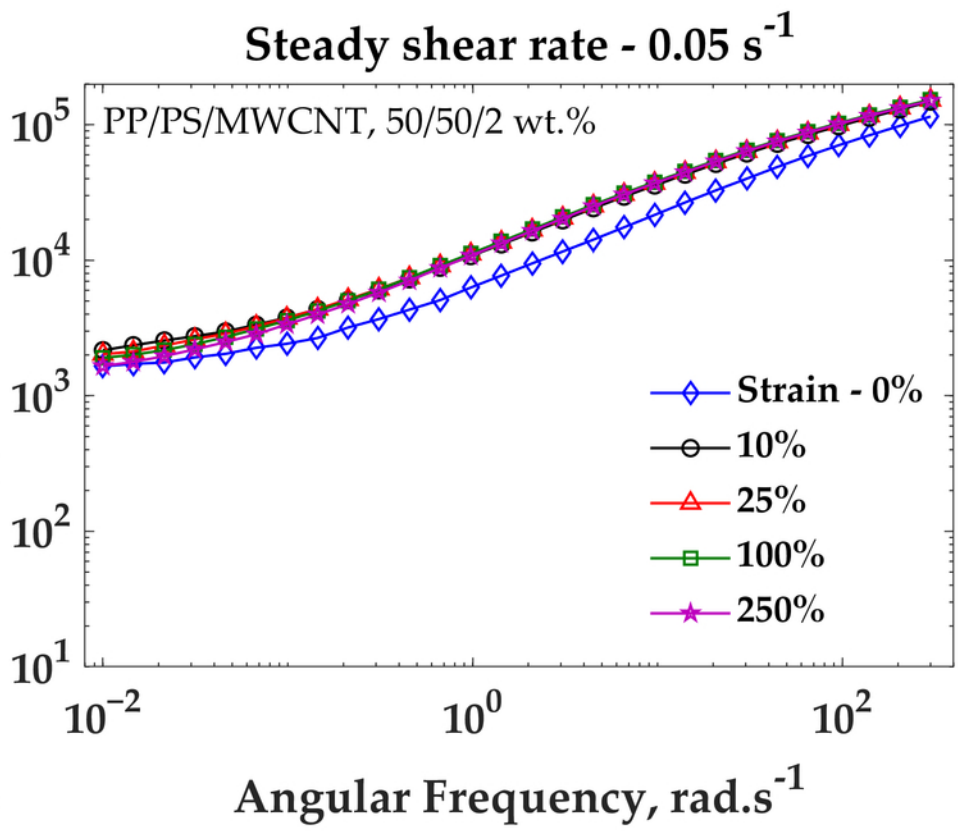
This is the author's peer reviewed, accepted manuscript. However, the online version of record will be different from this version once it has been copyedited and typeset.  
PLEASE CITE THIS ARTICLE AS DOI: 10.1122/1.5000000

Storage Modulus, Pa



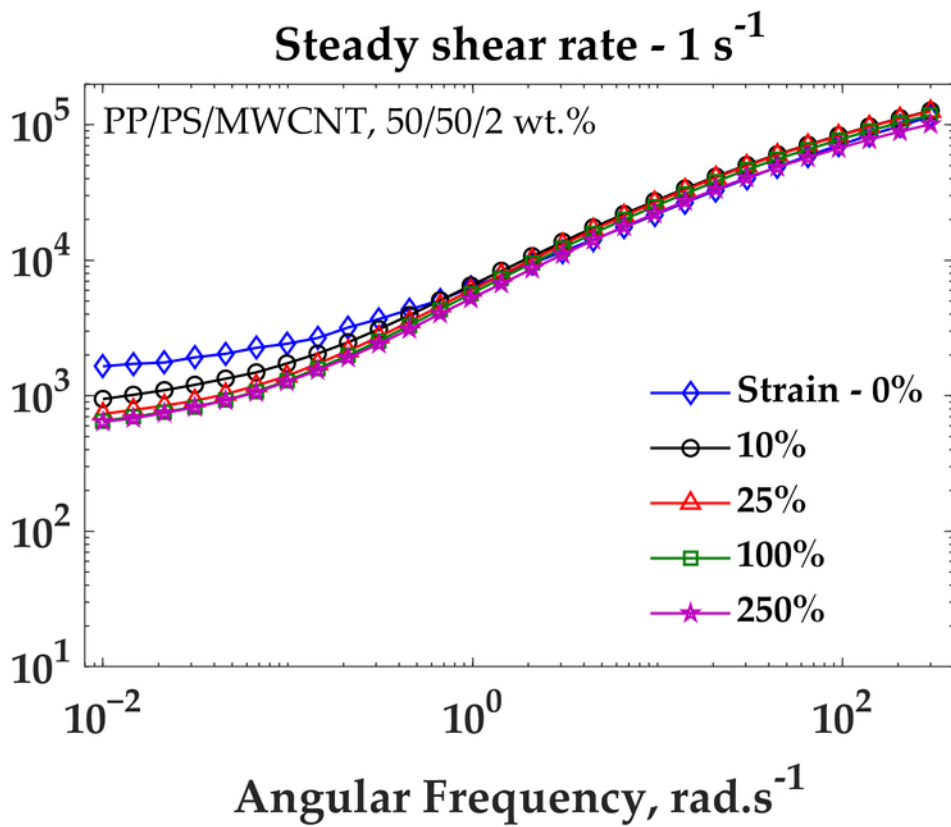
This is the author's peer reviewed, accepted manuscript. However, the online version of record will be different from this version once it has been corrected and typeset.  
 PLEASE CITE THIS ARTICLE AS DOI: 10.1122/1.5000064

Storage Modulus, Pa



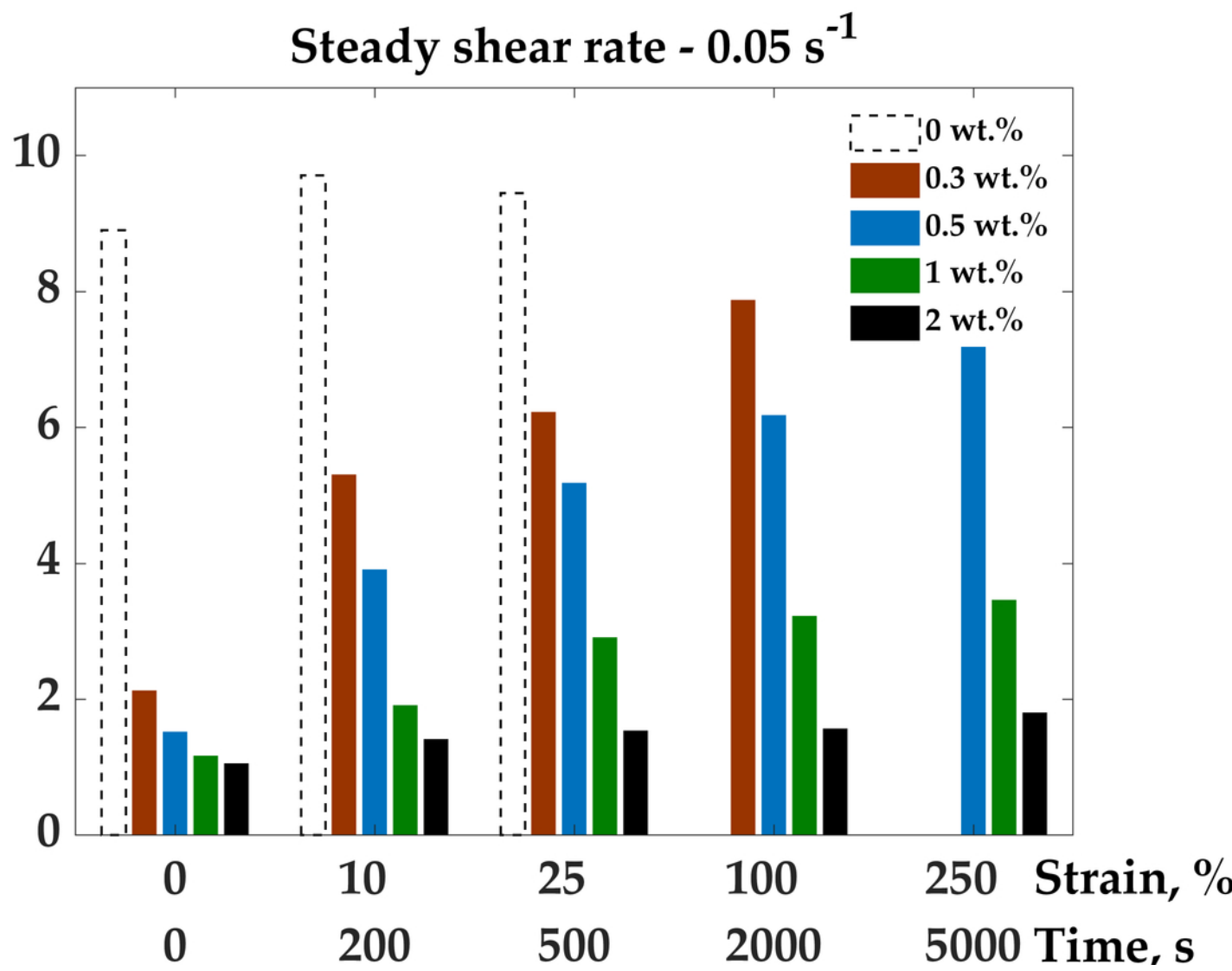
This is the author's peer reviewed, accepted manuscript. However, the online version of record will be different from this version once it has been corrected and typeset. PLEASE CITE THIS ARTICLE AS DOI: 10.1122/1.5116647

Storage Modulus, Pa



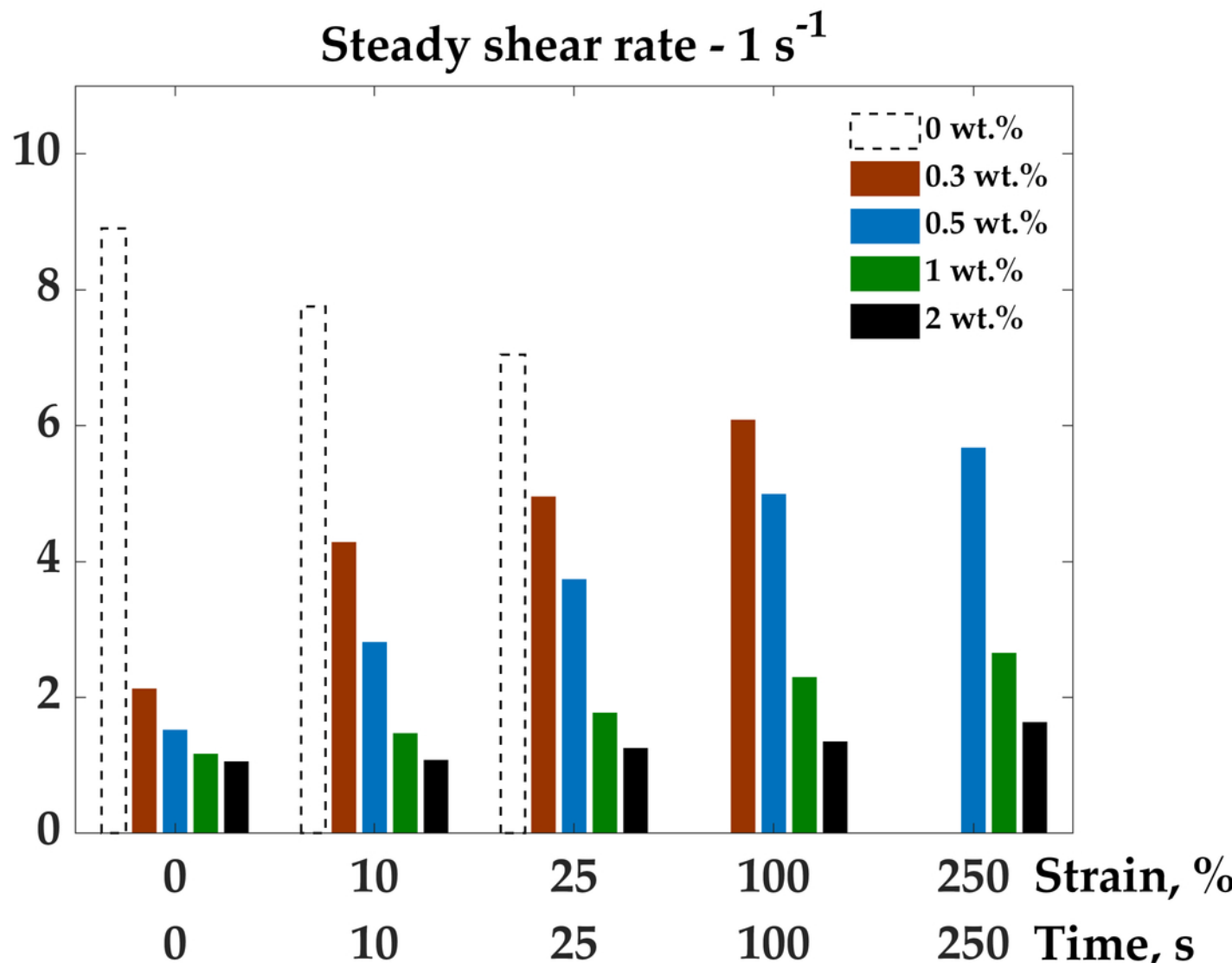
This is the author's peer reviewed, accepted manuscript. However, the online version of record will be different from this version once it has been copyedited and typeset.  
PLEASE CITE THIS ARTICLE AS DOI: 10.1122/8.0000647

**Domain Size,  $\mu\text{m}$**



This is the author's peer reviewed, accepted manuscript. However, the online version of record will be different from this version once it has been copyedited and typeset.  
 PLEASE CITE THIS ARTICLE AS DOI: 10.1122/8.0000647

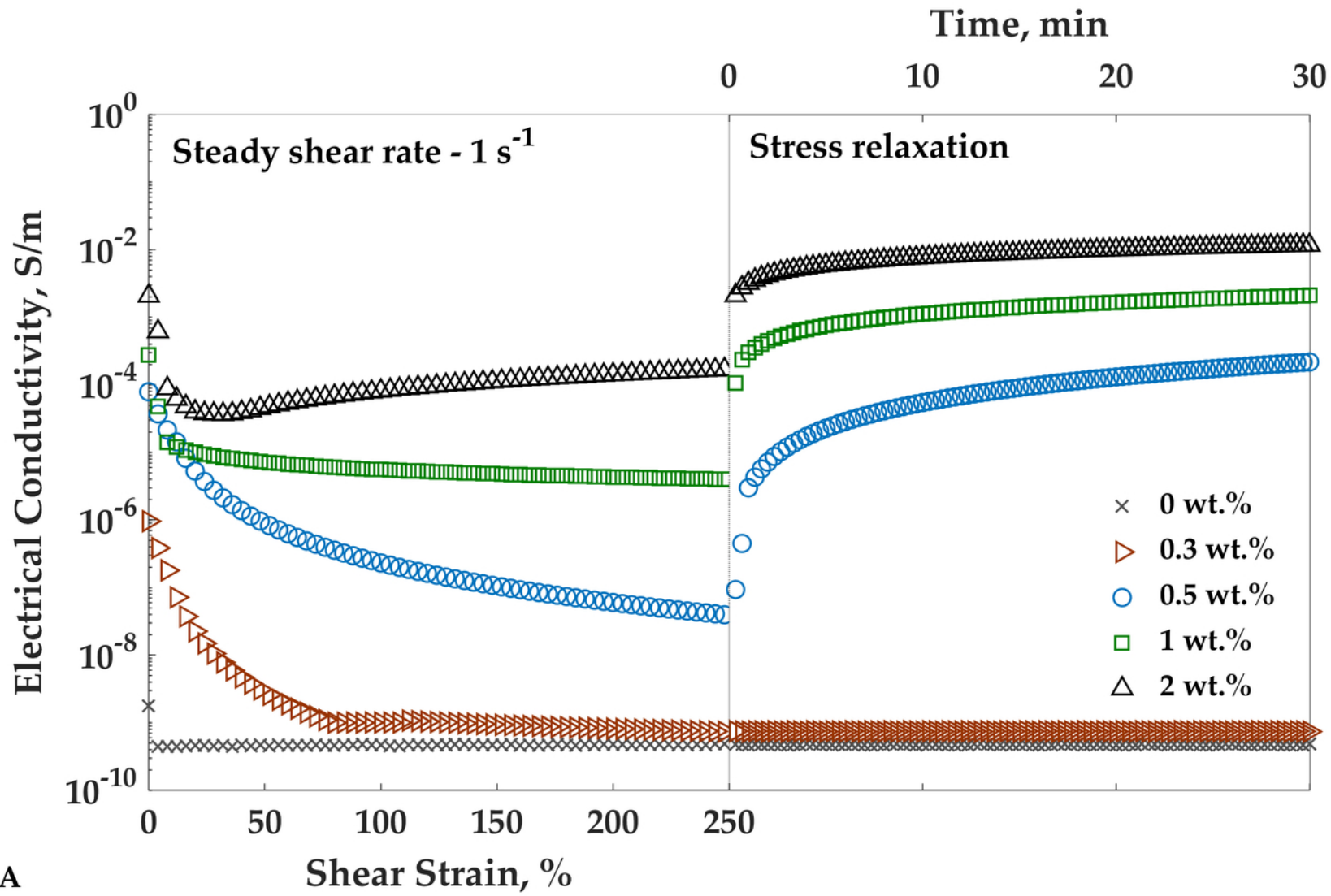
**Domain Size,  $\mu\text{m}$**





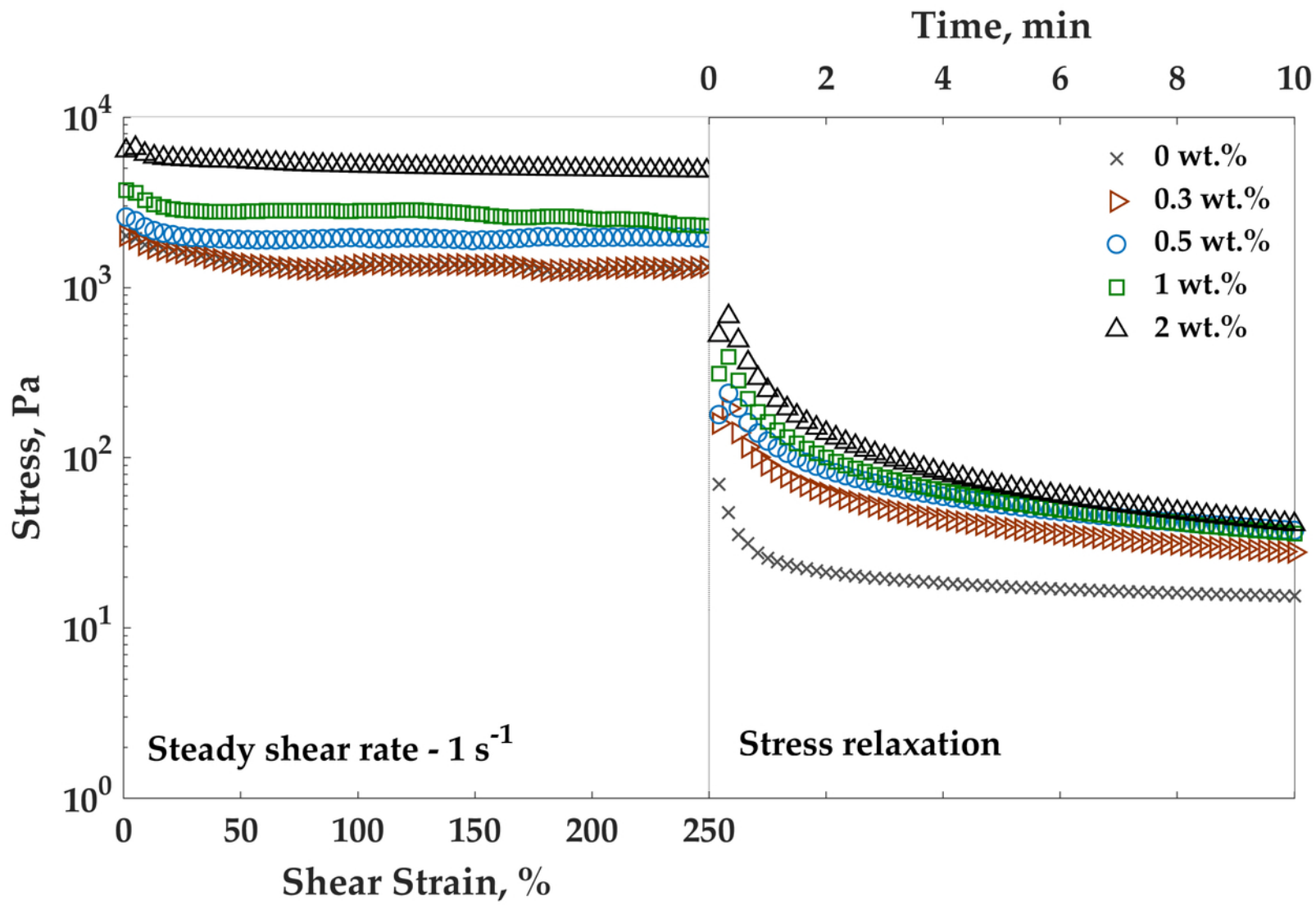
This is the author's peer reviewed, accepted manuscript. However, the online version of record will be different from this version once it has been copyedited and typeset.  
PLEASE CITE THIS ARTICLE AS DOI: 10.1122/8.0000647

A

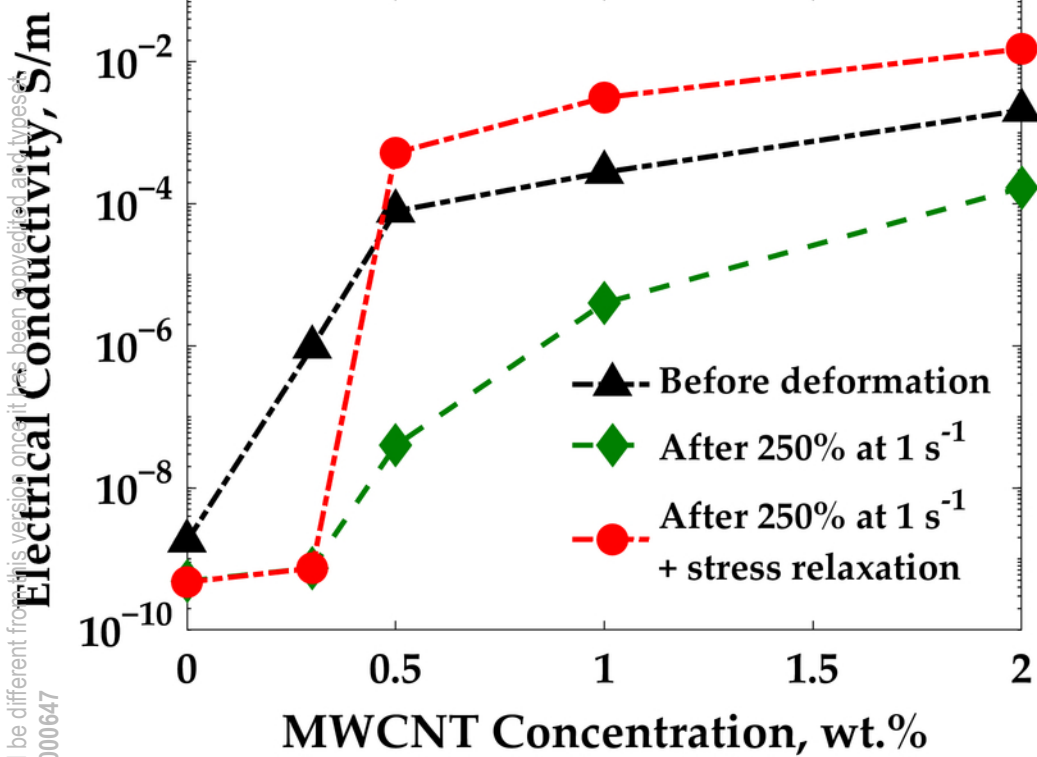


This is the author's peer reviewed, accepted manuscript. However, the online version of record will be different from this version once it has been copyedited and typeset.  
 PLEASE CITE THIS ARTICLE AS DOI: 10.1122/1.50000647

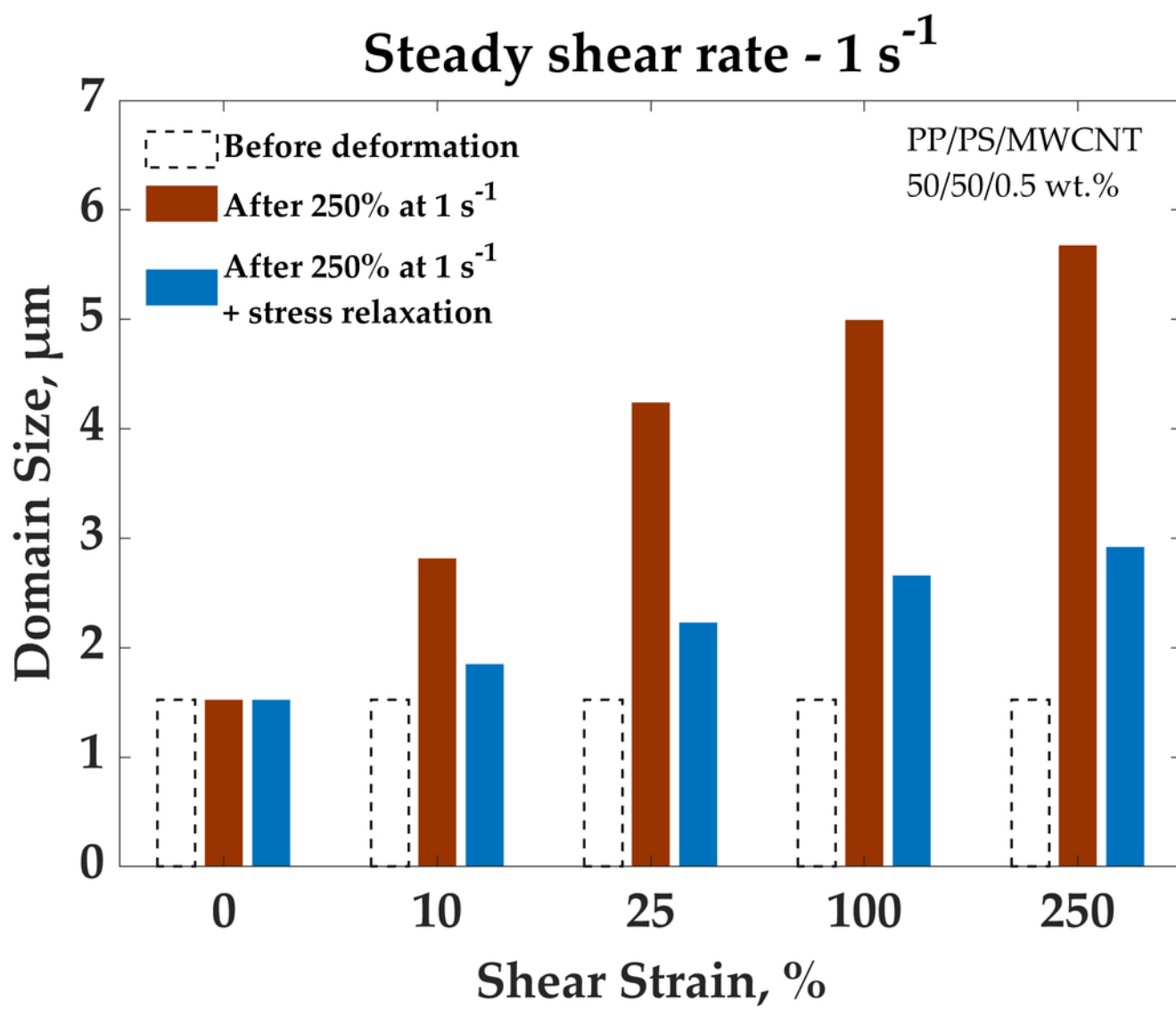
**B**



This is the author's peer reviewed, accepted manuscript. However, the online version of record will be different from this version once it has been copyedited and typeset.  
 PLEASE CITE THIS ARTICLE AS DOI: 10.1122/8.0000647

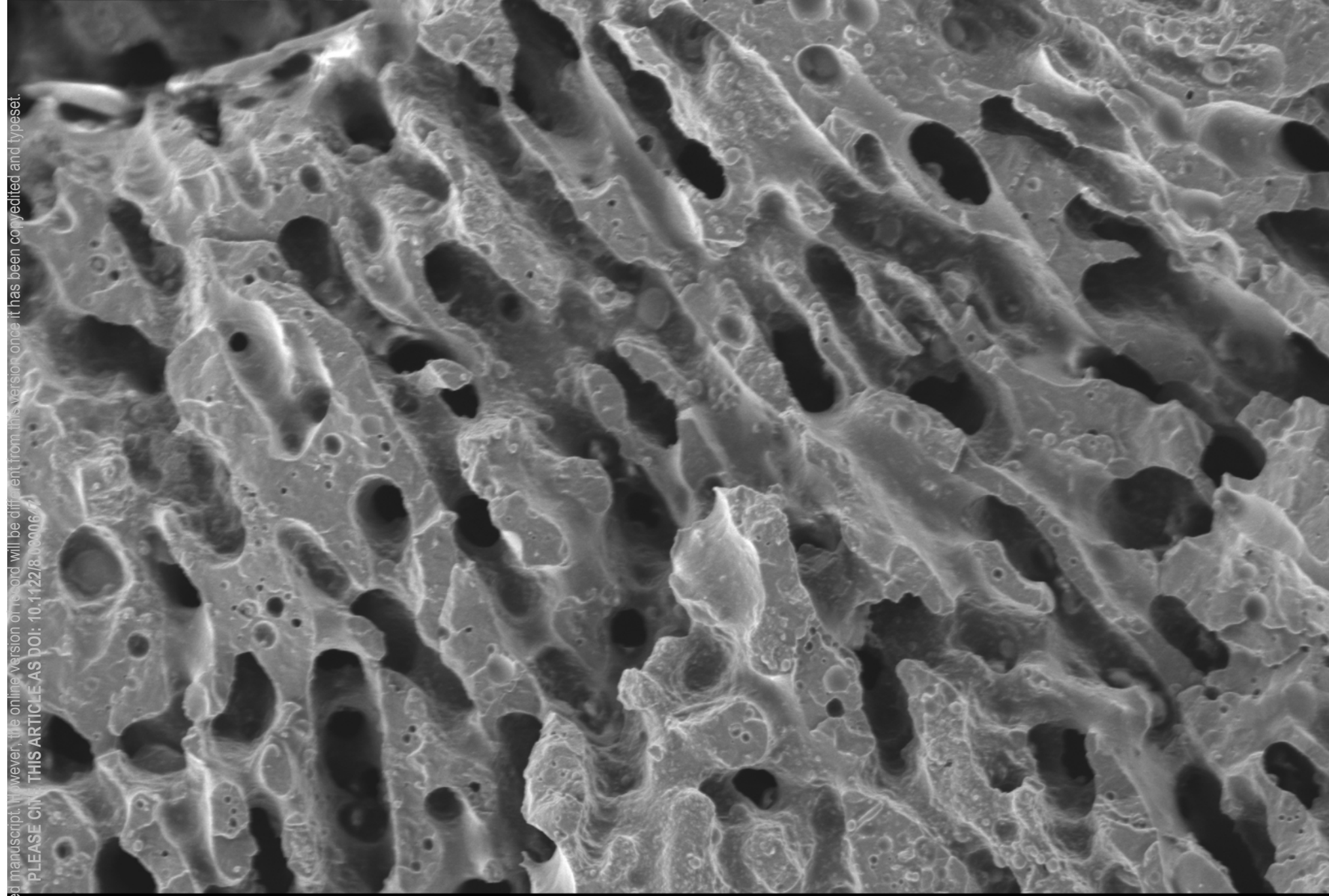


This is the author's peer reviewed, accepted manuscript. However, the online version of record will be different from this version once it has been copyedited and typeset.  
 PLEASE CITE THIS ARTICLE AS DOI: 10.1122/8.0000647



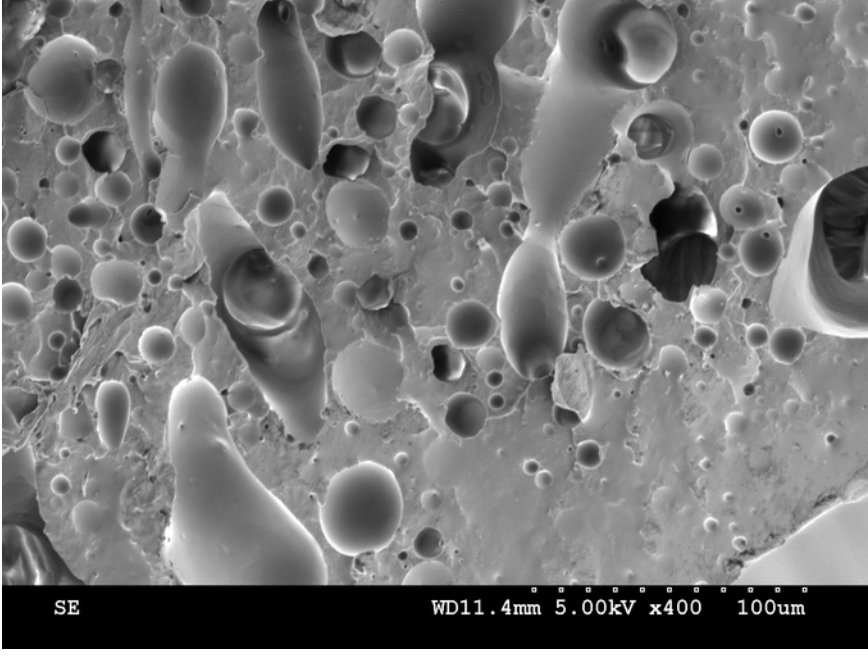
This is the author's peer reviewed, accepted manuscript. However, the online version of record will be different from this version once it has been copyedited and typeset.  
PLEASE CITE THIS ARTICLE AS DOI: 10.1122/1.5000677

**A**

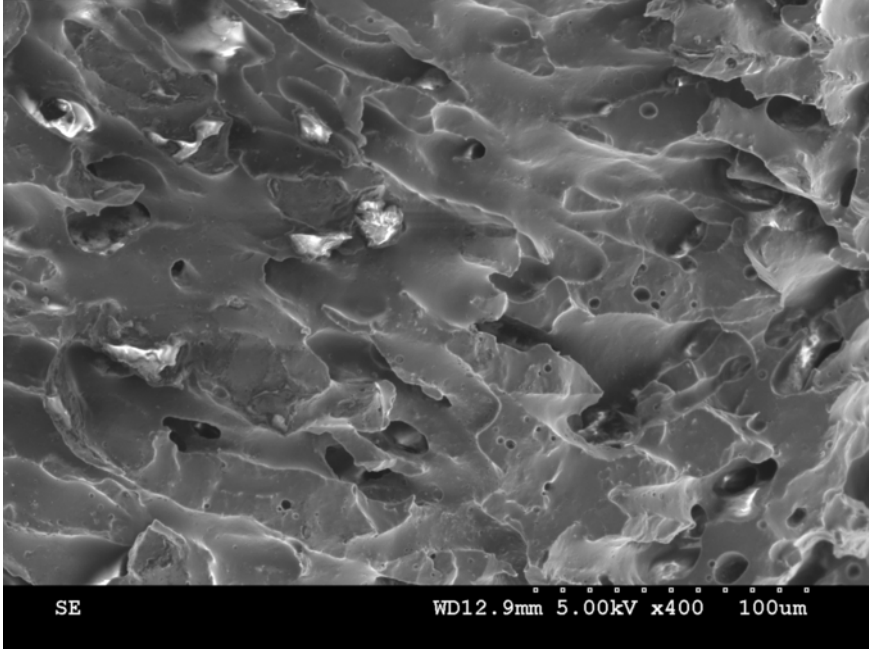


WD 9.7mm 5.00kV x400 100um

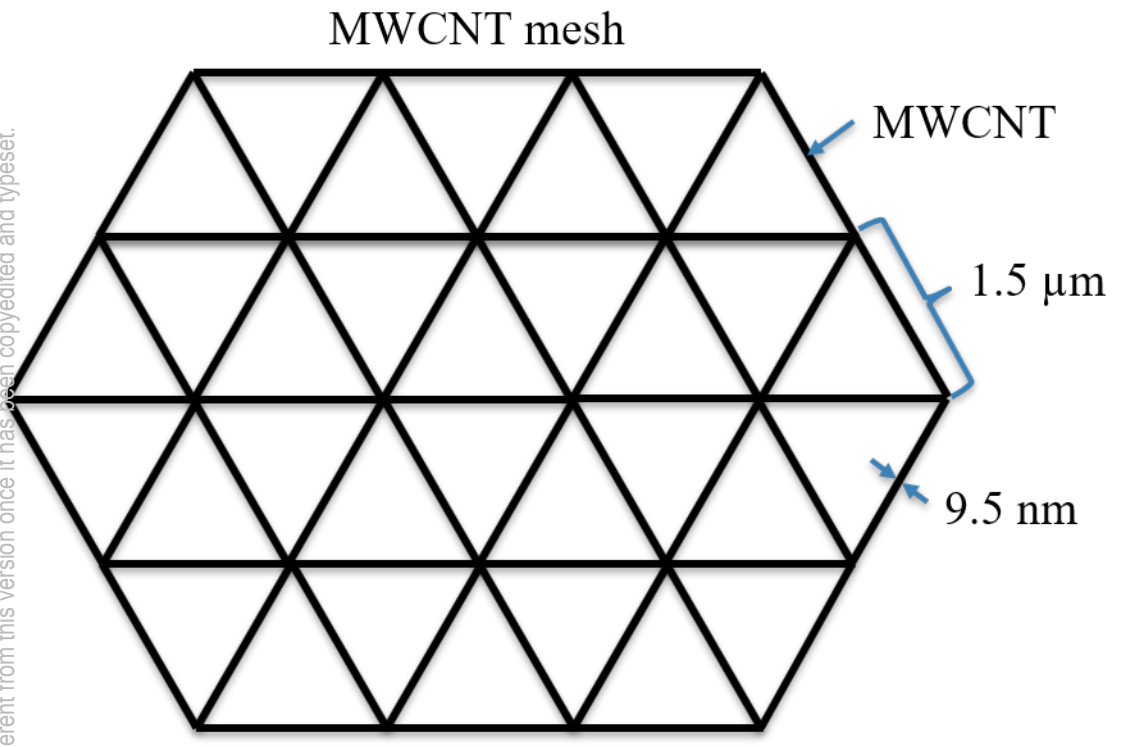
This is the author's peer reviewed, accepted manuscript. However, the online version of record will be different from this version once it has been copyedited and typeset.  
PLEASE CITE THIS ARTICLE AS DOI: 10.1122/8.0000647



This is the author's peer reviewed, accepted manuscript. However, the online version of record will be different from this version once it has been copyedited and typeset.  
PLEASE CITE THIS ARTICLE AS DOI: 10.1122/8.0000647



This is the author's peer reviewed, accepted manuscript. However, the online version of record will be different from this version once it has been copyedited and typeset.  
PLEASE CITE THIS ARTICLE AS DOI: 10.1122/8.0000647







This is the author's peer-reviewed, uncorrected manuscript. It is not for distribution. Please refer to the version on the journal website for the final copy. PLEASE CITE THIS ARTICLE AS: DOI: 10.1122/JRR-2019-00000

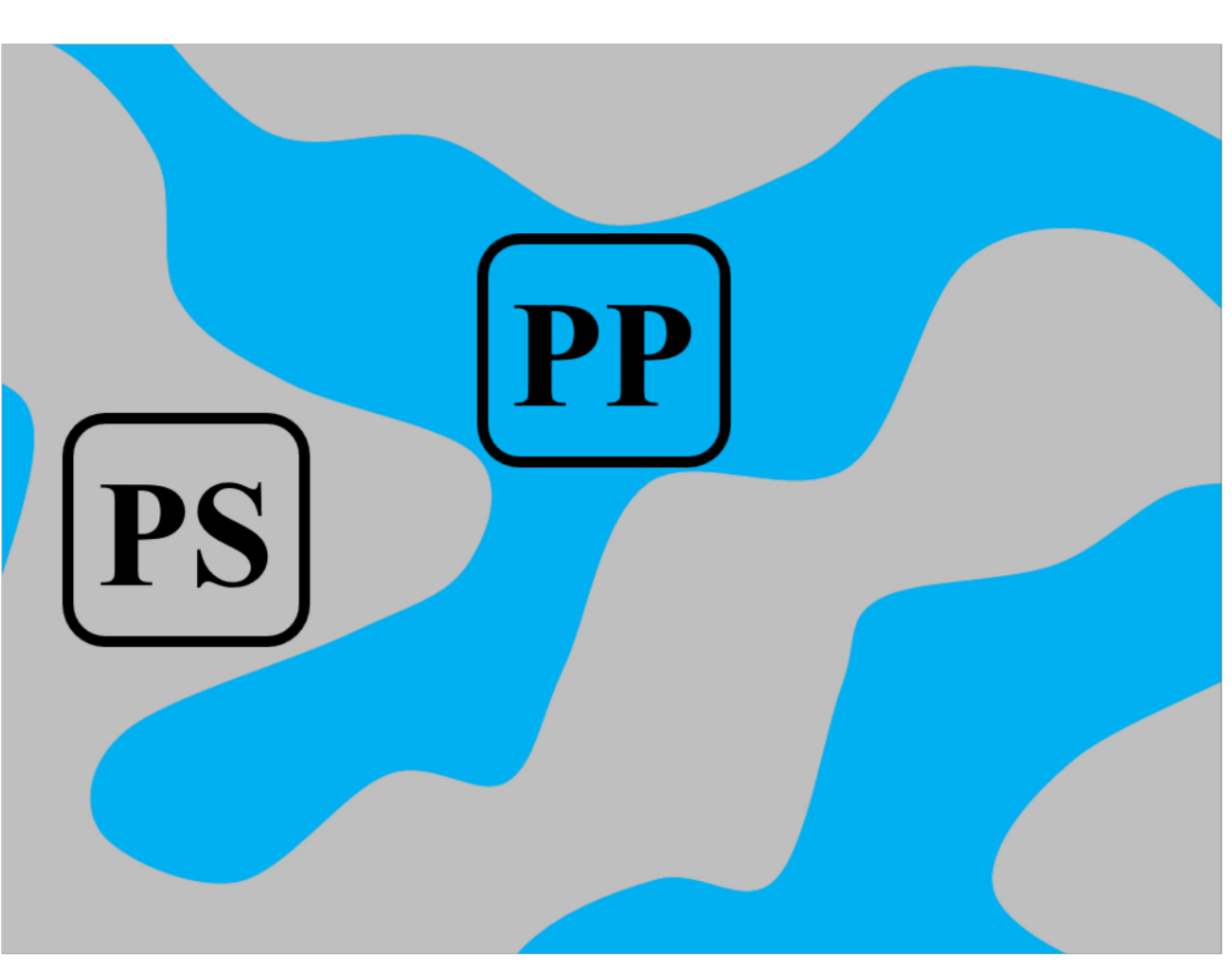
**Before any deformation**

**After 250% of strain at a steady shear rate of:**

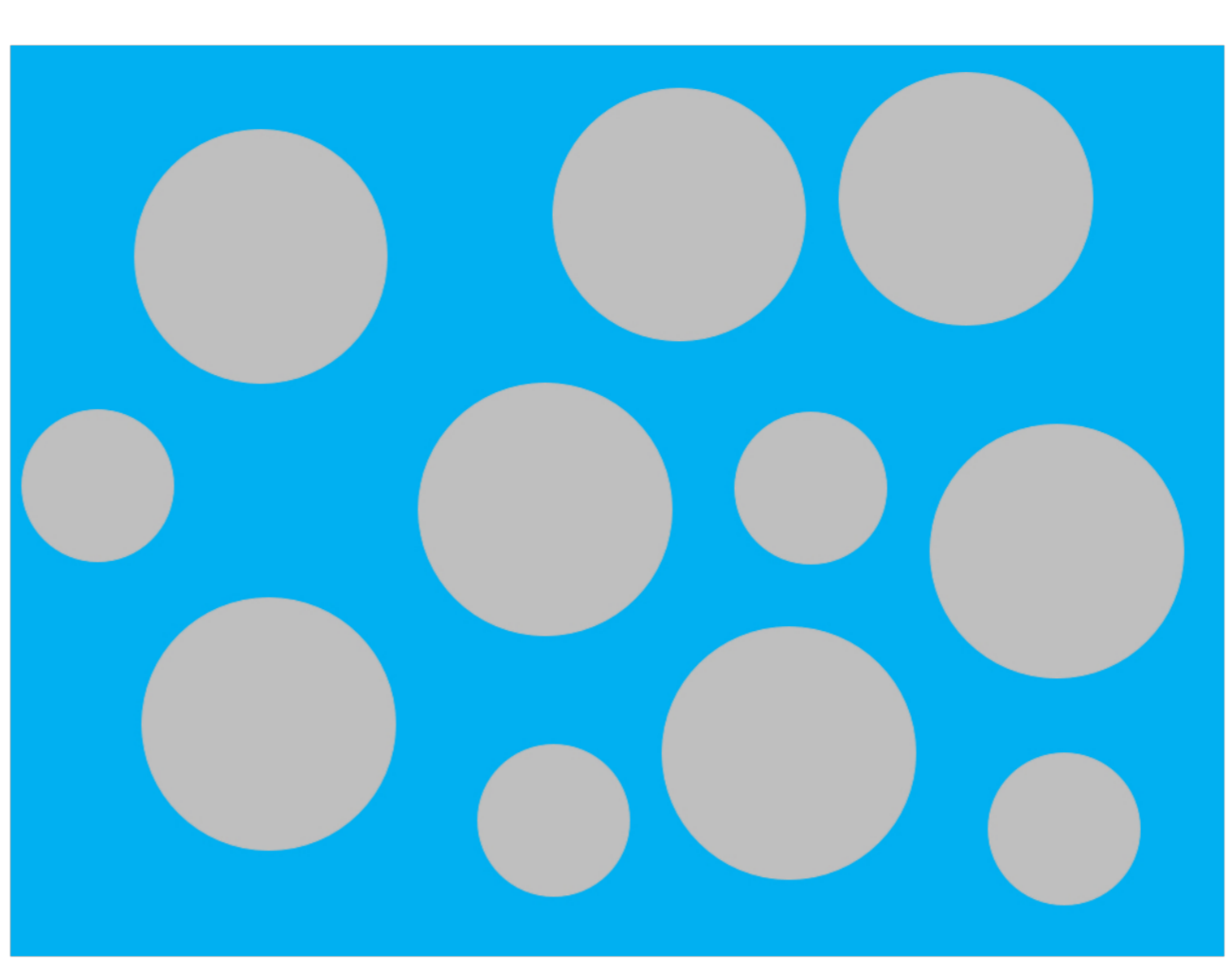
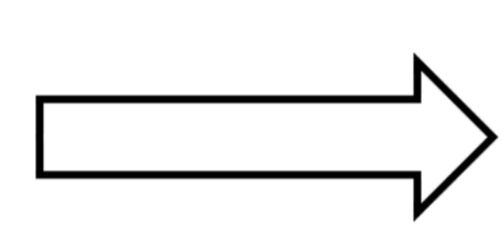
**0.05/s**

**1/s**

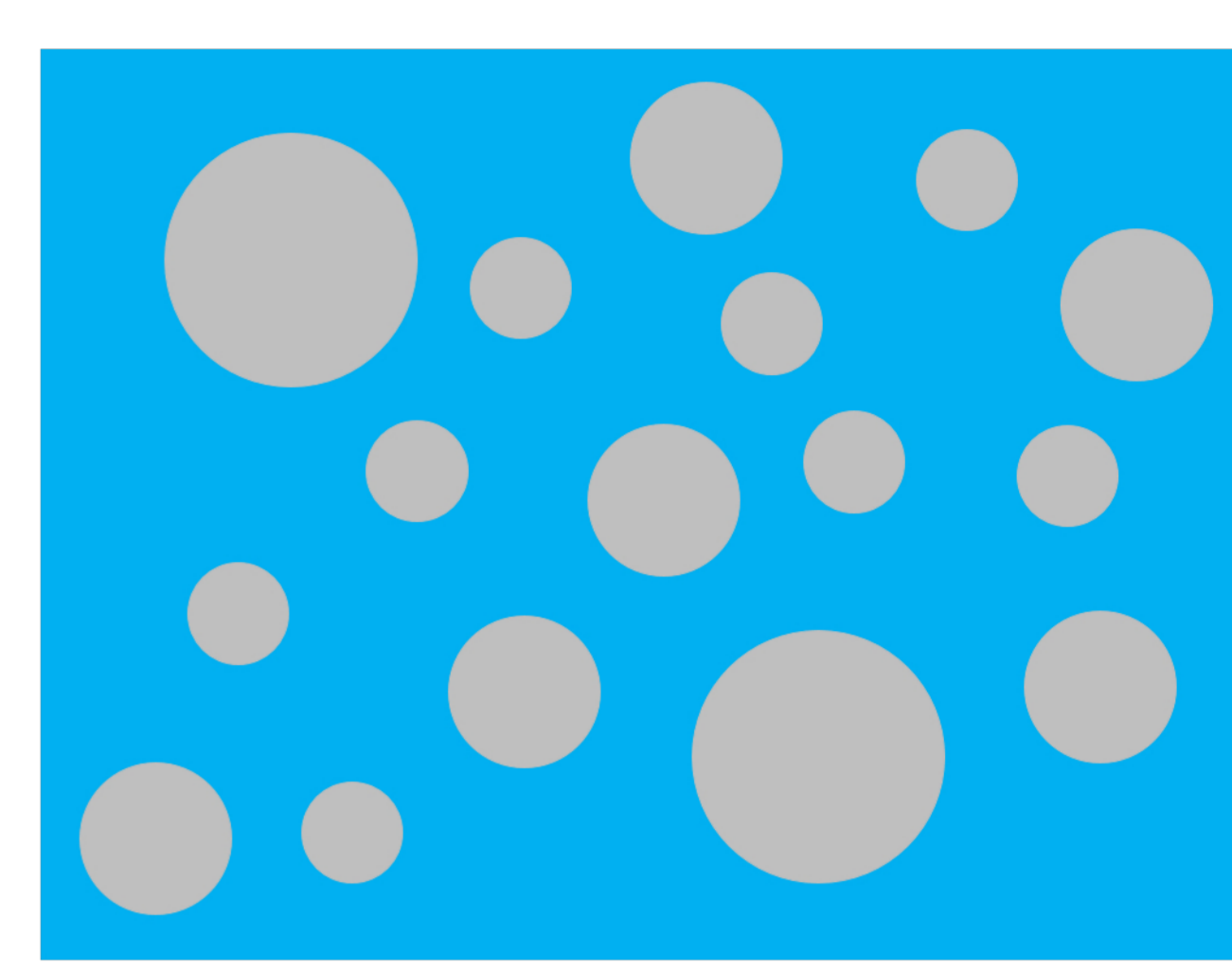
**0 wt.%**



$10^{-10} \text{ S/m}$

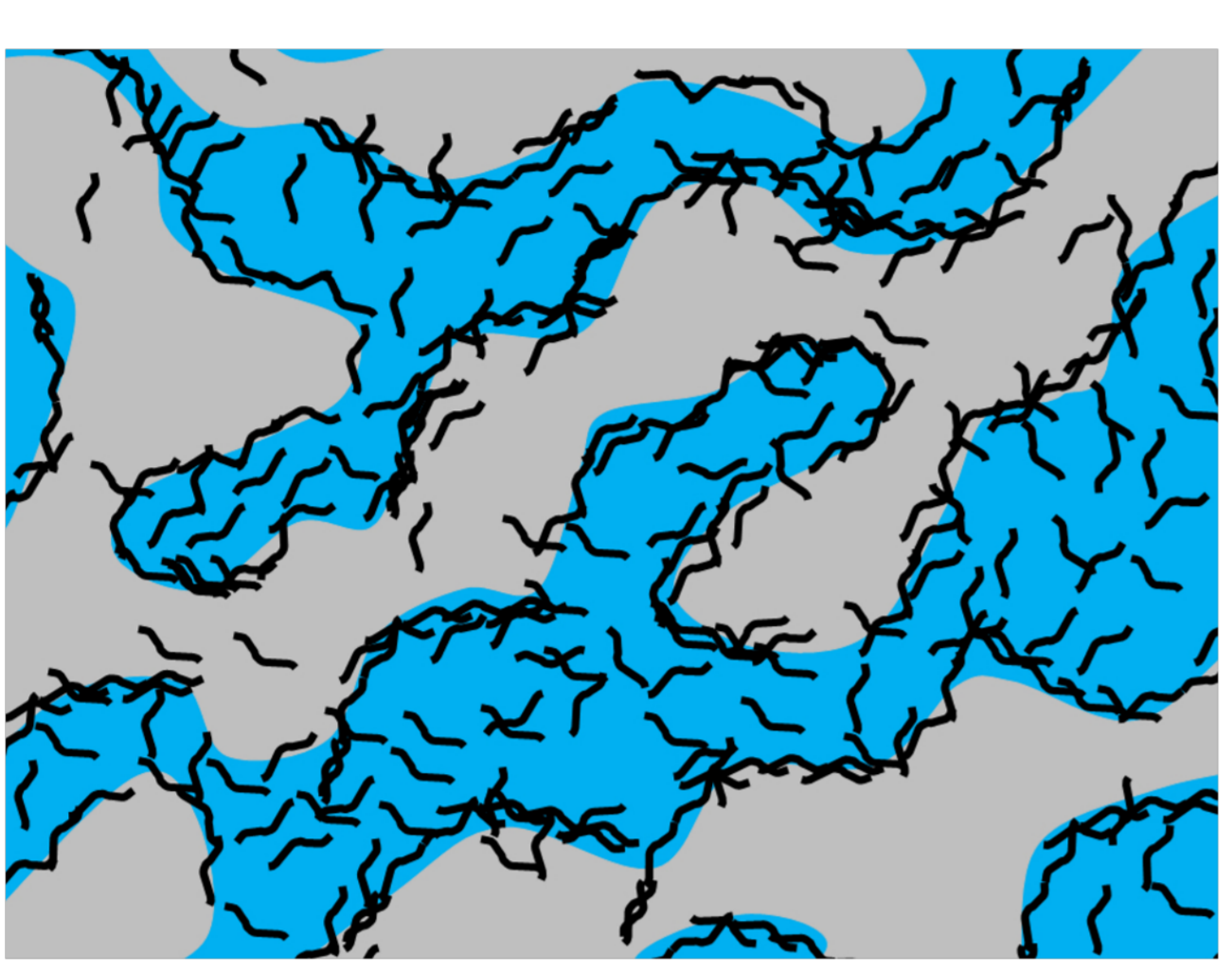


$10^{-10} \text{ S/m}$

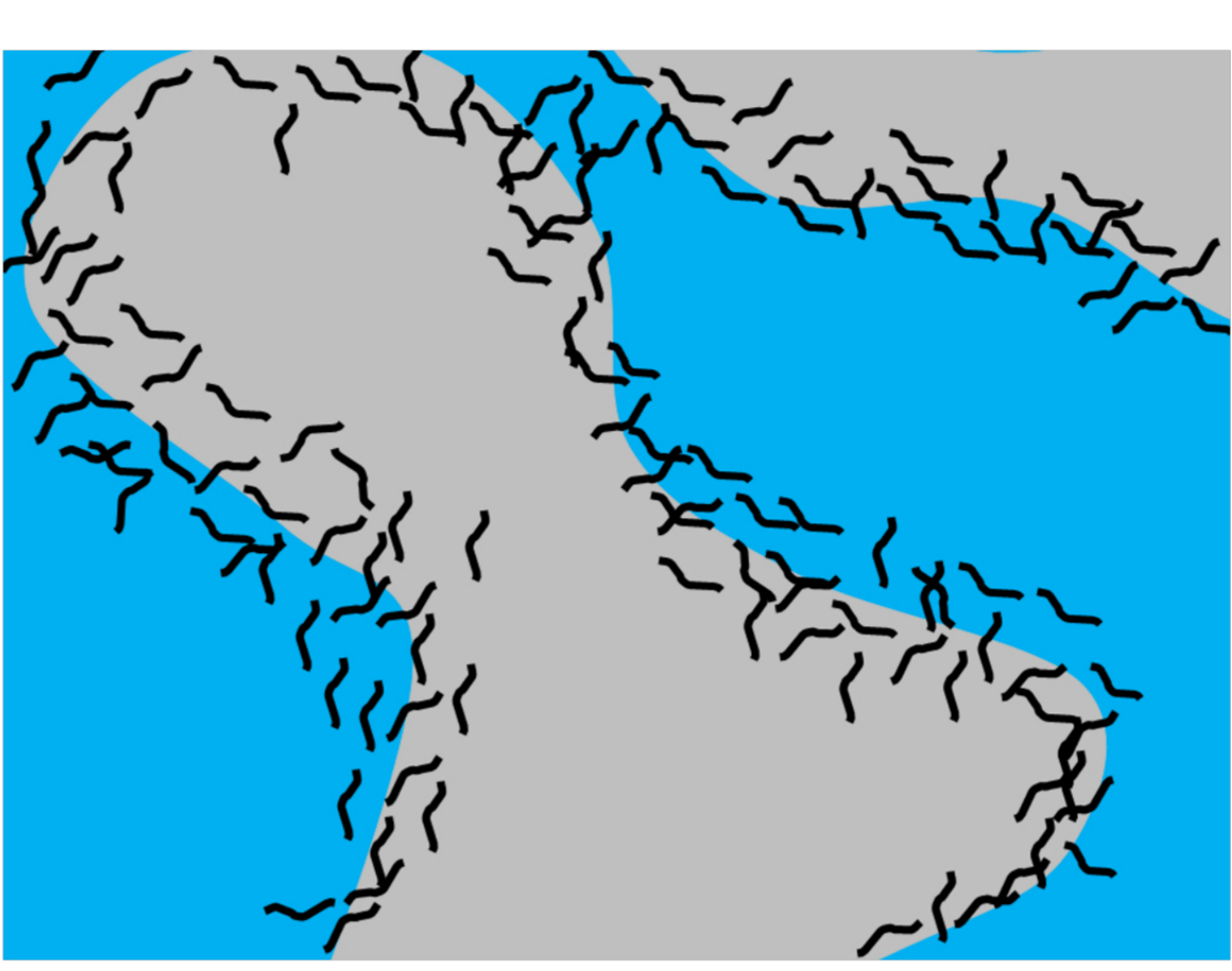
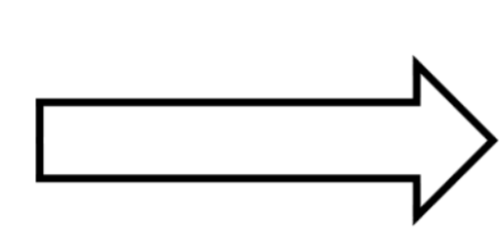


$10^{-10} \text{ S/m}$

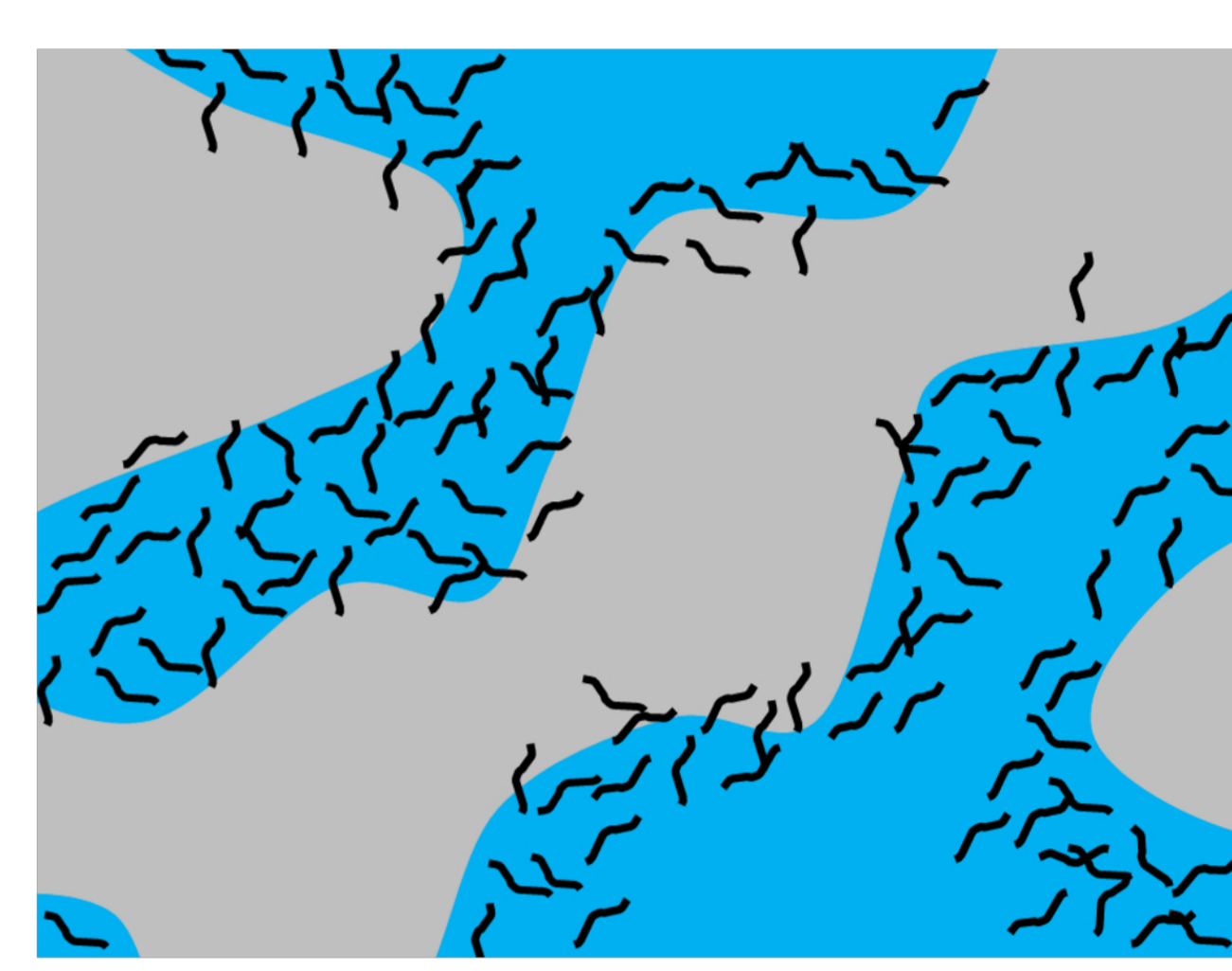
**0.5 wt.%**



$10^{-4} \text{ S/m}$



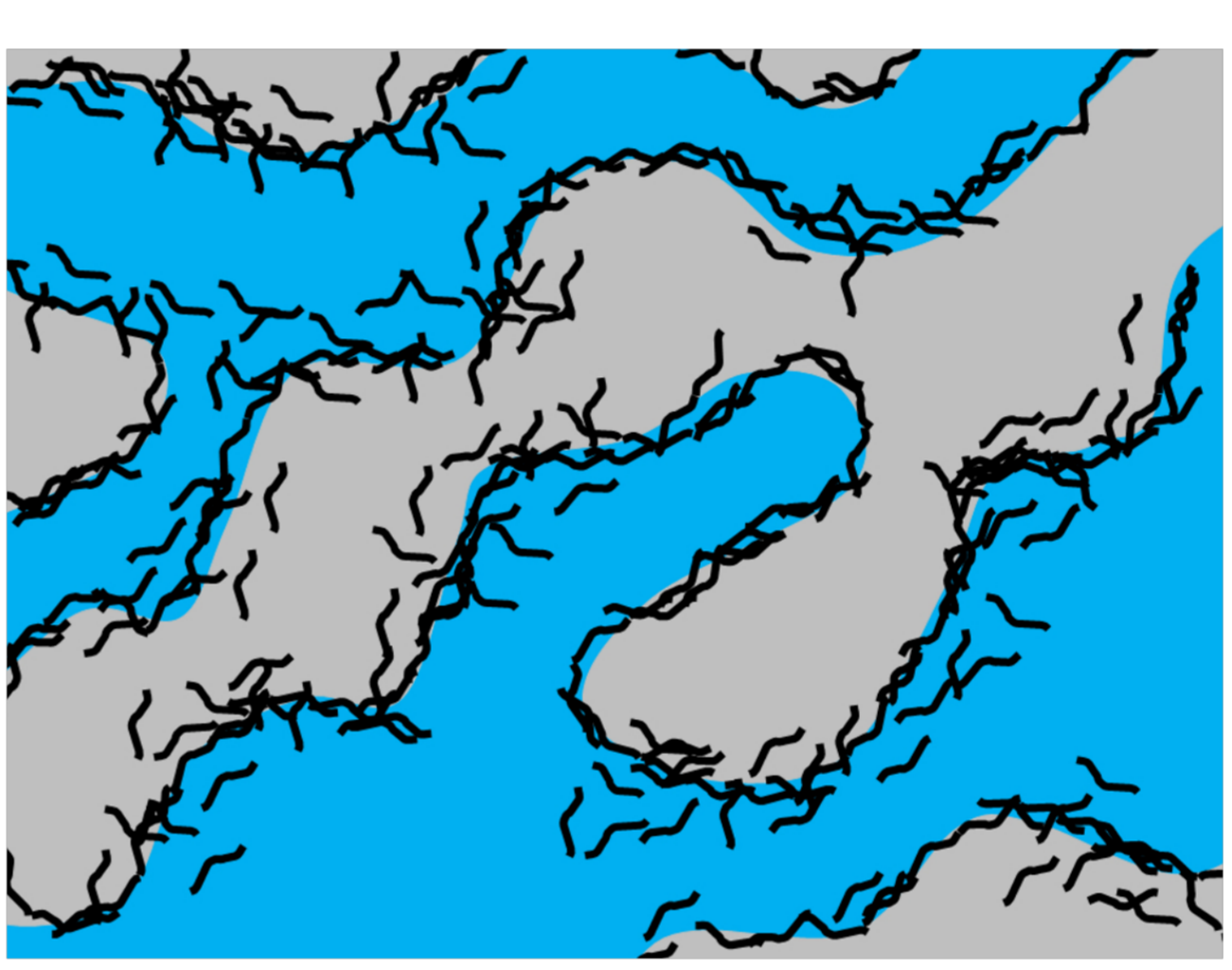
$10^{-6} \text{ S/m}$



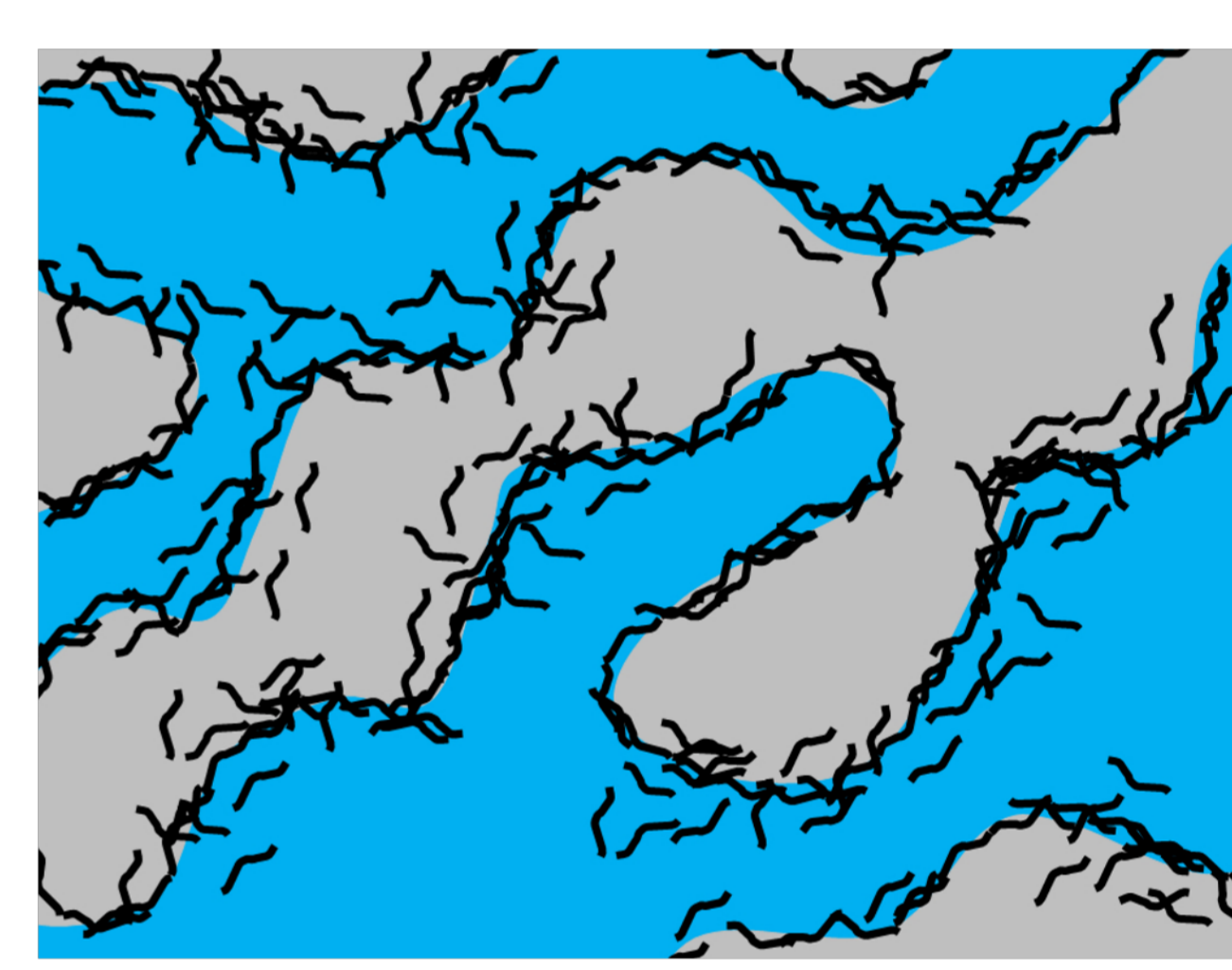
$10^{-8} \text{ S/m}$

**After stress relaxation**

**Total recovery of electrical conductivity**

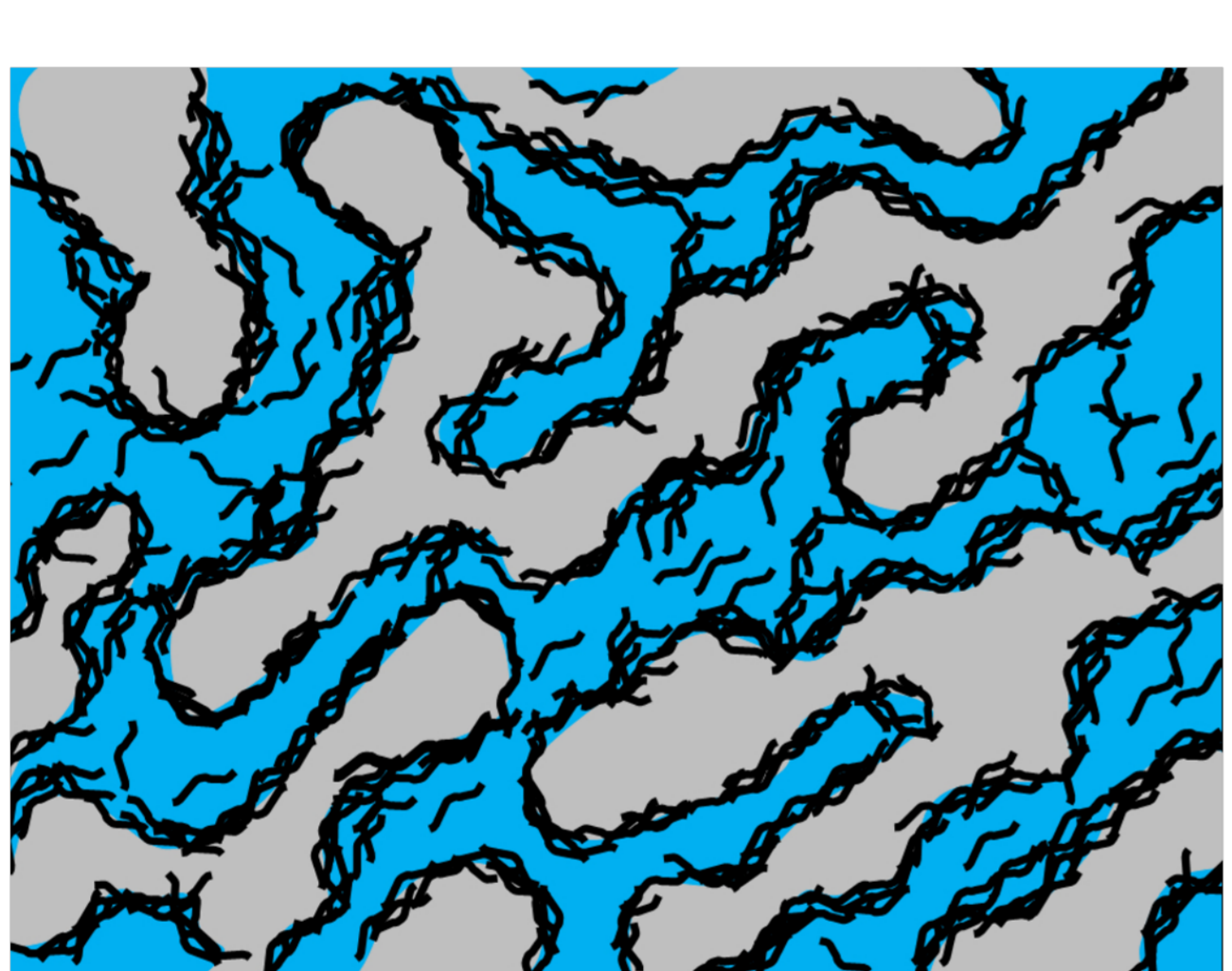


$10^{-4} \text{ S/m}$

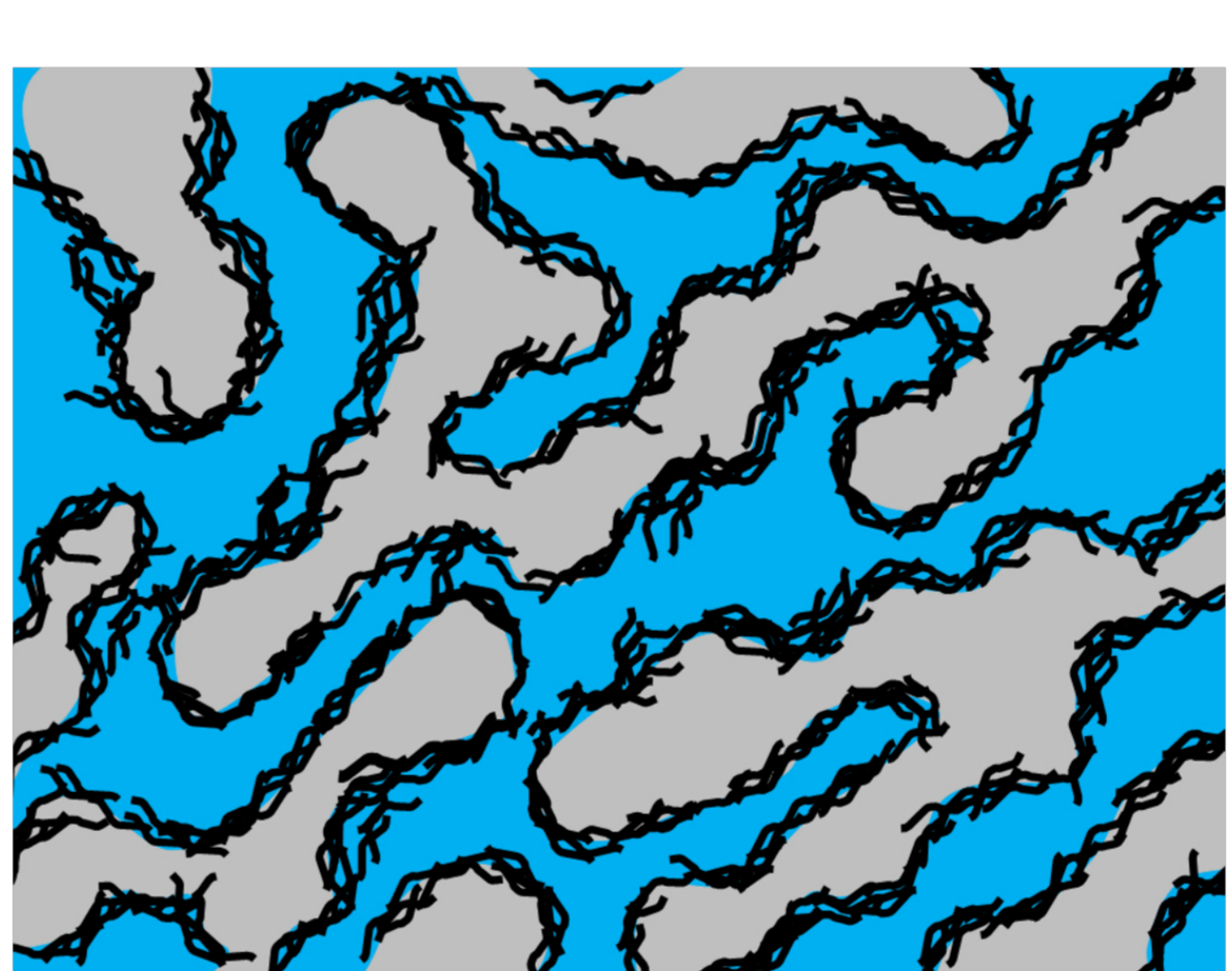
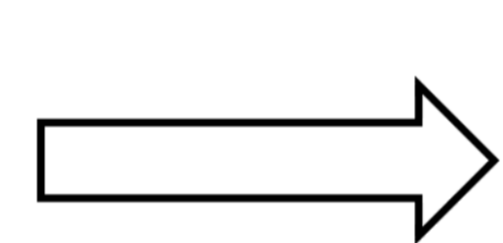


$10^{-4} \text{ S/m}$

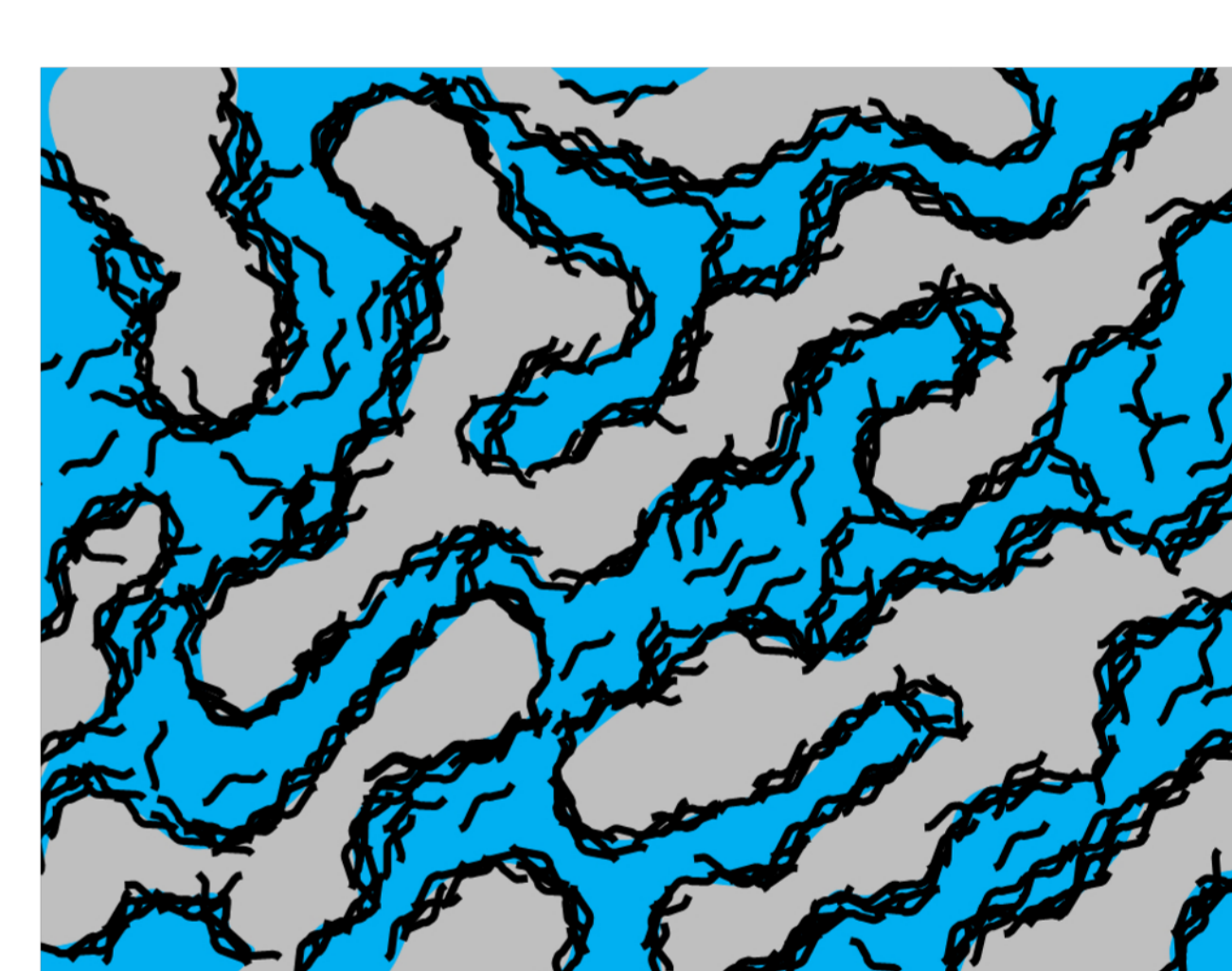
**2 wt.%**



$10^{-3} \text{ S/m}$

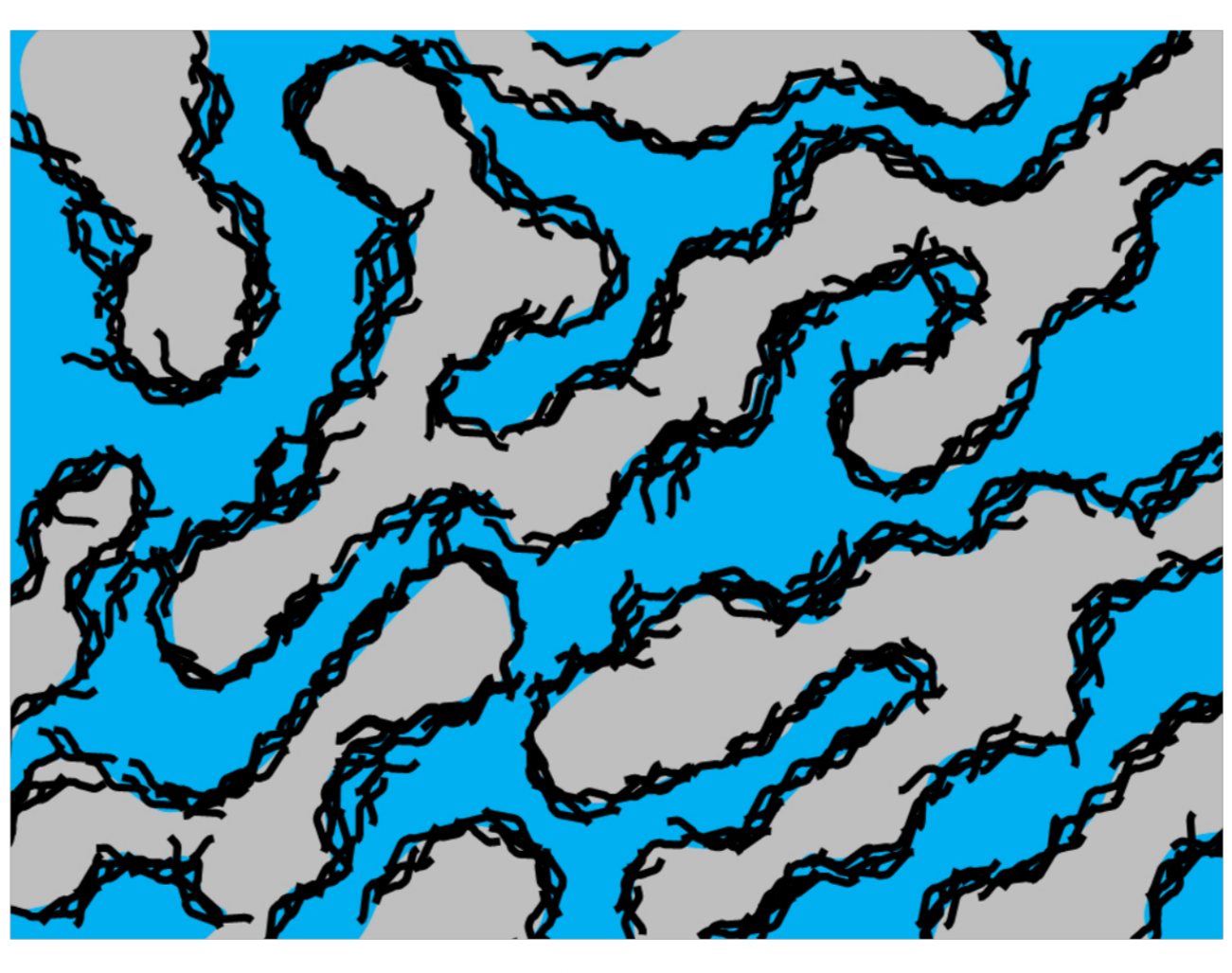


$10^{-3} \text{ S/m}$

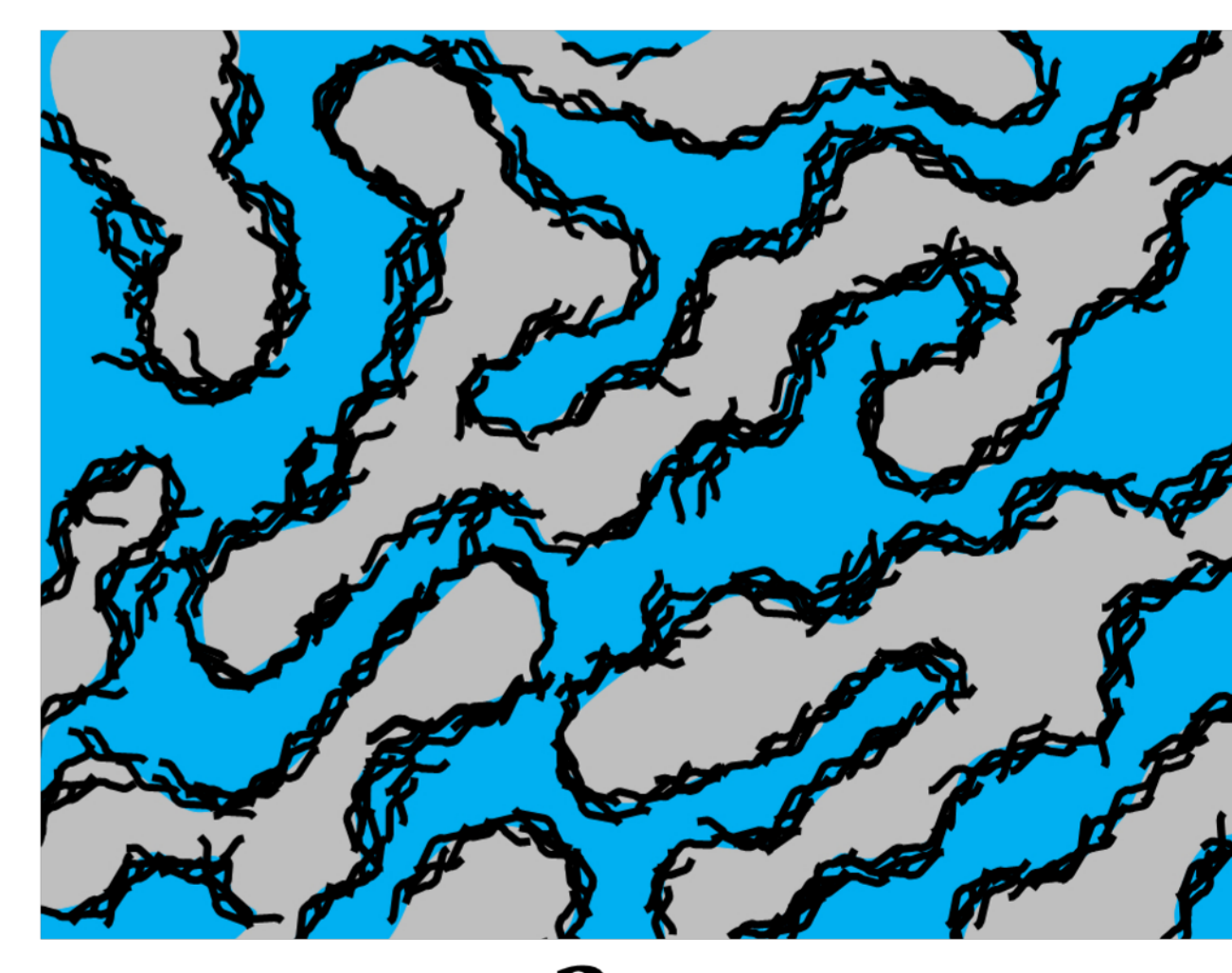


$10^{-4} \text{ S/m}$

**After stress relaxation**



$10^{-2} \text{ S/m}$



$10^{-2} \text{ S/m}$